UNIVERSITY OF SOUTHAMPTON

FACULTY OF ENGINEERING AND APPLIED SCIENCE

DEPARTMENT OF ELECTRONICS AND COMPUTER SCIENCE

NARROW-LINEWIDTH ERBIUM-DOPED FIBRE LASERS

By

Gregory John Cowle

A thesis submitted for the degree of Doctor of Philosophy

October 1991.

UNIVERSITY OF SOUTHAMPTON

ABSTRACT

FACULTY OF ENGINEERING AND APPLIED SCIENCE

DEPARTMENT OF ELECTRONICS AND COMPUTER SCIENCE

Doctor of Philosophy

NARROW-LINEWIDTH ERBIUM-DOPED FIBRE LASERS

by Gregory John Cowle

This thesis describes research towards narrow-linewidth and single-longitudinal-mode erbium-doped fibre lasers operating on the 1.55μm region. The work is concerned with the physics and technology of narrow-linewidth fibre lasers. Factors which affect the spectral width and number of modes oscillating in an erbium-doped fibre laser are described, with particular reference to spatial holeburning, the primary cause of multi-mode oscillation.

Novel resonator configurations for narrow-linewidth operation are described, in both standing-wave and travelling-wave arrangements, with linewidths as narrow as 10kHz being achieved. The development of narrow-bandwidth distributed Bragg reflectors is discussed.

Resonator configurations discussed include short fibre lasers with narrow bandwidth reflectors, polarimetric coupled-cavity fibre lasers, travelling-wave fibre ring lasers and travelling-wave fibre loop lasers. Travelling-wave operation is demonstrated to be a powerful technique for realising single-frequency fibre laser operation. Linewidths as narrow as 10kHz are demonstrated in long fibre laser resonators. The potential for high efficiency and broad tuning ranges are illustrated.

The statistics of phase noise in erbium-doped fibre amplifiers are characterised, by measurements of spectral broadening of a signal passing through the amplifier. The process of spectral broadening is modelled using a rotating vector approach. The implications for amplification of narrow bandwidth signals are discussed.

ACKNOWLEDGEMENTS

During the course of my studies I have had the opportunity to work with the majority of the members of the Optical Fibre Group, and although too numerous to list in full, I would like to acknowledge their assistance during this time. Particular thanks are due to Dr P.R Morkel with whom I collaborated in some of the work presented in this thesis, and to Dr W.L. Barnes, Dr R.I. Laming, Dr J.D. Minelly and Dr J.E. Townsend. I also thank Prof. W.A. Gambling for allowing me to study in the Optical Fibre Group and Prof. D.N. Payne for his supervision in my studies.

Thanks to D. Reid and C.M. Ragdale of Plessey Research Caswell Ltd for the loan of a fibre Bragg reflector.

Many thanks are due to Dr W.L. Barnes, Dr R.I. Laming, Dr P.R. Morkel and Dr C.N. Pannell for their valuable comments on this manuscript.

I am grateful to the Association of Commonwealth Universities for providing me with a scholarship to study in Britain and to the British Council for administering my award.

Finally, thanks to my family and friends for their encouragement and support during my studies in Britain.

Table of Contents

Table of Figures

Chapter One

Introduction

1.1 INTRODUCTION

Interest in rare-earth-doped fibre lasers and fibre amplifiers has been intense in the last few years, stemming from when low-loss silica optical fibres were fabricated with rare-earth dopants incorporated in the fibre core [Poole]. However the recent attention generated by these devices represents a renewed interest, stimulated by advances in technology allowing the development of a reliable fabrication technique, in a topic which began only a few years after the operation of the first ruby laser when Snitzer and Koester published results on amplification of light in glass [Snitzer] [Koester].

Fibre lasers and amplifiers are based on well-developed optical fibre and laser technology, taking a form in which the active lasing ions, rare-earth ions, are

incorporated in the core of the fibre [Mears]. If the fibre is optically pumped by a beam of light at a wavelength corresponding to an absorption band of the rare-earth ion, the light is attenuated as the electrons of the ion are excited to higher energy levels. Once in a higher energy level the electron will decay to a lower energy level, either non-radiatively producing one or more phonons or radiatively producing a photon. Radiative decays can occur spontaneously or be stimulated by a photon with energy equal to the energy difference between two of the rare-earth-ion energy levels. Stimulated emission, in which the photon created by de-excitation of the electron is in phase with the stimulating photon is the basis of lasing action. Gain can occur as stimulated photons promote further stimulated photons. Gain can be sustained if the number of ions in an excited state of a transition exceeds the number in the lower level of the transition. This condition is known as population inversion. Mirrors on the ends of the gain medium which reflect a proportion of the stimulated photons provide a resonant structure in which the stimulated photons are fed back into the gain medium to stimulate the emission of more photons with the same energy [Siegman].

Fibre lasers have certain advantages over other glass and solid-state lasers due to the waveguiding structure and small active volume provided by the optical fibre. The waveguiding properties of the optical fibre produces very good overlap between pump and signal modes, with the consequent interaction between the pump mode and active ions giving rise to highly efficient lasing operation [Reekie]. With core diameters typically only a few microns, pump intensities can be very high, often leading to significantly lower pump threshold powers than can be achieved with bulk lasers. As a result, some three-level laser systems which were previously not possible in bulk lasers are often easily demonstrated in continuous-wave oscillation in fibre form [Alcock] [Reekie 1986a]. The long lengths associated with active fibre devices allow very low concentrations of rare-earth ions to be used, allowing ion-ion interactions and concentration quenching effects to be kept low so as not to degrade device performance [Wyatt 1989a]. The long resonator lengths possible in fibre form could

also provide long interaction lengths for non-linear effects, such as Brillouin scattering, to be investigated within fibre laser resonators [Tkach] [Culverhouse]. The optical fibre waveguide structure also results in good thermal properties because of the surface area to volume ratio of the structure, resulting in more efficient heat dissipation than from bulk lasers [Urquhart]. The waveguide structure also ensures that the plane-wave nature of the guided mode is not affected by heating of the core, and hence heat stress will not affect the alignment of the resonator. In addition, because fibre lasers are based on well-developed single-mode optical fibre technology, they can incorporate the devices which have been developed in this technology, such as fibre couplers and distributed Bragg reflectors. The incorporation of these devices makes it possible to fabricate complex laser resonator structures to achieve desired spectral properties while maintaining low excess loss for efficient operation. Resonator structures can be designed which produce outputs with low temporal coherence and good temperature stability for certain sensors such as fibre gyroscopes [Digonnet], while other structures have been used to demonstrate extremely narrow-linewidth spectra or very short pulse generation [Kafka].

1.2 FIBRE LASERS AND AMPLIFIERS

Rare-earth-doped fibre lasers and amplifiers have been demonstrated at several wavelengths by using a variety of rare-earth ions as dopants in the fibre and by operating on numerous transitions of the ions. Of particular interest are the operation of neodymium-doped fibre devices in the 1.3μm region and erbium-doped fibre lasers and amplifiers in the 1.5μm region, these wavelength regions representing the low-loss windows in silica optical fibres utilised for long-distance optical communication systems. The 1.5μm region is the lowest loss silica optical fibre window and hence attracts most interest for long distance communications. The 1.3μm region exhibits more loss but is still important for amplifiers and laser sources due to the quantity of

installed fibre systems at this wavelength. Neodymium-doped fibres are promising as amplifiers in the 1.3μm region, however silica-based fibres are unlikely to be suitable hosts because of dominant excited-state absorption [Miyajima][Dakss]. Fluoro-zirconate fibres doped with neodymium ions have demonstrated gain of 10dB at 1.33μm and may in future result in practical amplifiers.

This thesis is concerned with the operation of active erbium-doped fibre devices in the 1.55μm region, and in particular the operation of these devices when the output characteristics are limited by the phase noise of the gain medium. The development of narrow-linewidth and single-longitudinal-mode fibre lasers, and the phase noise properties of fibre amplifiers, are discussed in the following chapters. The remainder of this chapter will give a brief introduction to the physics and technology of resonator design for single-frequency fibre lasers. The following chapters will expand on the principles of operation, and describe the development of some novel fibre laser devices for narrow-linewidth and single-longitudinal-mode operation in the 1.55μm region.

1.3 ERBIUM-DOPED FIBRE LASERS

Erbium-doped single-mode fibre lasers with outputs in the 1.55μm region operate on the $^4I_{13/2}$ to $^4I_{15/2}$ transition of the Er^{3+} ion sited in a glass host, and were first demonstrated in 1986 [Mears 1986]. Many variations on erbium-doped fibre laser devices have been demonstrated in this useful wavelength region in Fabry-Perot [Mears 1986] and ring [Scrivener] configurations, showing high efficiency and broad tuning ranges [Wyatt 1989]. The $^4I_{13/2}$ to $^4I_{15/2}$ transition in Er^{3+} is part of a three-level system, and since the laser is end-pumped, significant variations in the output characteristics occur with length variations and pump power [Barnes] [Kimura]. For a given pump power there is an optimum length for low-threshold operation. If the length is shorter than

the optimum length the gain will be less than the optimum case, while if the length is longer than the optimum length reabsorption of the signal photons will occur. These variations arise because of axial variations in population inversion which result in axial variations in gain and absorption. The fluorescence spectrum of an erbium-doped silica single-mode fibre is very broad, ~80nm [Ainslie], which is valuable for producing a tunable source [Kimura], [Reekie], [Wyatt 1989], however it places constraints on cavity wavelength selectivity for the design of narrow-linewidth and single-longitudinal-mode fibre lasers. The broad fluorescence spectrum results from the electronic structure of the rare-earth ion and on the modifying effect of the host glass.

Various pump bands are available for 1.55μm operation of erbium fibre lasers and amplifiers. Early Er^{3+}-doped fibre devices were pumped at 514.5nm by argon-ion lasers [Mears 1986]. Other pump bands to have been used are 807nm [Millar], 980nm [Laming] and 1.48μm [Snitzer 1988]. For telecommunications applications of fibre lasers and amplifiers a prime considerations for pump lasers will be reliability, and for this reason, diode laser pumping is attractive. 980nm pumping is most attractive because of its high efficiency and because it suffers from negligible Excited State Absorption (ESA) [Laming]. All fibre lasers and amplifiers discussed in the following chapters are pumped in the 980nm band with either dye, Ti:sapphire or diode lasers.

1.4 NARROW LINEWIDTH LASERS

Narrow-linewidth lasers have many applications such as in interferometry, high-resolution spectroscopy, metrology and communications. Single-longitudinal-mode lasers operating in the 1.5μm region are important devices for transmitters in single-mode optical fibre communication systems. Typically distributed feedback (DFB) semiconductor injection lasers are used in such systems, but such devices have broad

intrinsic linewidths, limiting linewidths to typically 1-10MHz. These devices can however be directly modulated via changes in drive current, although normally resulting in unwanted frequency chirps arising from changes in refractive index of the active layer with modulation current variations [Whalen]. Coherent communication systems, currently under development in research laboratories around the world, may offer significant performance advantages over presently used intensity modulation direct detection schemes, and allow many channels to be multiplexed on a single fibre [Linke]. Coherent techniques offer great potential in multichannel systems as a result of the very high receiver sensitivities that can be achieved. However these coherent schemes, operating with phase or frequency modulation, require single frequency lasers with narrow linewidths. Another drawback of coherent schemes is their additional complexity as compared with intensity modulation direct detection schemes.

To date most experimental coherent communication systems have employed either external cavity semiconductor lasers or helium-neon gas lasers as sources to achieve suitably narrow linewidths. Semiconductor laser sources such as external cavity lasers [Wyatt] and multisection distributed Bragg reflector lasers [Öberg] are promising candidates for commercial systems, however they are not yet fully developed for commercial operation in telecommunications environments. Erbium-doped fibre lasers may be attractive for producing single-longitudinal-mode operation because, as this thesis will show, erbium-doped fibre can be configured into suitable laser cavities to produce single-frequency operation, with linewidths several magnitudes narrower than those typically achieved with semiconductor lasers. If stable, tunable, diode-pumped single-longitudinal-mode fibre lasers can be developed, they may be future competitors to semiconductor laser diodes for applications such as communication systems.

1.5 SINGLE-LONGITUDINAL-MODE BEHAVIOUR

The most significant effect leading to multi-mode operation in lasers is spatial inhomogeneity of the population inversion, especially spatial holeburning [Siegman]. Some of the effects of spatial holeburning will be discussed in Section 3.4. Single-longitudinal-mode operation can be achieved by several methods, designed such that the effects of spatial holeburning in the gain medium cannot lead to multi-mode operation. In practice single-longitudinal-mode lasers can be realised by several methods including:

- a short laser resonator in which the passive cavity modes are widely spaced so that only one mode falls within the gain bandwidth. This method is suited to lasers with narrow gain bandwidths, such as some gas lasers. Other examples of this type of single-frequency resonator are miniature solid-state lasers [Zayhowski].

- multiple-mirror resonators which use interferometric mode selection to reduce the number of modes oscillating [P.W. Smith]. Such techniques have been investigated since the early years of laser experimentation [Kogelnik].

- a travelling-wave configuration which has no standing-wave pattern, first demonstrated in 1963 by Tang et. al. [Tang].

- modulating the position of the standing-wave field inside a laser cavity in order to achieve average uniform population inversion [Danielmeyer].

- injection locking of laser by a weak monochromatic signal injected into the laser from another laser, so that the injected laser captures the injected signal and is controlled by the injected signal [Stover].

Many of these techniques have been successfully applied to fibre laser resonators to achieve single-longitudinal-mode operation. The first demonstration of a single-longitudinal-mode fibre laser was a Nd^{3+}doped fibre laser operating at 1.082nm. The resonator was a short Fabry-Perot cavity in which a distributed Bragg reflector was incorporated in the doped fibre. To achieve single-longitudinal-mode operation the fibre length was cut back to 51mm to increase the passive cavity mode spacing so that only one mode lased [Jauncey 1988]. The doped fibre had a Nd^{3+} concentration of 0.1%, numerical aperture (NA) of 0.2 and cut-off wavelength, λ_c, of 940nm. Pumped at 594nm the laser exhibited a threshold of 6mW with slope efficiency 2.3%.

Single-longitudinal-mode erbium-doped fibre lasers had been demonstrated by only one technique when the work described in this thesis was commenced. Barnsley et. al. [Barnsley] demonstrated single-longitudinal-mode oscillation in an erbium-doped fibre Fox-Smith cavity. A fused tapered coupler was fabricated from Er^{3+}-doped fibre with Er^{3+} concentration 300 ppm and $\lambda_c = 1.0\mu m$ and a Fox Smith coupled-cavity resonator formed with path length ratios $L_2/L_1 = 1.13 \pm 0.02$. This cavity, although providing periodic loss, did not provide sufficient discrimination to achieve lasing on one pass-band of the Fox-Smith cavity, therefore a diffraction grating in the Littrow configuration was used as one of the reflectors. The fibre laser was pumped at 514.5nm from an Argon-ion laser. Lasing threshold was observed for 175mW pump power, and the measured slope efficiency was 0.04%. The laser spectral width was less than 8.5MHz.

The travelling-wave fibre ring laser presented in Chapter 5 was the next technique for achieving single-longitudinal-mode operation to be demonstrated, for the first time demonstrating linewidths substantially less than 1MHz [Morkel]. The travelling-wave technique eliminates the cause for multi-mode operation, namely spatial holeburning. This fibre laser configuration represents the first time fibre lasers have been operated with a resonator configuration not supporting a standing-wave mode. Following the reporting of this work several authors have pursued this method of achieving very

narrow linewidth and tunable single-longitudinal-mode erbium fibre lasers [Iwatsuki 1990] [D.A. Smith] [Maeda]. Chapter 5 describes another novel travelling-wave cavity for achieving single frequency erbium fibre lasers, the travelling wave fibre loop laser [Cowle]. This work on travelling-wave fibre lasers is now being regarded as a significant contribution to fibre laser technology. A publication by Iwatsuki et. al. [Iwatsuki] predating this work on travelling-wave fibre lasers claimed single-frequency operation in a bi-directional single-polarisation fibre ring laser. The measurements and experimental configuration presented indicate, however, that single-frequency operation was not achieved, and that an intermode beat signal was probably being measured.

Another approach to have been successfully demonstrated is injection locking of an erbium fibre laser by an external cavity diode laser [Jones]. A 2.5m Fabry-Perot fibre laser resonator constructed from Er^{3+}-doped fibre with Er^{3+} concentration 500ppm and was pumped by an Argon-ion laser operating on the 528nm line. With the injection signal adjusted to be close to a mode of the fibre laser oscillator, single-frequency operation of the fibre laser was achieved.

Single-longitudinal-mode operation in an Nd^{3+}-doped fibre laser has been demonstrated by suppression of spatial holeburning by spatial modulation techniques [Sabert]. A 5.1m resonator with piezo-electric phase modulators at each end of the resonator was formed, and by modulating the standing-wave in a push-pull fashion at a frequency above the relaxation oscillation frequency, spatial averaging of the standing-wave pattern was achieved, resulting in single-longitudinal-mode operation.

More recently published developments in techniques for achieving single frequency erbium fibre lasers are standing wave coupled cavity arrangements [Gilbert] and standing wave Fabry-Perot resonators incorporating narrow-bandwidth photorefractive DBRs written into the Er^{3+}-doped fibre [Ball].

1.6 PHASE NOISE PROPERTIES

The ultimate linewidth which can be obtained in a single-longitudinal-mode laser is quantum-limited, determined by spontaneous emission from the gain medium. The effect of phase noise on fibre laser performance has not been experimentally characterised to date, and it is the aim of this work to develop fibre laser resonators in which the linewidth properties are determined by the phase noise characteristics of the doped fibre gain medium.

The performance of erbium-doped fibre amplifiers in coherent communication systems may also depend on the phase noise properties of erbium-doped fibre with a population inversion. In this thesis the effect of phase noise on the spectral width of a signal passing through a fibre amplifier is discussed, in order to determine whether such a source of noise will limit the performance of possible future coherent optical systems utilising narrow-linewidth lasers and erbium-doped fibre amplifiers.

1.7 SYNOPSIS

The work presented in this thesis concerns the physics and technology of laser resonators for single-frequency operation in fibre lasers. Several novel fibre laser resonators were experimentally developed during the course of the research and these devices are discussed and analysed. The lasers are all based on erbium-doped single-mode optical fibres, with the emphasis, except in Chapter 6, on resonator aspects of the laser rather than the characteristics of the erbium-doped fibre itself, which has been extensively studied in recent years, particularly since the advent of the erbium-doped fibre amplifier [Mears 1987]. In the course of this work the now well-known characteristics of erbium-doped fibres, determined by much recent work at the University of Southampton and at other research institutions on erbium-doped fibre

lasers and erbium-doped fibre amplifiers, are drawn upon.

Chapter 2 summarises the fundamental principles of optical fibre waveguide theory and the theory of three-level lasers of particular relevance to erbium-doped fibre lasers. Chapter 3 describes the typical spectral characteristics exhibited by fibre lasers, with a view to understanding how the spectral characteristics can be modified to achieve single-frequency operation. Chapter 4 contains experimental characterisation of narrow-linewidth fibre lasers which operate with standing-wave resonators, including short fibre lasers with narrow-band grating reflectors and a novel polarimetric coupled-cavity configuration. Chapter 4 also describes the development of a fabrication technique for producing narrow-band distributed Bragg reflectors. Chapter 5 recounts experimental results on travelling-wave erbium-doped fibre lasers, developed to eliminate spatial holeburning. It includes a description of the first demonstration of a travelling-wave fibre ring laser and a novel travelling-wave fibre loop laser. Chapter 6 is concerned with erbium-doped fibre amplifiers and is significant as it contains the first measurements performed to characterise the effect of phase noise generated in a fibre amplifier on the spectral characteristics of a signal passing through the amplifier. The common link with the preceding chapters on fibre lasers is that in each case the devices are operating in a regime where operation is limited by the phase noise resulting from spontaneously emitted photons from the erbium-doped fibre gain medium.

The research describes in the following chapters was carried out in the Optical Fibre Group, and the author is grateful for fruitful collaboration with members of the Optical Fibre Group and the Optoelectronics Research Centre. In particular, the experimental results on the polarimetric coupled-cavity fibre laser and travelling-wave ring laser were obtained in collaboration with Dr Paul Morkel, while Dr John Minelly and Dr Philip Russell contributed to the development of narrow-bandwidth distributed Bragg reflectors.

1.8 REFERENCES

Alcock, I.P., Ferguson, A.I. Hanna, D.C and Tropper, A.C., ''Continuous-Wave Oscillation of a Monomode Neodymium-Doped Fibre Laser at 0.9μm on the $^4F_{3/2} \rightarrow {}^4I_{9/2}$ Transition'', *Opt. Commun.*, **58**, 6, pp. 405-408, July, 1986.

Ainslie, B.J., Craig, S.P., and Davey, S.T., ''The Absorption and Fluorescence Spectra of Rare-Earth Ions in Silica-Based Monomode Fiber'', *J. Lightwave Tech.*, **6**, 2, pp. 287-293, 1988.

Ball, G.A., Morey, W.W. and Glenn, W.H., ''Standing-Wave Monomode Erbium Fiber Laser,'' *IEEE Phot. Tech. Lett.*, **3**, 7, pp. 613-615, July 1991.

Barnes, W.L., Poole, S.B., Townsend, J.E., Reelie, L., Taylor, D.J. and Payne, D.N., ''Er^{3+}-Yb^{3+} and Er^{3+} Doped Fiber Lasers'', *J. Lightwave Tech.*, **7**, 10, pp. 1461-1465, Oct. 1989.

Barnsley, P., Urquhart, P., Millar, C., and Brierley, M., ''Fiber Fox-Smith Resonators: Application To Single-Longitudinal-Mode Operation of Fiber Lasers'', *J. Opt. Soc. Am. A.*, **5**, 8, 1988.

Cowle, G.J., Payne, D.N. and Reid, D., ''Single-frequency Travelling-wave Erbium-doped Fibre Loop Laser'', *El. Lett.*, **27**, 3, pp. 229-230, Jan. 1991.

Culverhouse, D., Kalli, K. and Jackson, D.A., ''Stimulated Brillouin Scattering Ring Resonator Laser for SBS Gain Studies and Microwave Generation'', *El. Lett.*, **27**, 22, pp .2033-2035, Oct. 1991.

Dakss, M.L. and Miniscalco, W.J., ''A Large-Signal Model and Signal/Noise Ratio Analysis for Nd^{3+}-Doped Fiber Amplifiers at 1.3μm'', *Fiber Laser Sources and Amplifiers II*, SPIE Vol. 1373, pp. 111-124, 1990.

Danielmeyer, H.G. and Turner, E.H., ''Electro-optic Elimination of Spatial Hole Burning in Lasers'', *Appl. Phys. Lett.*, **17**, 12, pp. 519-521, Dec. 1970.

Digonnet, M.J.F., ''Theory of Superfluorescent Fiber Lasers'', *J. Lightwave Tech.*, **4**, 11, pp. 1631-1639, Nov. 1986.

Gilbert. S.L., ''Frequency Stabilisation of a Tunable Erbium-doped Fiber Laser,'' *Opt. Lett.*, **16**, 3, pp. 150-152, Feb. 1991.

Iwatsuki, K., Takada, A., Hagimoto, K., Saruwatari, M., Kimura, Y., and Shimizu, M., ''Er^{3+}-doped Fiber-Ring-Laser With Less Than 10kHz Linewidth'', *Proc. OFC'89,* PD, 1989.

Iwatsuki, K., Okamura, H. and Saruwatari, M., ''Wavelength-tunable Single-frequency and Single-polarisation Er-doped Fibre Ring Laser with 1.4kHz Linewidth,'' *El. Lett.*, **26**, p. 2033 1990.

Jauncey, I.M., Reekie, L., Mears, R.J., and Rowe, C.J., ''Narrow-Linewidth Fiber Laser Operating at 1.55μm'', *Opt. Lett.*, **12**, p. 164, 1987.

Jauncey, I.M., Reekie, L., Townsend, J.E., Payne, D.N., and Rowe, C.J., ''Single-Longitudinal-Mode Operation of an Nd^{3+}-doped Fibre Laser'', *El. Lett.*, **24**, 1, 1988.

Jones, J.D.C. and Urquhart, P., ''An Injection-Locked Erbium Fibre Laser'', *Opt. Comm.*, **76**, 1, pp. 42-46, April 1990.

Kafka, J.D., Baer, T. and Hall, D.W., ''Mode Locked Erbium Doped Fibre Laser with Soliton Pulse Shaping'', *Opt. Lett.*, **14**, 22, pp. 1269-1271, Nov. 1989.

Kimura, Y. and Nakazawa, M., ''Lasing characteristics of Er^{3+}-doped Silica Fibers from 1553 up to 1603nm'', *J. Appl. Phys.*, **64**, 2, pp. 516-520, July 1988.

Koester, C.J., and Snitzer, E., ''Amplification in a Fiber Laser'', *Appl. Opt.*, **3**, pp. 1182-1186, 1963.

Kogelnik, H. and Patel, C.K.N., ''Mode suppression and Single Frequency Operation in Gaseous Optical Masers'', *Proc. IRE*, **50**, pp. 2365-2366, Nov. 1962.

Laming, R.I., Farries, M.C., Morkel, P.R., Reekie, L., Payne, D.N., Scrivener, P.L., Fontana, F., and Righetti, A., ''Efficient Pump Wavelengths of Erbium-Doped Fibre Optical Amplifier'', *El. Lett.*, **25**, 1, pp. 12-14, 1989.

Linke, R.A., and Gnauck, A.H., ''High-Capacity Coherent Lightwave Systems'', *J. Lightwave Tech.*, **6**, 11, pp. 1750-1769, 1988.

Maeda, M.W., Patel, J.S., Smith, D.A., Chinlon Lin, Saifa, M.A. and Von Lehman, A., ''An Electronically Tunable Fiber Laser With a Liquid-Crystal Etalon Filter as the Wavelength-Tuning Element,'' **2**, 11, pp. 787-789. Nov. 1990.

Mears, R.J., Reelie, L., Poole, S.B. and Payne, D.N., ''Neodymium-doped Silica Single-mode Fibre Lasers'', *El. Lett.*, **21**, 17, pp. 738-740, Aug. 1985.

Mears, R.J., Reekie, L., Poole, S.B., and Payne, D.N., ''Low Threshold Tunable CW and Q-switched Fibre Laser Operating at 1.55μm'', *El. Lett.*, **22**, pp. 884-885, 1986.

Mears, R.J., Reekie, L., Jauncey, I.M. and Payne, D.N., ''Low-noise Erbium-doped Fibre Amplifier Operating at 1.54μm'', *El. Lett.*, **23**, 19, pp. 1026-1028, Sept. 1987.

Millar, C.A., Miller, I.D., Ainslie, B.J., Craig, S.P., and Armitage, J.R., ''Low-threshold CW Operation of an Erbium-doped Fibre Laser Pumped at 807nm Wavelength'', *El. Lett.*, **23**, 99.865-867, 1987.

Miyajima, Y., Komukai, T., Sugawa, T. and Katsuyama, Y., ''Nd^{3+}-doped Fluoro-zirconate Fiber Amplifier Operated Around 1.3μm'', *Proc. OFC'90*, PD16, 1990.

Morkel, P.R., Cowle, G. and Payne, D.N., ''Single-Frequency Operation of a Travelling-Wave Erbium Fibre Ring Laser'', *Proc. OFC'90*, PD18, Jan 1990.

Öberg, M., Nilsson, S., Klinga, T. and Ojala, P., ''A Three-Electrode Distributed Bragg Reflector Laser with 22nm Wavelength Tuning Range'', *IEEE Phot. Tech. Lett.*, **3**, 4, pp. 299-301, April 1991.

Poole, S.B., Payne, D.N., and Fermann, M.E., ''Fabrication of Low-loss Optical Fibres Containing Rare-Earth Ions'', *El. Lett.*, **21**, pp. 737-738, 1985.

Reekie, L., Mears, R.J., Poole, S.B., and Payne, D.N., ''Tunable Single-Mode Fiber Lasers'', *J. Lightwave Tech.*, **4**, 7, pp. 956-960, 1986.

Reekie,L., Mears, R.J., Poole, S.B. and Payne, D.N., ''A Pr^{3+} Doped Singlemode Fibre Laser'', *IOP Meeting on Solid-State Lasers*, London, 1986.

Sabert, H. and Ulrich, R., ''Single Longitudinal Mode Operation of Nd^{3+}-Fibre Laser'', *Proc. 15th ACOFT*, Sydney, Dec. 1990.

Scrivener, P.L., Tarbox, E.J. and Malton, P.D., ''Narrow-linewidth Tunable Operation of Er^{3+}-doped Single-mode Fibre-laser,'' *El. Lett.*, **25**, 8, pp. 549- 1989.

Siegman, A.E., *Lasers*, University Science Books, Mill Valley, California, 1986.

Smith, D.A., Maeda, M.W., Johnson, J.J., Patel, J.S., Saifi, M.A. and Von Lehman, A., ''Acoustically Tuned Erbium-doped Fiber Ring Laser,'' *Opt. Lett.*, **16**, 6, pp. 387-389, Mar. 1991.

Smith, P.W., ''Mode Selection in Lasers'', *Proc. IEEE*, **60**, 4, pp. 423-440, April 1972.

Snitzer, E., ''Neodymium Glass Laser'', *Proc. 3rd Int. Conf. Solid State Lasers*, pp. 999-1019, Paris, 1963.

Snitzer, E., Po, H., Hakimi, R., Tumminelli, R., and MaCollum, B.C., ''Erbium Fiber Laser Amplifier at 1.55μm with Pump at 1.48μm and Yb Sensitized Er Oscillator'', *Proc. OFC'88*, PD2, 1988.

Stover, H.L. and Steier, W.H., ''Locking of Laser Oscillators by Light Injection'', *Appl. Phys Lett.*, **8**, 91, 1966.

Svelto, O., *Principles of Lasers*, 2nd Ed., Plenum Press, New York, 1982.

Tang, C.L., Statz, H. and deMars, G., ''Regular Spiking and Single-mode Operation of Ruby Laser'', *Appl. Phys. Lett.*, **2**, pp. 222-224, June 1963.

Tkach, R.W. and Chraplyvy, A.R., ''Fibre Brillouin Amplifiers'', *Opt. & Quant. Electron.*, **21**, S105-S112, 1989.

Urquhart, P., ''Review of Rare Earth Doped Fibre Lasers and Amplifiers'', ''*IEE Proc. J*, **135**, 6, pp. 385-407, Dec. 1988.

Whalen, M.S., Wood, T.H., Miller, B.I., Koren, U., Burrus, C.A. and Raybon, G., ''Variation of Frequency Chirp with Wavelength in an InGaAsP/InP Multiple-Quantum-Well (MQW) Waveguide Electroabsorption Modulator'', *IEEE Phot. Tech. Lett.*, **3**, 5, pp. 451-452, May 1991.

Wyatt, R., Cameron, K.H. and Matthews, M.R., ''Tunable Narrow Line External Cavity Lasers for Coherent Optical Systems'', *Br. Telecom Tech. J.*, **3**, 4, pp. 5-11, Oct. 1985.

Wyatt, R., ''High-power Broadly Tunable Erbium-doped Silica Fibre Laser,'' *El. Lett.*, **25**, 22, pp. 1498- 1989.

Wyatt, R., ''Spectroscopy of Rare Earth Doped Fibres'', *Fiber Laser Sources and Amplifiers*, **SPIE 1171**, pp. 54-64, 1989.

Zayhowski, J.J. and Mooradian, A., ''Single-frequency microchip Nd lasers'', *Opt. Lett.*, **14**, pp. 24-26, Jan. 1989.

Chapter Two

Fibre Laser Theory

2.1 INTRODUCTION

Much has been written in recent years on the application of laser theory to fibre lasers and amplifiers. This chapter aims to summarise from published work the important aspects of the theory which are the bases of the operation of fibre lasers and amplifiers, and to point out factors of most relevance when designing and building experimental fibre lasers. The waveguiding nature of optical fibres is important in determining the modal properties of fibre lasers and amplifiers and is discussed in Section 2.2. As this work is concerned with erbium fibre lasers operating in the 1.55μm region, Section 2.3 reviews three-level laser theory and its application to fibre lasers.

2.2 OPTICAL FIBRE WAVEGUIDES

Fibre lasers are glass lasers fabricated in the form of optical fibres, with active ions, for example, rare-earth ions, incorporated in the fibre core [Poole]. Many of the benefits of constructing glass lasers as fibre lasers arise from the waveguiding properties of the optical fibre [Armitage]. Such benefits include high efficiency arising from the good overlap obtainable between the pump mode, signal mode and the rare-earth-ion dopant distribution, inherent compatibility with optical fibres used as transmission and sensing media, and good heat dissipation properties [Reekie] [Urquhart] [Millar]. Important characteristics relevant in the description of fibre lasers arise from optical waveguide theory, and include the pump and signal mode profiles and the number of transverse modes supported by the fibre at a given wavelength.

Single-mode optical fibres are generally modelled as ideal circularly-symmetric step-index fibres in which the refractive index profile n(r) varies with radial distance r from the centre of the fibre as:

$$\begin{aligned} n(r) &= n_{co} \qquad 0 \le r \le a \\ n(r) &= n_{cl} \qquad r > a \end{aligned} \tag{1}$$

where n_{co} and n_{cl} are the core and cladding refractive indices respectively and a is the core radius. For modelling purposes the cladding is assumed to be infinite, i.e., no outer boundary. These parameters, and the free-space wavelength λ of the light passing through the fibre, are used to define the profile height parameter Δ and the waveguide parameter V, defined by Snyder and Love as [Snyder] [Gloge]:

$$\Delta = \frac{n_{co}^2 - n_{cl}^2}{2n_{co}^2}$$
$$V = \frac{2\pi}{\lambda} a (n_{co}^2 - n_{cl}^2)^{\frac{1}{2}} \quad (2)$$

The complete theoretical description of such a waveguide has been well documented [Snyder], however it is useful to summarise the important parameters required to characterise fibre lasers and amplifiers. A scalar wave approximation is used to obtain solutions to the electromagnetic equations of the modes in step-index fibres, this approximation being allowable since $\Delta \ll 1$. The solutions to Maxwell's equations for the fibre structure produce a finite number of modes, which in the weak-guidance approximation, $\Delta \ll 1$, simplify to the LP or linearly polarised modes. The number of guided modes at a given wavelength depends on the value of V.

The single-mode regime for a step-index profile fibre is defined by the condition:

$$0 < V < 2.405 \quad (3)$$

Provided this condition is met only two degenerate orthogonally polarised modes can propagate in a step-index circular core fibre [Jeunhomme]. This condition will normally be met by the signal wavelength and often by the pump wavelength in single mode fibre lasers and amplifiers. Hence using Equation 2.2 the cutoff wavelength λ_c above which the fibre becomes single-mode is:

$$\lambda_c = \frac{2\pi a (n_{co}^2 - n_{cl}^2)^{\frac{1}{2}}}{2.405} \quad (4)$$

As the V number increases the fibre supports more than one mode. When $2.405 \leq$

$V < 3.832$ another set of modes propagate, with more modes being supported as V further increases [Snyder]. The wave fronts of the field are perpendicular to the fibre axis, i.e., they have a plane-wave nature or have constant phase across any axial point at a given time.

The mode field shapes which result from the solutions of Maxwell's equations are given by combinations of Bessel functions [Snyder]. The fields can be conveniently described in cylindrical coordinates (r,ϕ,z) with the z-axis coinciding with the fibre axis of symmetry. The normalised intensity profile $f(r,\phi)$ for the LP_{lm} modes are [Jeunhomme] [Armitage]:

$$f(r,\phi) = \begin{cases} AJ_l^2\left(\frac{ur}{a}\right)\cos^2 l\phi & r<a \\ A\left(\frac{J_l(u)}{K_l(w)}\right)^2 K_l^2\left(\frac{wr}{a}\right)\cos^2 l\phi & r>a \end{cases} \tag{5}$$

where J_l are Bessel functions of order l and K_l are modified Bessel functions of order l, and A is chosen for normalisation so that:

$$\int_{r=0}^{\infty}\int_{\phi=0}^{2\pi} f(r,\phi) r \, dr \, d\phi = 1 \tag{6}$$

A LP mode is one which is linearly polarised and the subscripts l and m of an LP mode refer to the number of azimuthal and radial zeros in the field distribution. The normalised propagation constants, u and w, are solutions of the eigenvalue equation:

$$\frac{uJ_{l+1}(u)}{J_l(u)} = \frac{wK_{l+1}(w)}{K_l(w)} \tag{7}$$

where $u^2 + w^2 = V^2$.

The fundamental LP_{01} mode the shape is similar to a Gaussian, and hence a Gaussian is often used to approximate the field shape for design and application calculations [Marcuse]. The radial intensity $S_{p,s}(r)$ of the pump and signal modes are thus approximated, for $V > 1$, by a characteristic shape [Snyder]:

$$S_{p,s}(r) = \frac{1}{\pi \omega_{p,s}^2} \exp\left(-\frac{r^2}{\omega_{p,s}^2}\right) \tag{8}$$

where $\omega_{p,s}$ is the spot size at the pump and signal wavelengths (1/e intensity). Optical fibres used for fibre lasers and amplifiers are normally designed to be single mode at both the pump and signal wavelengths, and hence this approximation to the radial intensity is sufficient for most calculations. Typically between 30% and 50% of the mode power is carried in the fibre cladding [Gloge] [Jeunhomme]. The local gain and absorption coefficients in a doped fibre will vary with transverse position across a fibre core, according to the pump and signal intensity profiles and the profile of the dopant distribution. Used in conjunction with the radial profile of the rare-earth dopant, an overlap integral can be arranged with the pump mode intensity distribution and absorption cross-section in order to approximate the pump absorption in a doped fibre.

2.3 3-LEVEL FIBRE LASER THEORY

The triply-ionised erbium ion resident in a silica-glass matrix has energy levels as shown in Figure 2.1 for energies up to about 20,000cm^{-1}. Lasing in the 1.55μm region occurs between the $^4I_{13/2}$ metastable level and the $^4I_{15/2}$ ground state with the pump level being either the $^4I_{13/2}$ level or one of the higher levels. For the purposes of the following discussion only three or four levels are of interest, and the energy

level diagram can be replaced by the simplified diagram of Figure 2.2. Three or four levels are of interest, depending on whether the pump wavelength results in excited state absorption (ESA) or excitation of ions from the upper lasing level to a higher level.

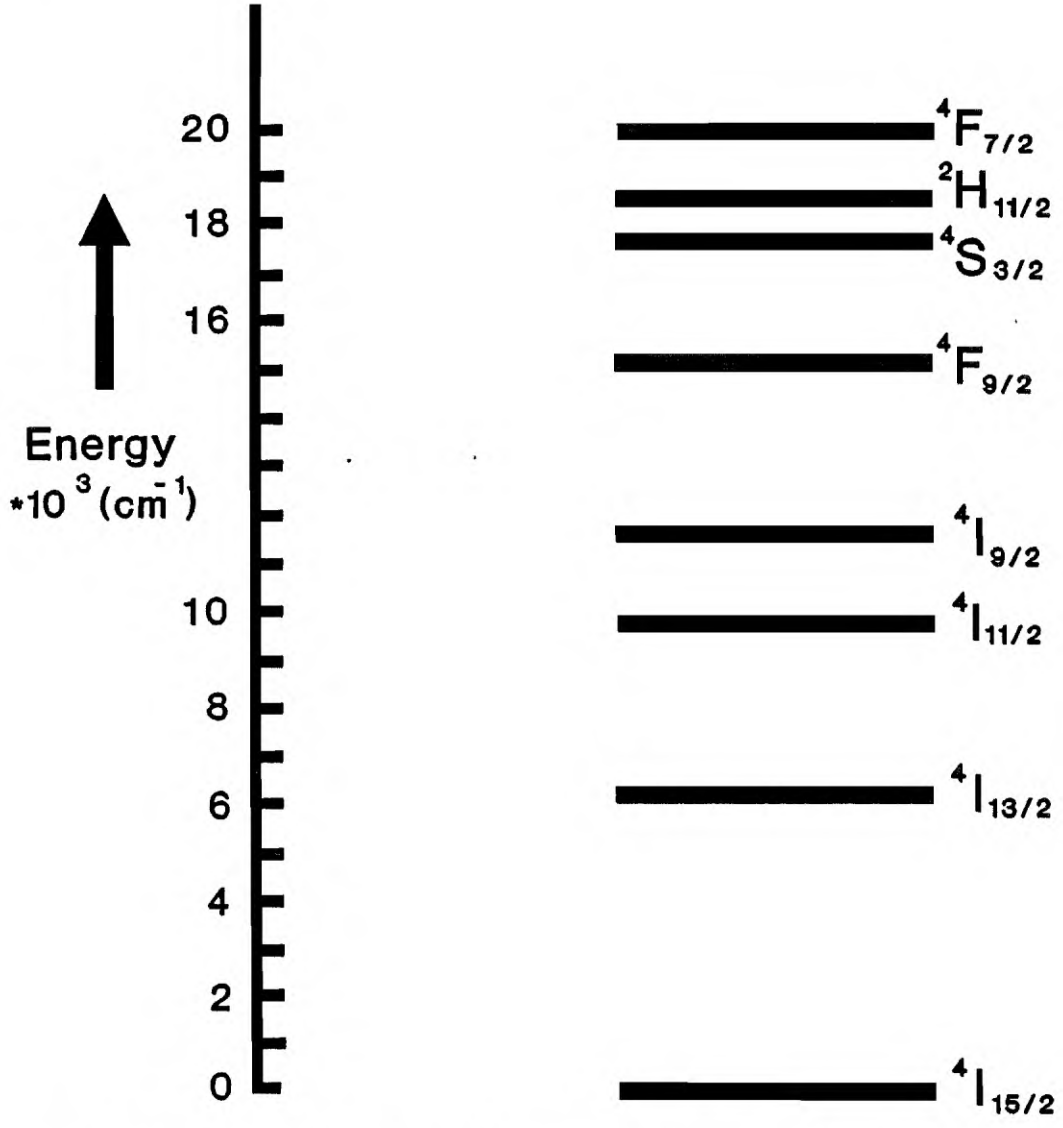

Figure 2.1 Partial erbium-ion energy level diagram. Lasing in the 1.55μm region occurs between the $^4I_{13/2}$ level and the $^4I_{15/2}$ ground state.

Ground state absorption (GSA) occurs from the ground state into the pump band by the absorption of pump photons. From the pump level the ion undergoes rapid

relaxation via phonon interactions with the host glass matrix into the metastable upper lasing level. For some pump wavelengths pump ESA, or absorption which does not originate from the ground state but from an excited state, may occur. Pump ESA is followed by rapid relaxation via multiphonon effects into the upper lasing level. Thus although the ions return to the upper lasing level, pump energy is lost for no increase in the useful inversion. The ratio of signal absorption rate (1→2) to signal emission rate (2→1) is unity for an ideal three level system, however different effective stimulated emission cross sections σ_e and absorption cross sections σ_a occur for Er^{3+} ions in a glass host due to the Stark split manifolds (to be described in Chapter 3), resulting in unequal signal absorption and emission rates.

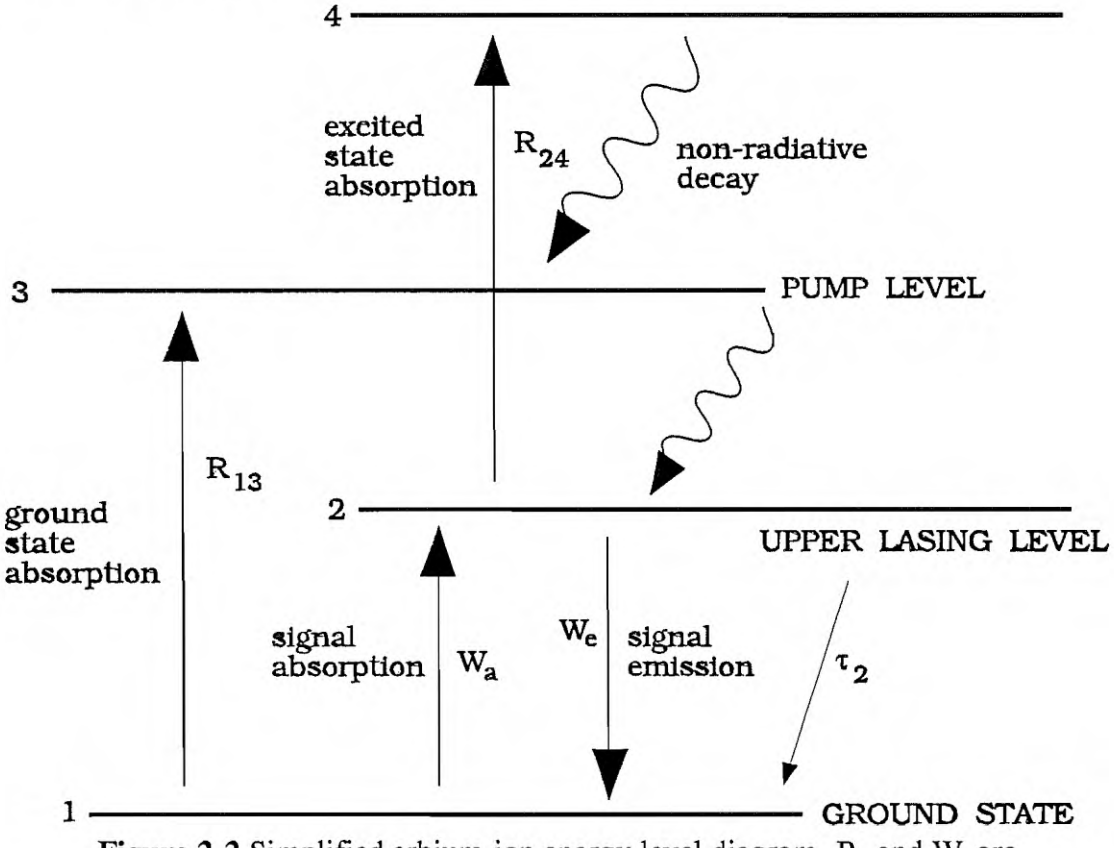

Figure 2.2 Simplified erbium-ion energy level diagram. R_{ij} and W_i are the stimulated absorption and emission transition rates.

Electrons in the Er^{3+} ion are excited or relax from one energy level to another by the

absorption or emission of a photon, or by absorption by the host matrix of one or more phonons. Consider an energy level k containing a ion density N_k. There exists a spontaneous decay rate for a downward transition, γ_k, or a decay time τ_k such that:

$$\left.\frac{dN_k}{dt}\right|_{spont} = -\gamma_k N_k = -\frac{N_k}{\tau_k} \qquad (9)$$

Neglecting ion-ion interactions (see Chapter 3), two components can make up this decay, radiative relaxation (spontaneous emission) and non-radiative relaxation in which energy goes to heating up the surrounding material. In addition to spontaneous transitions between energy levels, if an external light signal is applied to an ion, there is a probability that stimulated emission or absorption may occur. The emitted photon for stimulated transitions 2→1 is in phase with the stimulating photon. This process is the basis of the laser and maser and is possible because photons are bosons obeying Bose-Einstein statistics, in which there is no bar to having more than one particle in a particular state.

The transition rates of the simplified erbium three-level system of Figure 2.2, R_{ij}, W_a, $W_{e,}$, are defined by [Desurvire] [Digonnet 1989]:

$$\begin{aligned} R_{13} &= \frac{\sigma_{GSA} I_p}{h\nu_p} \\ R_{24} &= \frac{\sigma_{ESA} I_p}{h\nu_p} \\ W_a &= \frac{\sigma_a I_s}{h\nu_s} \\ W_e &= \frac{\sigma_e I_s}{h\nu_s} \end{aligned} \qquad (10)$$

where σ_{GSA}, σ_{ESA} are the pump GSA and ESA cross sections respectively, I_p, I_s are the pump and signal photon intensities respectively, υ_p, υ_s are the pump and signal frequencies respectively and h is Planck's constant. The pump and signal mode intensity profiles have forms as given by the Bessel function expressions or Gaussian approximation as described in Section 2.2 [Armitage][Digonnet]. In addition, the dopant ion distribution will have a radial profile which may have radial variation. The pump intensity, signal intensity and dopant ion profiles will thus have general forms $I_p(r,\phi,z)$, $I_s(r,\phi,z)$, $N_d(r)$. As an alternative to considering r,ϕ variations in intensity, a simpler approach is to use an infinite plane-wave approximation which ignores transverse variation of the pump, signal and dopant concentration. In the infinite plane-wave approximation the core size is introduced to normalise the power in the plane wave to the power carried in the core.

The manner in which the ion density in a given energy level varies with time is generally expressed as an atomic rate equation. The rate equation for ions in an energy level k can be written in a general form as:

$$\frac{dN_k(t)}{dt} = \left.\frac{dN_k(t)}{dt}\right|_{stim\ up} + \left.\frac{dN_k(t)}{dt}\right|_{stim\ down} + \left.\frac{dN_k(t)}{dt}\right|_{spont} \qquad (11)$$

and is made up of stimulated absorptions and emissions and spontaneous decay components.

Using the transition rates of the erbium system from Equation 2.10 in the general rate equations for the various levels, and solving for steady state conditions, the population densities of the energy levels become:

$$N_1 = \frac{W_e + \frac{1}{\tau_2}}{W_a + W_e + \frac{1}{\tau_2} + R_{13}} N_0$$

$$N_2 = \frac{W_a + R_{13}}{W_a + W_e + \frac{1}{\tau_2} + R_{13}} N_0 \qquad \textbf{(12)}$$

with N_3, N_4 negligible and the total ion population density, N_0, hence given by $N_0 = N_1 + N_2$, and where levels 1,2,3,4 are the ground state, upper lasing level, pump level and excited state absorption levels respectively.

As the absorption and emission cross-sections for transitions between the upper lasing level and the ground state are very similar, to achieve gain a pump rate R_{13} is required such that the situation $N_2 > N_1$ or population inversion is achieved. This is conveniently achieved for reasonable pump powers over long lengths in the fibre form because of the high pump intensity which results from the small core diameter.

For a longitudinally-pumped fibre laser or amplifier, calculation of the unsaturated single-pass gain requires knowledge of the pump power evolution along the fibre. The evolution of pump power in these cases will determine the population inversion as a function of the fibre length and hence determine the evolution of signal power. Hence in the longitudinally-pumped case the ion population densities must be considered with axial variation, $N_k(z)$. The axial variation of the pump power, $P_p(z)$, assuming the relaxation time from the pump and ESA levels is rapid compared to the relaxation from the metastable level, can be written as [Morkel]:

$$\frac{dP_p(z)}{dz} = -P_p(z)\eta_p \left(\sigma_{GSA} N_1(z) + \sigma_{ESA} N_2(z)\right) \qquad \textbf{(13)}$$

where η_p is the pump overlap fraction, arising from the overlap of the pump beam

with the dopant distribution, which can be calculated from the Gaussian approximation [Morkel]. The local axial gain, $\gamma(z)$, can be written:

$$\gamma(z) = \eta_s\left(\sigma_e N_2(z) - \sigma_a N_1(z)\right) \tag{14}$$

where η_s is the overlap fraction between the signal mode and the population inversion (from the Gaussian approximation).

The signal power axial variation can be expressed in terms of the local gain (ignoring background losses):

$$\frac{dP_s^{\pm}(z)}{dz} = \pm P_s^{\pm}(z)\gamma(z) \tag{15}$$

where $P_s^{+}(z)$, $P_s^{-}(z)$ are the co- and counter-propagating signals respectively. Similarly the axial dependence of amplified spontaneous emission power can be determined [Morkel]. Numerical analysis is required to solve the coupled equations with axial dependence, however such calculations are not required in this work. Rather the purpose of this description is to define the parameters of the end-pumped three-level fibre laser system, in order to give some insight into the important parameters required when designing experimental erbium fibre lasers. A full numerical analysis of pump and signal evolution has been considered by several authors [Digonnet 1990], [Morkel], [Matsas]. While considering erbium amplifiers from theoretical modelling is important to optimise performance, in experiments to date the absolute gain and spectral properties are still generally evaluated experimentally [Suzuki], [Nakazawa], [Simpson], while modelling is used to understand trends as device parameters are varied.

When considering erbium fibre lasers the gain in a given length of doped fibre is of prime importance and would normally be measured in a laser experiment if required.

An attractive approach to modelling the gain medium of an erbium fibre laser is the lumped element method developed by P.R. Morkel in which the distributed amplifier is considered as a lumped element [Morkel]. The lumped element approach to modelling amplifier gain requires approximations to be made regarding the effective core area and is only valid when no ESA exists, and is a good approximation in the case of 980nm pumping of erbium in which ESA is negligible. The approach is possible because the single pass gain can be expressed in terms of the integral of the population inversion along the fibre length. In this way only the summation of the gain, not the actual distribution is important. The approach is attractive for fibre lasers and amplifiers with their well-defined waveguide geometry, since the integral of the population inversion is proportional to the absorbed pump power, and hence it becomes possible to relate gain to absorbed pump power [Morkel]. The approximation becomes exact when there is negligible signal and pump variation over the doped region, i.e., when the dopant is confined to the centre of the core.

Following this approach the single pass gain in nepers in terms of absorbed pump power for a fibre length l is:

$$\gamma(l) = \sigma_{21}\left((1+\alpha)\frac{\eta\tau_{21}P_{abs}}{h\nu_p A_{eff}} - \alpha N_0 l\right) \qquad (16)$$

where $\alpha=\sigma_{12}/\sigma_{21}$, η is the pump quantum efficiency, P_{abs} is the absorbed pump power and A_{eff} is the effective core area [Morkel]. The effective area is calculated from mode overlaps of the Gaussian approximation, and is given by:

$$A_{eff} = \frac{\pi\left(\omega_p^2+\omega_s^2\right)\left(1-e^{-d^2/\omega_p^2}\right)}{1-e^{-d^2\left(1/\omega_s^2+1/\omega_p^2\right)}} \qquad (17)$$

where $\omega_{p,s}$ are the spot sizes at the pump and signal wavelengths and d is the radius of the dopant profile. The lumped element formalism arises from energy conserva-

tion, by considering that under small signal equilibrium conditions the rate of absorption of pump photons in an elemental length of fibre, multiplied by the pump quantum efficiency, is equivalent to the natural decay rate from the population inversion in the length. Integrating over the length of the amplifier the integral of the population inversion can be determined in terms of the pump power, which can be used to calculate the single-pass gain of Equation 2.16. The umpumped erbium transition is absorbing at the lasing wavelength, and significant depopulation of the ground state must be achieved before there is any gain. A transparency condition exists where there is no net gain or loss, when the pump rate out of the ground state is approximately equal to the fluorescence rate of the lasing transition. Hence there is an optimum length, for a given amount of pump power, for maximum gain from an amplifier or maximum output from an oscillator.

By considering the loss in a laser resonator, the laser threshold power can be expressed as [Morkel]:

$$P_{th} = \frac{h\nu_p A_{eff}((L+T) + 2\alpha\sigma_{21}N_0 l)}{2(1+\alpha)\eta\tau_{21}\sigma_{21}} \qquad (18)$$

where L is the resonator intrinsic loss and T is the output coupling. It is because the core area is small, allowing high pump intensities to be achieved, that low threshold operation is possible even for three-level fibre lasers.

2.4 SUMMARY

This chapter has summarised some of the important aspects of optical waveguide theory and the theory of three-level lasers used to model erbium-doped fibre lasers and amplifiers. Section 2.2 discussed the theory of optical fibre waveguides.

Important parameters used to design fibre lasers arising from this theory are the single-mode regime for determining cutoff wavelengths for the pump and signal modes and the shape of the guided mode, which is used in conjunction with the dopant profile to determine gain.

Section 2.3 briefly outlined the theory of three-level lasers. Significant properties to come out of this were the transition rates and rate equations, the conditions for lasing threshold, axial dependence of gain, and the gain available from a length of erbium-doped fibre.

2.5 REFERENCES

Armitage, J.R., ''Three-level Fiber Laser Amplifier: A Theoretical Model'', *Appl. Opt.*, **27**, 23, pp. 4831-4836, Dec. 1988.

Desurvire, E., Simpson, J.R and Becker, P.C., ''High-gain Erbium-doped Travelling-wave Fiber Amplifier'', *Opt. Lett.*, **12**, 11, pp. 888-890, 1987.

Digonnet, M.J.F. and Gaeta, C.J., ''Theoretical Analysis of Optical Fiber Laser Amplifiers and Oscillators'', *Appl. Opt.*, **24**, 3, pp. 333-342, Feb. 1985.

Digonnet, M.J.F., ''Theory of Operation of Three- and Four-level Fiber Amplifiers and Sources'', SPIE **1171** Fiber Laser Sources and Amplifiers, pp. 8-26, 1989.

Digonnet, M.J.F., ''Closed-Form Expressions for the Gain in Three- and Four-Level Laser Fibers'', *IEEE J. Quant. El.*, **26**, 10, pp. 1788-1796, 1990.

Gloge, D., ''Weakly Guiding Fibers'', *Appl. Opt.*, **10**, pp. 2252-2258, Oct. 1971.

Jeunhomme, L.B., *Single-Mode Fiber Optics, Principles and Applications*, Marcel Dekker, Inc., New York, 1983.

Marcuse, D., ''Gaussian Approximation of the Fundamental Modes of Graded Index Fibres'', *J. Opt. Soc. Am.*, **68**, 1, pp. 103-109, 1978.

Matsas, V., *Mode Locking of Fibre Lasers*, Mini-thesis, University of Southampton, April 1991.

Millar, C.A., Whitley, T.J. and Flemming, S.C., ''Thermal Properties of an Erbium-Doped Fibre Amplifier'', *IEE Proc. J*, **137**, 3, pp. 155-162, June 1990.

Morkel, P.R., *Active Neodymium and Erbium Doped Fibre Devices*, Ph.D. Thesis, University of Southampton, August 1990.

Nakazawa, M., Kimura, Y. and Suzuki, K., ''Efficient Er^{3+}-doped Optical Fiber

Amplifier Pumped by a 1.48μm InGaAsP Laser Diode'', *Appl. Phys. Lett.*, **54**, 4, pp. 295-297, Jan. 1989.

Poole, S.B., Payne, D.N., Mears, R.J., Fermann, M.E. and Laming, R.I., ''Fabrication and Characterisation of Low-Loss Optical Fibres Containing Rare-Earth Ions'', *J. Lightwave Tech.*, **LT-4**, 7, pp. 870-876, July 1986.

Simpson, J.R., Mollenauer, L.F., Kranz, K.S., Lemaire, P.J., Olsson, N.A., Shang, H.T. and Becker, P.C., ''A Distributed Erbium Doped Fiber Amplifier'', *Proc. OFC'90.*, PD19, Jan. 1990.

Shimoda, K., ''Introduction to Laser Physics'', 2nd Ed., Springer Series in Optical Sciences, Springer-Verlag, Berlin, 1986.

Snyder, A.W., and Love, J.D., *Optical Waveguide Theory*, Chapman and Hall, London, 1983.

Suzuki, K., Kimura, Y. and Nakazawa, M., ''High Gain Er^{3+}-doped Fibre Amplifier Pumped by 820nm GaAlAs Laser Diodes'', *El.Lett.*, **26**, 13, pp. 948-949, June 1990.

Urquhart, P., ''Review of Rare Earth Doped Fibre Lasers and Amplifiers'', *IEE Proc. J*, **135**, 6, pp. 385-407, Dec. 1988.

Chapter Three

Fibre Laser Spectral Characteristics

3.1 INTRODUCTION

Fibre laser resonators can be formed with a variety of cavity configurations. The simplest cavity structure is a section of rare-earth-doped fibre onto which dielectric mirrors are incorporated on both ends. The doped fibre is then longitudinally pumped through one of the dielectric mirrors by a light source with a wavelength corresponding to one of the absorption bands of the rare-earth ion. With sufficient pumping, lasing may occur in one of the gain bands. Depending on cavity and pumping conditions, optical linewidths for such fibre lasers may be typically in the range 1-15nm [Mears][Kimura]. Such broad spectra can occur in a laser with a primarily

homogeneously-broadened transition, such as alumino-silicate erbium-doped fibre operating at room temperature [Guy][Tachibana][Zyskind], because of the broad gain bandwidth. The effect of spatial holeburning on the gain medium allows much of the gain bandwidth to be utilised [Siegman]. Spatial holeburning is induced by the standing-wave pattern in the laser cavity and can reduce the gain competition between axial modes. This effect, combined with the width of the gain-bandwidth in doped fibre, allows lasers without wavelength-selective resonators to oscillate over spectral widths equivalent to hundreds or thousands of passive cavity modes. The spectral characteristics of a fibre laser and the number of modes oscillating in a given laser cavity are determined by the combined effects of spatial holeburning, the shape and width of the gain spectrum of the rare-earth ion and the passive cavity mode structure.

This chapter examines the factors which determine spectral characteristics of erbium fibre lasers. An understanding of these factors will allow fibre laser cavities to be designed to produce output which have spectral widths smaller than those of the simple fibre laser. Some of the pertinent factors, including the shape and width of the gain spectrum, are determined primarily by the glass structure and modification of these parameters are beyond the scope of this work, however other properties such as the spacing of the modes and the effects of spatial holeburning can be modified by suitable resonator design. Chapter 4 dealing with standing-wave fibre resonators for narrow-linewidth operation and Chapter 5 dealing with single-frequency travelling-wave resonators will demonstrate how the spectral characteristics of erbium fibre lasers can be altered by varying the resonator properties, leading eventually to single-longitudinal-mode operation.

This chapter firstly discusses, in Section 3.2, the spectroscopy of Er^{3+} in silica glass, followed by a description of passive cavity modes in Section 3.3. Section 3.4 describes spatial holeburning and some of its possible effects on laser spectra. Section 3.5 reviews the statistics exhibited by monochromatic laser light once single-longitudinal-mode operation is achieved, and discusses the ultimate quantum limits

on laser linewidth.

3.2 ERBIUM IONS IN GLASS HOSTS

The energy levels of the Er^{3+} ion are shown in Figure 3.1 for energy levels up to 20,000cm^{-1}. The energy levels are described by the LSJ notation, with the superscript L referring to the electron spin, S referring to the orbital angular momentum and the subscript J giving the total angular momentum of the electron. When used in a fibre laser or amplifier the ion is present in a glass host, normally silica glass. Significant changes in the spectral lineshape and broadening mechanisms are observed between fibres with different glass compositions [Dybdal][Guy][Tachibana][Zemon]. At room temperature both homogeneous and inhomogeneous broadening mechanisms contribute to the lineshape. Homogeneous broadening mechanisms act on all ions in the same manner, whereas inhomogeneous mechanisms affect different ions to different extents. The Er^{3+} ion is sensitive to changes in the surroundings determined by the glass host composition. As a result erbium-doped fibres exhibit behaviour characteristic of homogeneous or inhomogeneous systems depending on the type of glass matrix [Guy].

Spectroscopic parameters which are of importance in the design of erbium fibre lasers and amplifiers for experimental purposes have been well characterised [Barnes 1991], [Ainslie], [Briançon], [Dybdal], [Wyatt], [Zemon]. These parameters include optical absorption and emission strengths, transition rates and absorption and emission widths. These parameters determine important properties such as available gain, pump rates required for threshold, and so on.

The spontaneous radiative transition rate of an electron within the rare-earth ion from an excited state 2 to ground state 1, $A_r(2,1)$, can be determined from a measured

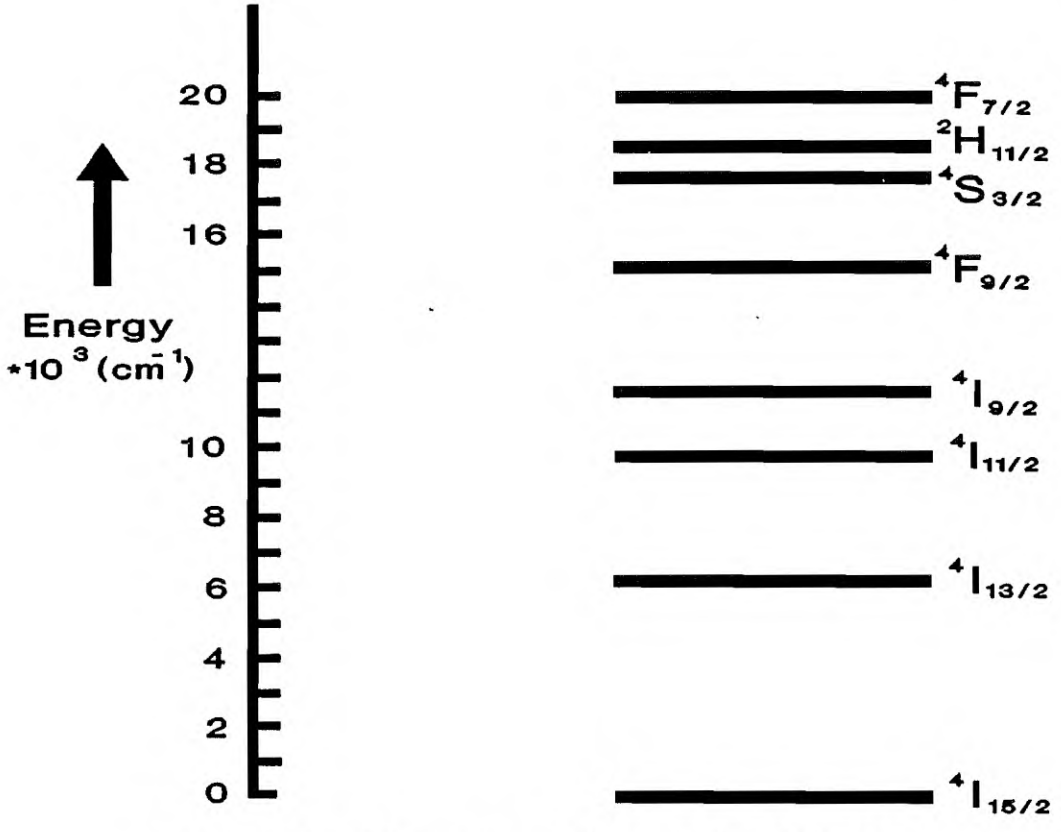

Figure 3.1 Partial energy level diagram of the Er^{3+} ion.

absorption cross-section spectrum by:

$$A_r(2,1) = \frac{1}{\tau_r} = \frac{8\pi n^2}{\lambda^2} \frac{2J_1+1}{2J_2+1} \int \sigma_a(\nu) d\nu \qquad (1)$$

where J_i is the angular momentum quantum number, τ_r is the radiative lifetime, n is the refractive index of the glass host and the absorption cross section, σ_a, is determined from the attenuation of light intensity I(z) in a thickness z′:

$$\sigma_a = \frac{\ln\left(\frac{I(0)}{I(z')}\right)}{\rho z'} \qquad (2)$$

where ρ is the Er^{3+} concentration [Dybdal].

The emission cross section is given by:

$$\sigma_e(\nu) = \frac{\lambda^2}{8\pi n^2} A_r(2,1) g(\nu) \qquad (3)$$

where the normalised line shape function $g(\upsilon)$ is obtained from the fluorescence intensity $I(\upsilon)$ at frequency ν in units of photon rate per unit frequency interval to yield:

$$g(\nu) = \frac{I(\nu)}{\int I(\nu) d\nu} \qquad (4)$$

These expressions are only approximations for the case of an ideal host. Measured values may be different to the approximations for the case of Er^{3+} in silica because the Stark splitting of the energy levels is comparable or longer than the thermal spread kT. If the Stark splitting is taken into account, requiring a correction of 15-20% [Dybdal], these expressions yield good approximations, since in silica with phonon energy $\approx 1100 cm^{-1}$ other relaxation processes do not compete with radiative decay from the $^4I_{13/2}$ level to the $^4I_{15/2}$ ground state. Detailed measurements of absorption and emission cross-sections for various silica hosts show that emission cross-sections are in the range $4.4\text{-}6.7\times10^{-25} m^2$ while absorption cross-sections are in the range $4.7\text{-}7.9\times10^{-25} m^2$ [Barnes 1991]. A typical absorption spectrum of an Er^{3+}-doped silica fibre is shown in Figure 3.2 for visible and near infra-red

wavelengths.

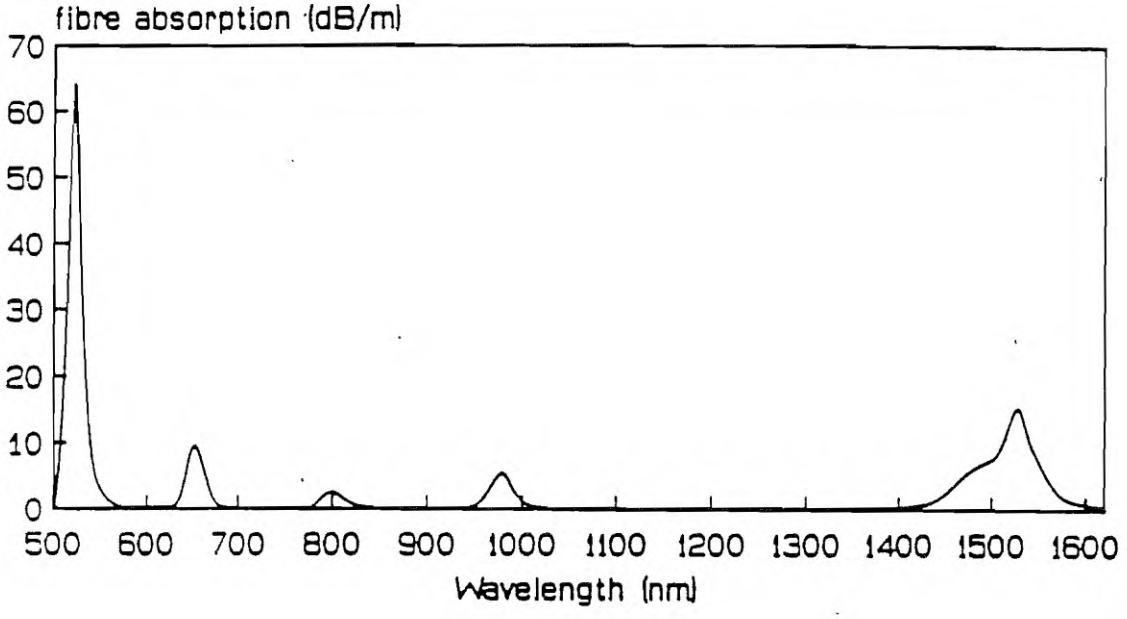

Figure 3.2 Absorption spectrum in the visible and near infra-red wavelengths for an Er^{3+}-doped alumino-silica fibre. (After [Morkel]).

Non-radiative decay can occur via interactions between the excited ions and the glass lattice through multiphonon emissions, and is inversely proportional to the energy gap between two levels [Miniscalco]. Glasses with high phonon energies require fewer phonons to bridge the gap. The lifetime will generally be temperature dependent if the gap is less than ten times the effective phonon frequency and completely quenched if it is less than four times [Shinn]. Measurements of the fluorescence lifetime of the $^4I_{13/2}$ level in silica glass typically result in values $\sim$10ms [Dybdal], [Wyatt]. Low concentrations, $<$0.1wt%, show smooth exponential decays however higher concentrations exhibit decays with more than one component [Wyatt]. Several effects are believed to occur leading to non-exponential decays for high Er^{3+} concentrations.

High concentrations of erbium ions may be required for narrow linewidth operation to allow short fibre lengths to be used, as will be discussed in Chapter 4. Fibres with concentration >2wt% Er^{3+} can show strongly non-exponential decays for high input powers (~ 100mW) while exhibiting nearly exponential decays for input powers ~ 1mW. This effect has been attributed to cooperative upconversion, illustrated schematically in Figure 3.3. In this upconversion process neighbouring ions in the $^4I_{13/2}$ level interact, the resulting energy transfer leaving one ion excited to the $^4I_{9/2}$ level and the other returning to the ground state. This effect is dependent both on the Er^{3+} concentration and the level of excitation. The process requires two interacting ions and will hence not be evident at low pumping levels [Miniscalco]. High concentrations of Er^{3+} can also result in clustering of the dopant, yielding an extremely rapid decay rate in the clustered regions [Ainslie 1989]. The degree of clustering is dependent on the composition of the host, more erbium ions being able to be incorporated in an alumina co-doped host than a germania co-doped host before the onset of clustering. Hence to avoid upconversion problems erbium concentrations must be kept low, <0.1wt%. Short erbium-doped fibre lasers requiring high erbium concentrations may as a result be less efficient than long lasers with low erbium concentrations [Laming].

The width of the absorption and emission bands are established by the splitting of the energy levels by the host field into Stark components and the homogeneous widths of the individual components. The individual Stark levels have been measured for various glass matrix types by fluorescence line narrowing, a technique in which a laser line, narrow with respect to the absorption band, is used to excite a subset of optically active sites [Guy][Zemon]. The $^4I_{15/2}$ ground state is split into 8 Stark doublets by the host field while the $^4I_{13/2}$ level is split into 7 Stark levels. The separation of adjacent Stark levels is 20-80cm^{-1} (4-15nm) with total Stark splitting 335-400cm^{-1} (80-90nm). The Stark energies vary from 0-60cm^{-1} (10nm) among Er^{3+} sites, indicating that site-to-site variations are of the same order as the Stark splitting. Measurements of homogeneous and inhomogeneous linewidths indicate that for

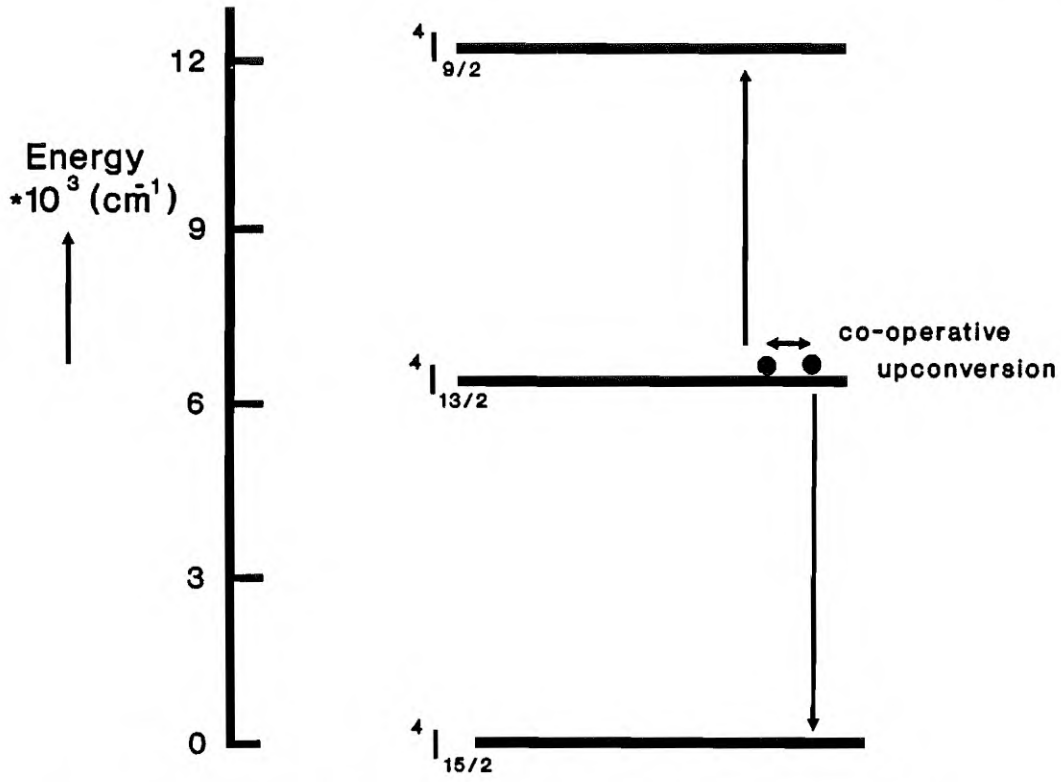

Figure 3.3 Co-operative upconversion process. Two ions in the same energy level interact to excite one ion and de-excite the other.

alumino-silicate glass fibres the homogeneous linewidth is 11.5nm and the inhomogeneous linewidth is 12.5nm [Desurvire]. For germano-silicate glass fibres the homogeneous width is 3.2nm and the inhomogeneous width is 6.4nm [Guy]. The amount of spectral overlap between sites depends on the relative magnitude of the inhomogeneous and homogeneous widths and mixed homogeneous and inhomogeneous behaviour is expected. In germano-silicate fibres the inhomogeneous component is dominant and inhomogeneous saturation behaviour is observed [Laming 1989a]. In alumino-silicate fibres the homogeneous and inhomogeneous components are of the same order and strong spectral overlap is expected between emission originating from different sites, with homogeneous broadening dominating. In alumino-silicate fibres homogeneous broadening should be a good approximation for room temperature luminescence spectra [Tachibana][Zyskind].

The splitting of the energy levels by the glass host also means that spectral variation of gain occurs depending on the degree of inversion [Ainslie 1990], [Kimura]. As a consequence the fibre length and the pumping wavelength can determine the shapes of the absorption and emission spectra and the peak lasing wavelength [Barnes]. If, for example, the fibre is too long for a given level of pump power an unbleached section of fibre remains at the output end which preferentially absorbs wavelengths from the short wavelength part of the fluorescence spectrum.

Erbium-doped fibre lasers and amplifiers have been demonstrated with various pump lasers corresponding to the absorption bands shown in Figure 3.2. Early Er^{3+}-doped devices were pumped at 514.5nm from an argon-ion laser [Mears]. Other pump bands to have been demonstrated are 807nm [Millar], 980nm [Laming 1989] and 1.48μm [Snitzer]. For telecommunications applications prime considerations for pump lasers are lifetime, reliability and efficiency, and for these reason diode laser pumping is attractive. Low-cost AlGaAs diode lasers are easily available for the 800nm band, but a drawback of this pump band is considerable excited state absorption in much of this pump band which limits performance. However, by appropriate fibre design and the use of a large numerical aperture, good results can be obtained [Horiguchi]. With high-power laser diodes being available at both 980nm and 1480nm the most attractive wavelength for low-noise amplification at this stage appears to be the 980nm band. Reasons for its preference are its freedom from ESA (like 1.48μm pumping) and the noise figure advantage over 1.48μm pumping when used as an amplifier for telecommunications applications, the noise figure advantage arising because higher inversion can be achieved for 980nm pumping [Morkel 1990a]. Pumping in-band, the pump wavelength is a compromise between short wavelengths for low-noise amplification and long wavelengths for high pump conversion efficiency [Giles]. An alternative approach to exciting the $^4I_{13/2}$ level is to co-dope the fibre with Yb^{3+} allowing the fibre to be diode pumped or pumped with a mini-YAG into the broad absorption band of the triply-excited Yb ion, with the energy then transferred to the erbium ion [Barnes 1989].

3.3 PASSIVE CAVITY MODES

A fibre laser cavity provides to certain wavelengths of electromagnetic radiation a resonance condition such that after each round-trip of the cavity the fields add in phase. The resonance conditions determine the discrete mode frequencies of the laser spectrum within the gain bandwidth. The conditions for phase matching which give rise to the cavity modes can be seen from the steady-state conditions. For a simple Fabry-Perot cavity as illustrated in Figure 3.4, which is comprised of two mirrors with a gain medium between the mirrors, the steady-state conditions for phase-matching on a round-trip require that the two signals E_1, E_2 satisfy the equality:

$$E_2 = r_1 r_2 e^{j2aL_a n} e^{-j\frac{2\omega Ln}{c}} E_1 \qquad (5)$$

where a is the gain coefficient, r_1, r_2 are the mirror reflectivities, L is the cavity length, L_a is the length of the gain medium and n is the cavity effective phase refractive index. In this simple model the index is assumed constant throughout the resonator.

The phase term leads to the phase matching condition:

$$e^{-j\frac{2\omega Ln}{c}} = e^{-jk2\pi} \qquad k \ \ integer \qquad (6)$$

meaning that frequency solutions take the form of discrete frequencies, the passive cavity mode frequencies given by:

$$\omega = k \times 2\pi \times \frac{c}{2nL} \qquad k \ \ integer \qquad (7)$$

where the quantity c/2nL is known as the cavity free spectral range.

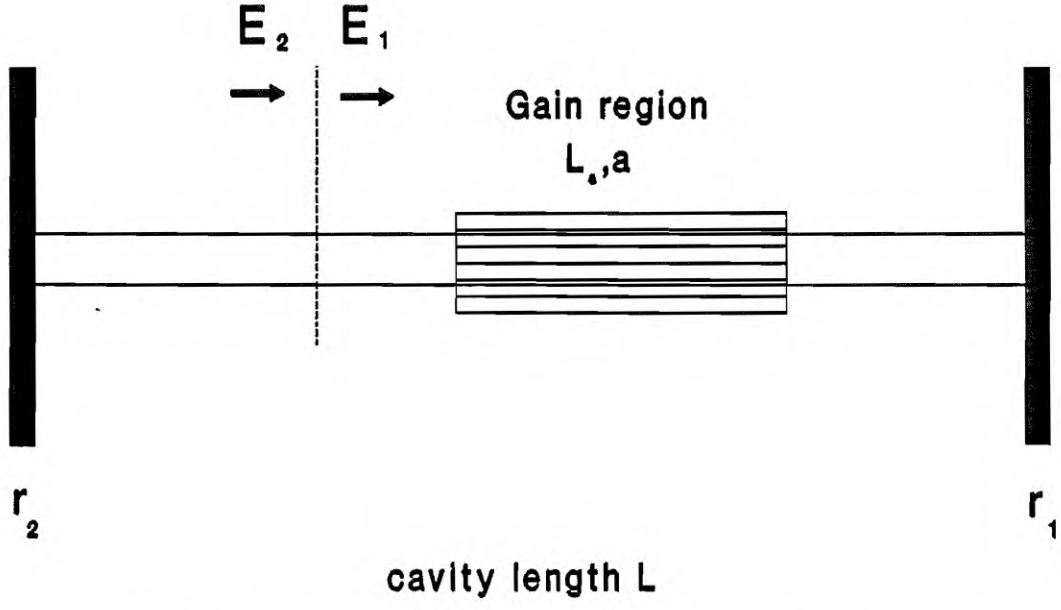

Figure 3.4 Resonator model of Fabry-Perot laser cavity. $E_1=E_2$ for phase-matching.

In the case of a ring resonator, illustrated schematically in Figure 3.5, phase-matching requires that E_1, E_2 satisfy the equation:

$$E_2 = l\, e^{jaL_a n}\, e^{-j\frac{\omega L n}{c}}\, E_1 \qquad (8)$$

where l represents the loss associated with the round-trip pass. The resonator is assumed to have the same refractive index throughout the ring. Again taking the phase term the following phase-matching term becomes:

$$e^{-j\frac{\omega L n}{c}} = e^{-jk2\pi} \qquad k \ \ integer \qquad (9)$$

This time the discrete frequency solutions take the form:

$$\omega = k \times 2\pi \times \frac{c}{nL} \qquad k \ \ integer \tag{10}$$

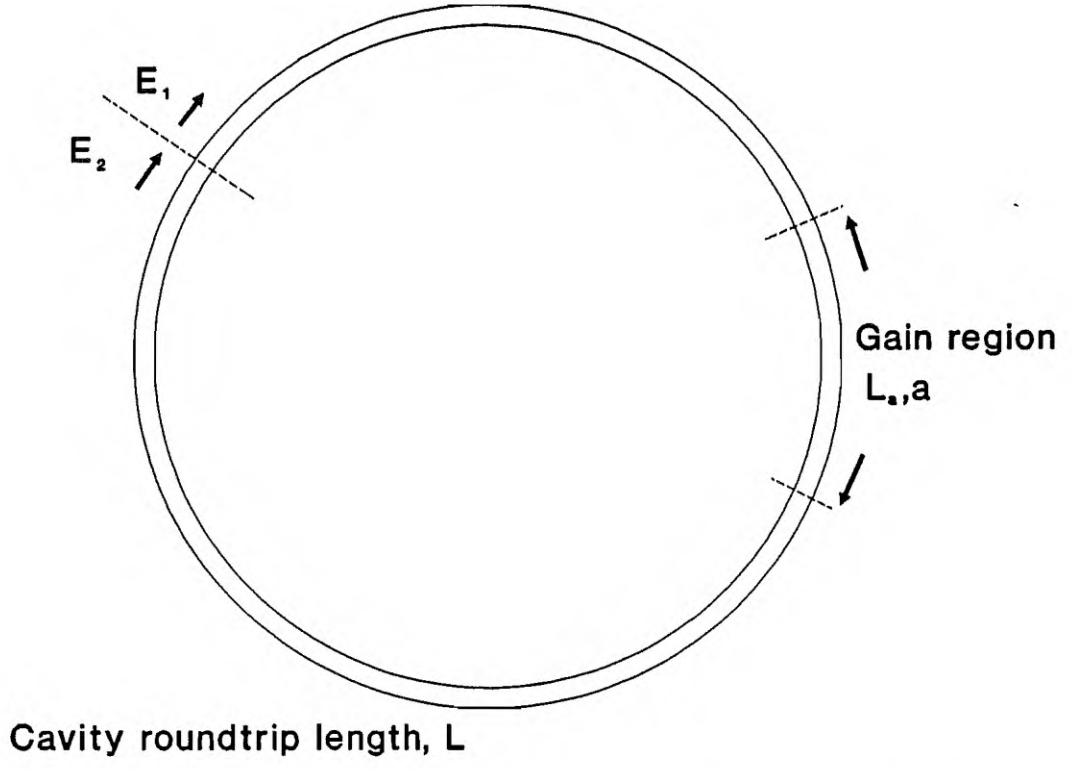

Figure 3.5 Model of ring laser resonator. For phase-matching $E_1 = E_2$.

The cavity modes determine the discrete frequencies within the lasing medium gain bandwidth at which lasing is possible. For this simple model the refractive index was assumed constant. The index in a real resonator may be different if different materials are comprising different sections of the resonator, and an average effective index for the cavity round-trip will result. In addition the index may vary in a fibre laser resonator with absorption, intensity, and so on. Clearly to reduce the number of modes oscillating in a standing-wave cavity the resonator length needs to be minimised. For erbium fibre lasers there are other factors, such as concentration quenching described in Section 3.2, which limit how short the laser cavity can be fashioned for efficient operation. There are however several mechanisms which can

reduce the number of cavity modes oscillating in a resonator of given length, including the use of coupled cavity resonators.

Multiple-mirror cavities or interferometric cavities offer a means of determining the spacing of cavity modes from several cavity properties and not just simple length considerations. When using these techniques, several linear or ring cavities are interconnected, with the phase matching conditions for resonance having to satisfy all coupled cavities simultaneously. These techniques generally result in increased cavity mode spacing, and are thus often considered for linewidth control applications [Smith]. An example of coupled-cavity operation of an erbium-doped fibre laser is discussed in Chapter 4.

3.4 SPATIAL HOLEBURNING

The number of modes making up a laser spectrum can thus be seen to be determined by several factors, including the gain bandwidth and the spacing of the passive cavity modes. However the most important phenomenon which will lead to the onset of multi-mode oscillation is the effect of spatial holeburning on the gain medium [Siegman]. The spatial distribution of the population inversion determines the gain of different cavity modes and, therefore, which mode or modes will lase [Zayhowski].

When a gain medium is pumped within a laser cavity, the cavity mode with the highest inversion and which therefore experiences most gain on a round-trip of the resonator will reach lasing threshold first. The presence of wavelength-selective elements in the cavity will influence which mode experiences most net gain. In addition, for a longitudinally-pumped three-level laser such as an Er^{3+}-doped fibre laser, the gain spectrum is strongly influenced by the length of the gain medium and the level of pump power. Once one mode is lasing and the pump rate is further

increased, another mode may or may not oscillate, depending primarily on the linewidth broadening mechanisms in the gain medium and on the presence or absence of spatial holeburning.

Under steady state conditions and in a gain medium which is ideally homogeneously broadened only the first mode to reach threshold should oscillate. Every ion in this ideal medium has exactly the same lineshape, thus as the material is pumped and the population inversion in a transition increases, the magnitude of the gain increases without changing the line-shape until one mode reaches threshold and begins to lase. Once this mode is lasing the gain profile is clamped in magnitude with only one mode above threshold. As the medium is pumped harder the gain profile cannot move higher, or the situation would arise in which gain exceeds the cavity losses for the lasing mode and the mode would continue to grow in power. Thus in this ideal situation only one mode will oscillate. Additional pumping will increase the power in the mode but will not allow more modes to oscillate.

In an inhomogeneously broadened transition by contrast many modes can oscillate simultaneously. Each ion in the gain medium can have a slightly different gain profile, and when one mode reaches threshold it saturates the gain medium only for that group of atoms resonant at the frequency of that mode. It saturates the gain profile at that frequency to the point at which gain equals loss, while at other frequencies gain can still increase as the medium is pumped. Thus depending on the width of the gain curve and the spacing of the passive cavity modes, many modes can simultaneously oscillate, given sufficient pump power. This behaviour is described as spectral holeburning.

Regardless of the broadening mechanism, the most dominant effect leading to multi-mode oscillation is spatial holeburning in the gain medium. Spatial holeburning can have several forms [Siegman] but the aspect of interest here arises due to two waves travelling in opposite directions giving rise to standing-wave pattern in the optical

intensity. Each laser mode in a standing-wave resonator sets up a well-defined standing-wave pattern within the gain medium, with peaks and nulls in the optical intensity spaced by $\lambda/2n$, where n is the effective index of the resonator. The population inversion will have a corresponding distribution and be periodically saturated with the same period, leading to the possibility of other modes being able to fit into the nulls left by the first mode to receive sufficient gain the achieve threshold.

The situation can be analysed by considering a low-loss cavity which allows a standing wave to be formed by the oppositely travelling waves $I_1(z,t)$, $I_2(z,t)$ (linearly polarised with the same polarisation) with propagation constants $\pm\beta$, such that a standing wave is formed in the optical intensity I(z):

$$I(z)=I_1(z)+I_2(z)+2\sqrt{I_1 I_2}\cos(2\beta z) \tag{11}$$

Only the axial component of the intensity is considered, and thus a plane-wave approximation for the mode profile is taken. In a homogeneously saturable gain medium the population inversion, $\Delta N(z)$, will be saturated according to the spatial distribution of the optical intensity and have a form given by [Siegman][Zayhowski]:

$$\begin{aligned}\Delta N(z) &= \frac{\Delta N_0}{1+\frac{I(z)}{I_{sat}}} \\ &= \frac{\Delta N_0}{1+\frac{I_1(z)+I_2(z)+2\sqrt{I_1 I_2}\cos(2\beta z)}{I_{sat}}}\end{aligned} \tag{12}$$

where ΔN_0 is the maximum population inversion and I_{sat} is the saturation intensity of the gain medium. The saturation intensity is that which reduces the gain coefficient to half its small signal value, and is defined by:

$$I_{sat} = \frac{h\omega}{2\pi\sigma_{21}\tau_{21}} \tag{13}$$

The form of the optical intensity of a mode and the resulting saturation of the population inversion are illustrated in Figure 3.6. The periodic nulls and peaks in the population inversion are known as spatial holeburning.

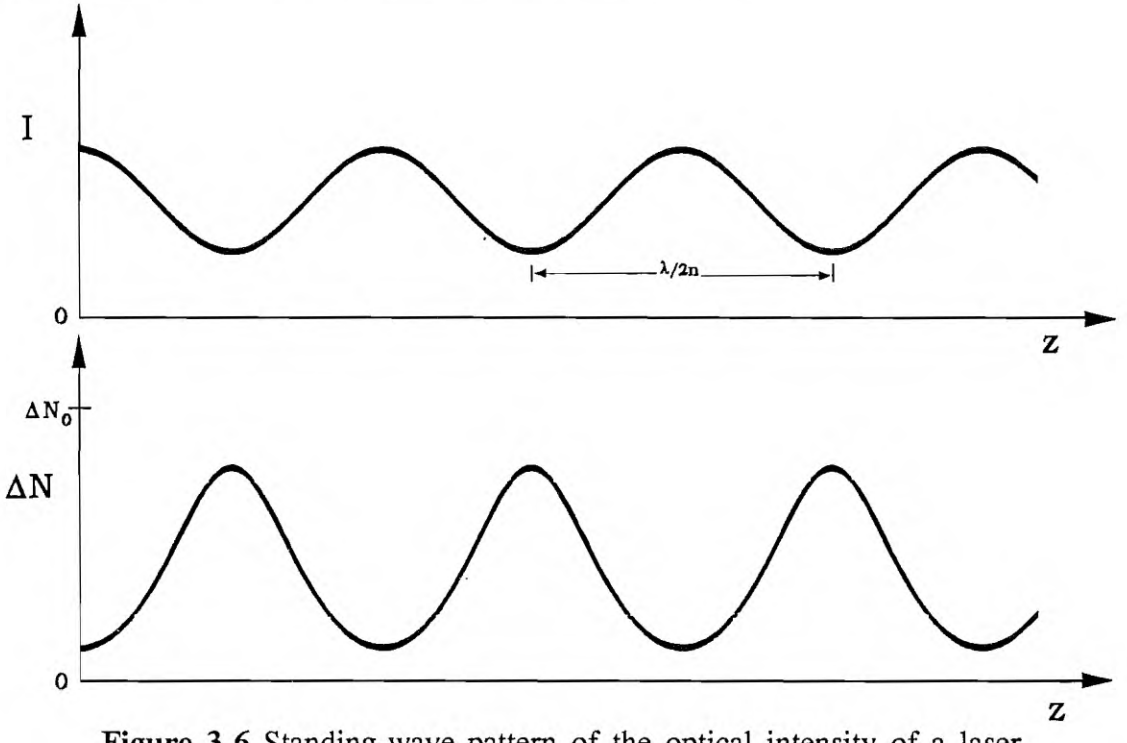

Figure 3.6 Standing-wave pattern of the optical intensity of a laser mode giving rise to spatial holeburning in the gain medium.

Spatial holeburning can have various consequences, such as reduced competition between certain modes, the strength of the effect depending on how the modes fill the cavity and how one mode will fit into the peaks and troughs of the population inversion spatial distribution caused by another mode. When spatial holeburning occurs it can affect the spectral content of a laser by favouring particular modes. As a result the spectrum may be made up of modes with a larger mode spacing than

would be indicated by the passive mode spacing. Rather than the adjacent mode experiencing most gain as would be indicated by the shape of the gain curve another mode for which the peaks of the optical intensity fall into the undepleted part of the gain medium may encounter more gain in the round-trip of a resonator.

Practical insight into the effects of spatial holeburning can be gained from calculations on the model illustrated in Figure 3.7. In this model a 1m length laser cavity is considered, with one mode oscillating with mode number k_1. This mode will set up a standing-wave pattern due to the two oppositely-travelling waves resulting in a depletion of the population inversion with spatial variation, $\Delta N_1(z)$, of the form:

$$\Delta N_1(z) = \frac{K_1}{1 + \frac{K_2 + \cos(\pi k_1 z)}{K_3}} \qquad (14)$$

where K_1, K_2 and K_3 are constants. If another mode with mode number k_2 is to oscillate then it will result in an intensity pattern, $I_2(z)$, of the form:

$$I_2(z) = K_4 + \cos(\pi k_2 z) \qquad (15)$$

where K_4 is a constant. With only the first mode oscillating the gain available for a second mode, G_2, will scale by the overlap integral:

$$G_2 \propto \int_a^b I_2(z)\Delta N_1(z)dz \qquad (16)$$

where the gain region extends from a to b as shown in Figure 3.7. Using this model calculations can be performed to determine which mode sees the most gain once the first mode is oscillating. In the following calculations the cavity length is assumed to be 1 metre and the mode number of the first mode to oscillate in each situation is

chosen to simulate operation at about 1.55μm. In practice, for a different cavity configuration it may not necessarily be the case that the same mode will be the first to lase, but this assumption does not affect the general results of the analysis. The calculations are intended to illustrate how spatial holeburning can affect modal structure without attempting calculate the exact mode structure, and hence the gain profile is assumed to be flat, the intensity of the mode uniform along the entire length, while only the region in which the gain occurs is varied. It is also assumed that the round-trip loss in the resonator is low, to allow the existence of a well-defined standing-wave pattern. For resonators with large loss the mode intensities will not oscillate as strongly spatially, and spatial holeburning effects will be reduced.

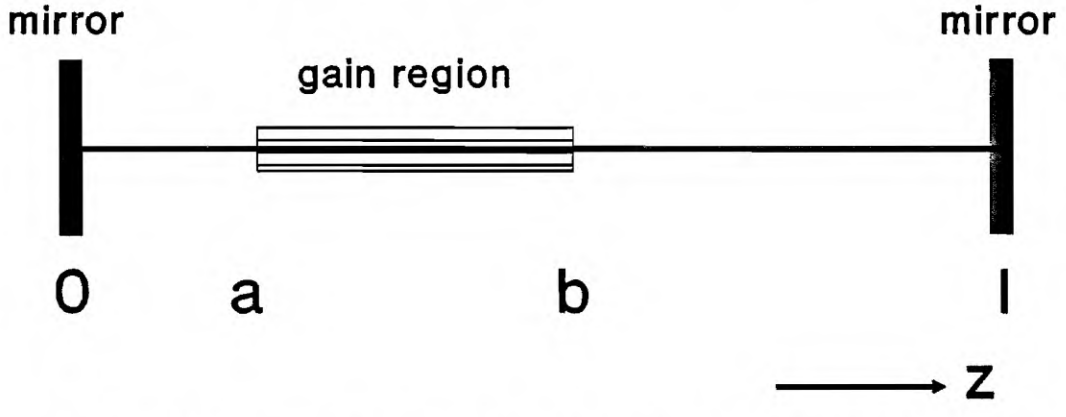

Figure 3.7 Resonator model used to model the effects of spatial holeburning. Cavity length 1m, with gain region extending from a to b.

Illustrative examples of the effect of spatial holeburning on the laser spectrum can be seen from considering a 1 metre laser cavity in which the gain medium occupies only a 10cm region. If the central mode is oscillating at a wavelength of about 1.55μm then Figures 3.8, 3.9 and 3.10 show which modes have the most gain if the gain region is at the end of the cavity, a quarter way along the cavity length and in the centre of the cavity respectively, with the gain being calculated from Equation 3.16 by numerical integration, with a and b defining the gain region. The gain is calculated

for individual modes close to the central mode. The mode with the most gain is at quite different spacing in each case, in this example spaced at the 14th mode for the case of the gain at the end of the cavity, the 4th mode with the gain medium centred a quarter distance along the length, while the second mode sees most gain if the gain medium is in the centre of the cavity.

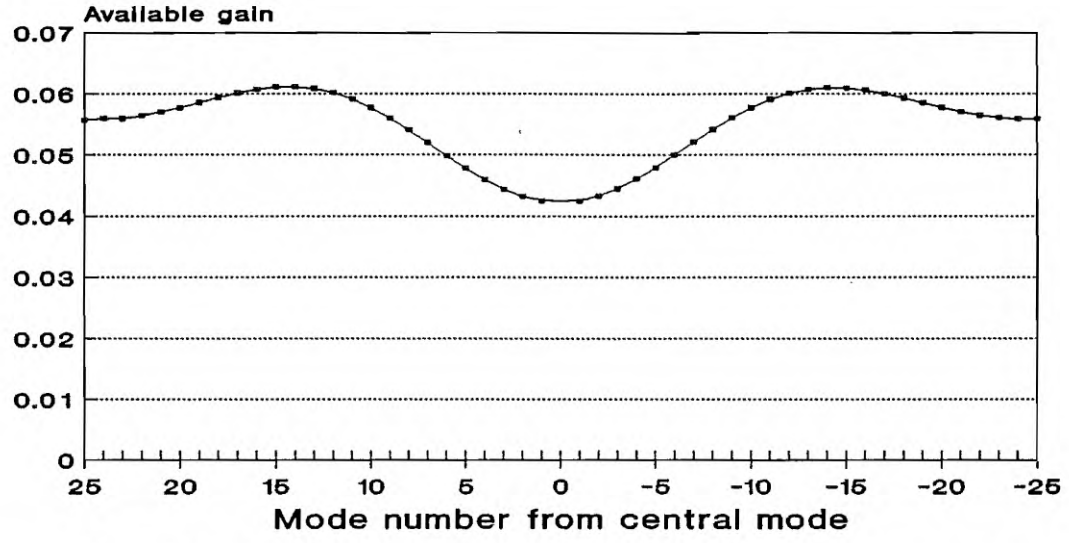

Figure 3.8 Gain available to modes close to central mode after central mode lasing. Gain in region 0-0.1m, cavity length 1m.

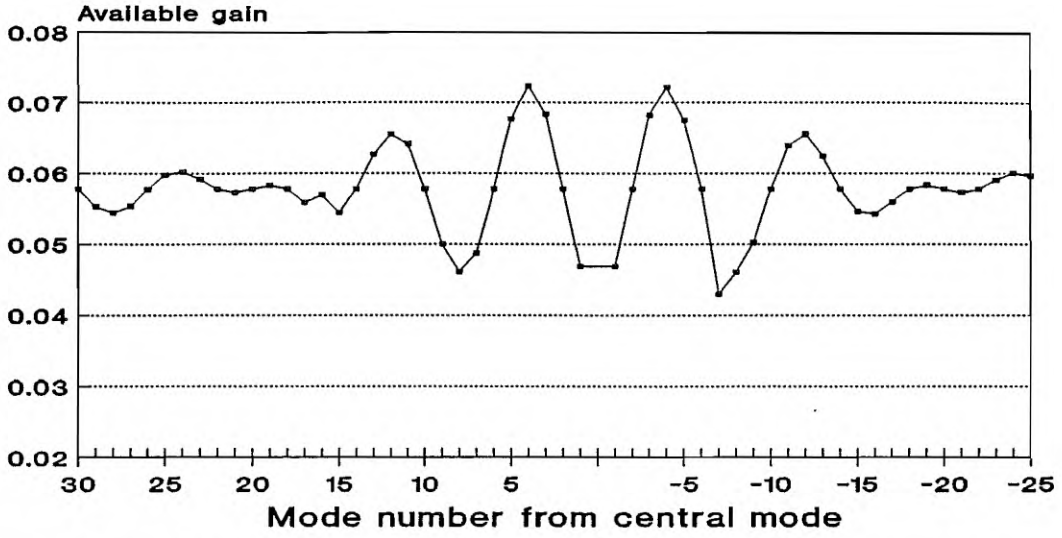

Figure 3.9 Gain available to modes close to central mode after central mode lasing. Gain region 0.2m-0.3m, cavity length 1m.

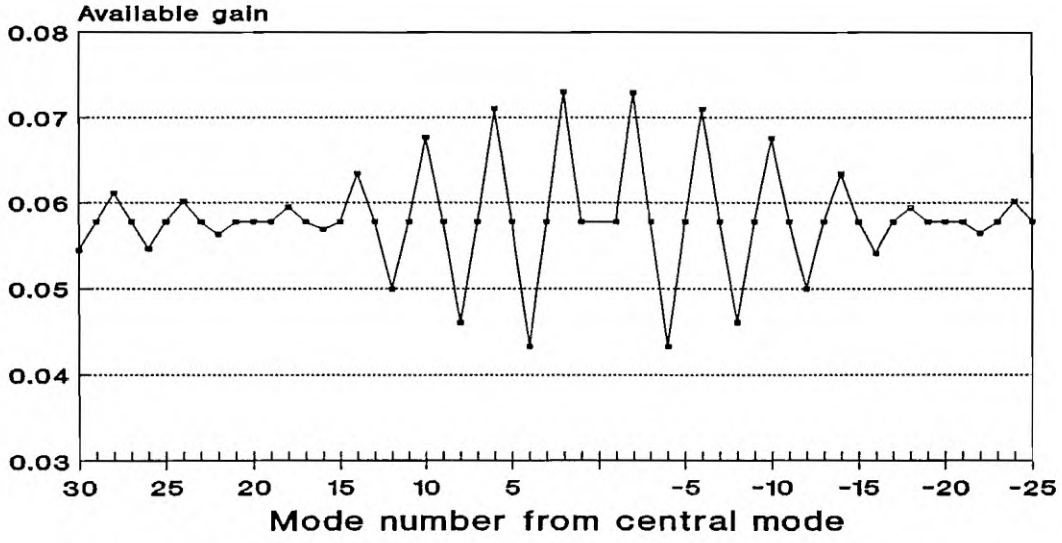

Figure 3.10 Gain available to modes close to central mode after central mode lasing. Gain region 0.45m-0.55m, cavity length 1m.

Gain region	Mode from central mode with most gain
0-0.1m	14^{th}
0-0.2m	7^{th}
0-0.3m	5^{th}
0-0.5m	3^{rd}
0.2-0.3m	4^{th}
0.15-0.35m	4^{th}
0.1-0.4m	4^{th}
0.45-0.55m	2^{nd}
0.4-0.6m	2^{nd}
0.3-0.7m	2^{nd}

Table III.I Next mode with most gain after central mode @1.55μm lasing. Resonator length 1m.

Table III.I indicates other examples of the next mode with most gain for various positions and lengths of the gain region in a 1 metre laser. Some general observations which arise from this analysis include:

- As the length of the gain medium increases the depth of modulation in the amount of gain available decreases. Eventually as the gain medium occupies the entire cavity all modes will have equal probability of having most gain after one mode is lasing.

- The maximum in the amount of gain available always occurs for a mode close to the central mode. This is because the correlation between modes decreases as the difference in mode numbers increases.

This will be accentuated in a real laser medium which not have a flat gain profile, but will generally have a gain peak at the wavelength of the central mode.

- Placing the gain medium at one end of the laser cavity maximises the spacing between preferred modes, placing the gain medium in the centre of the cavity minimises the spacing between preferred modes.

Spatial holeburning can thus have a significant effect on the spectral characteristics of a fibre laser when the spectrum is observed on the scale of individual modes. It is one of the most significant effects leading to multimode oscillation, but careful cavity design to eliminate spatial holeburning can lead to single-longitudinal-mode operation. However in the case of a standing-wave resonator, to ensure single-longitudinal-mode operation we require that the total gain is less than the round-trip loss for all other modes. This analysis has not been taken as far as defining formulas for the laser designer to design a single-longitudinal-mode laser, but as an indication of the possible effects of spatial holeburning. Chapter 5 describes experimental fibre laser configurations which operate in a uni-directional mode within the gain medium in order to eliminate spatial holeburning, resulting in single-longitudinal-mode operation.

It should be noted that although controlling spatial holeburning could be used to achieve single-longitudinal-mode operation in standing-wave resonators, such operation is not easily achievable in fibre lasers with long resonator lengths and long distributed gain regions in which the wavelength is considerably smaller than the length of the gain region. In addition, fibre laser resonators will often have complex structures leading to high round-trip losses, making the effects of spatial holeburning less dominant. Controlling spatial holeburning in standing-wave resonators is more suited to single-frequency operation in short lasers with short gain regions, such as microchip lasers [Zayhowski]. Chapters 4 and 5 will illustrate how single-frequency

operation can more easily be achieved in erbium-doped fibre lasers in resonators without spatial holeburning than in resonators with spatial holeburning.

3.5 STATISTICS OF LASER LIGHT

By designing a laser resonator to control the properties described above, i.e., the gain bandwidth, passive cavity mode spacing and the effects of spatial holeburning, single-longitudinal-mode operation can be achieved in Er^{3+}-doped fibre lasers, as will be described in the following chapters. Once single-longitudinal-mode operation is achieved the ultimate linewidth limit is determined by the statistics of the laser light. Ideal laser light can be considered as a purely monochromatic signal with fixed amplitude E_0, frequency ω_0 and phase ϕ, with the radiation field being:

$$\varepsilon(t) = Re\left\{E_0 e^{j(\omega_0 t+\phi)}\right\} \tag{17}$$

Real laser light, although being highly monochromatic compared to other light sources, has a finite spectral width with the ultimate linewidth limit of a single-longitudinal-mode laser being determined by the spontaneous emission noise generated by the gain medium and the linewidth or Q of the passive cavity.

A model commonly used to describe the effects of the spontaneous emissions and the resulting phase fluctuations of the laser signal is the rotating phasor model [Yariv], [Henry]. A variation on this model will be used in Chapter 6 when describing the effects of randomly-phased spontaneous photons from an erbium-doped fibre amplifier on the amplification of narrow-band signals. A real laser field undergoes random fluctuations of both phase and amplitude and hence can be represented by:

$$\varepsilon(t) = Re\left\{E(t) e^{j(\omega_0 t+\phi(t))}\right\} \tag{18}$$

The source of the fluctuations is the spontaneous emission of photons by the gain medium. Whereas stimulated photons are in phase with the stimulating photons, the spontaneous photons are not coherent with the laser field. The spontaneous photons add to the field, with the random nature of the photon phase giving rise to phase and amplitude fluctuations.

The phasor model is depicted in Figure 3.11. The ideal laser field can be represented by a rotating vector with rotation rate ω_0. The length of the vector is proportional to the signal strength. The phase of the signal can be altered by spontaneous emissions and by the effects of acoustic disturbances and thermal drift on the laser cavity. The effect of one spontaneous emission photon is to add one uncorrelated event of unit length. This gives rise to an angular variation ϕ and a change in the field phase $\Delta\theta$. The angle ϕ of the spontaneous photon is a random variable uniformly distributed on $(-\pi, \pi)$. The resulting random process is both stationary and ergodic, i.e., the statistical properties are independent of the time origin and a sample at any time will reveal the statistics of the process as a whole [Goodman].

The phase of the laser light is modelled as uniformly distributed on $(-\pi, \pi)$ or equivalently to undergo a random-walk process. The Weiner-Levy process is used to model the phase fluctuations [Moslehi]. The phase is modelled as a non-stationary zero-mean Gaussian random process for which the statistics of the phase difference are [Goodman], [Moslehi]:

$$\begin{aligned} \overline{[\phi(t_a)-\phi(t_b)]^2} &\propto t_b - t_a \\ \overline{\phi(t_a)\phi(t_b)} &\propto \min(t_a, t_b) \end{aligned} \qquad (19)$$

where t_a, t_b are arbitrary instants of time. These properties are also characteristic of a diffusion process and of Brownian motion of a free particle. The Weiner-Levy process has the property that although the process is non-stationary its first increments

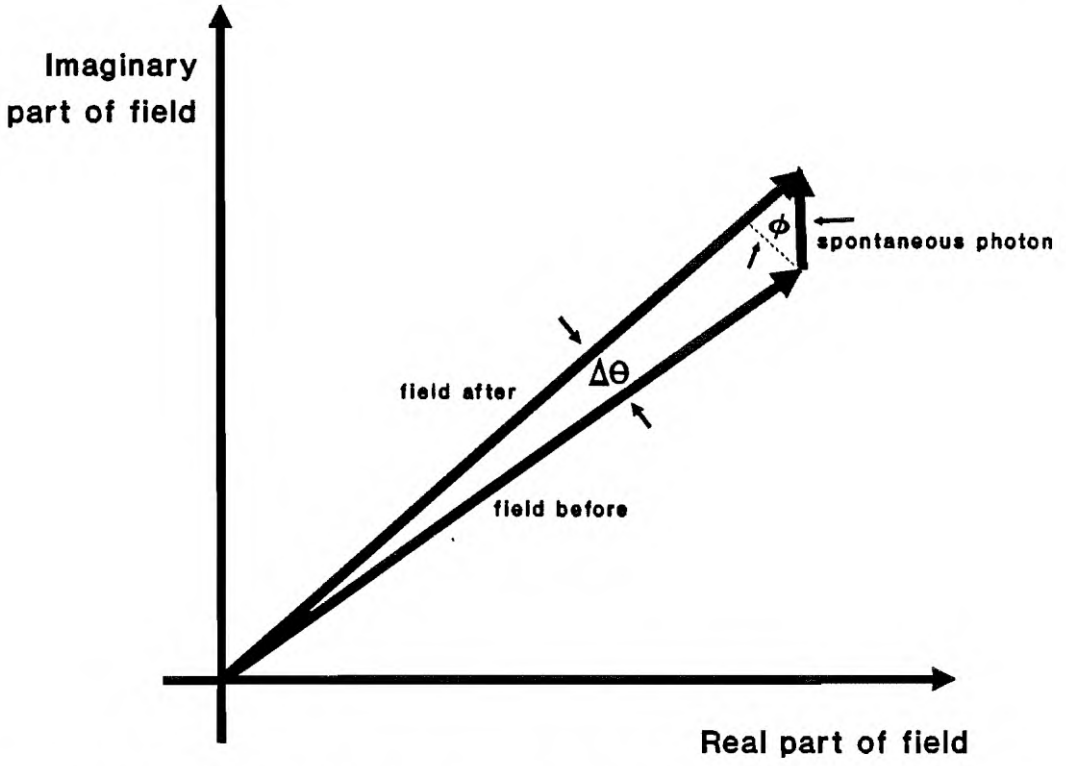

Figure 3.11 Rotating vector model used to model laser linewidth.

are stationary and independent. Thus the first increment of the phase, or the phase difference $\Delta\phi(t)=\Delta\phi(t)-\Delta\phi(0)$, is a zero-mean Gaussian random process. The probability density function (PDF) of $\Delta\phi(t)$ is hence of the form:

$$p_{\Delta\phi}(\Delta\phi) = \frac{1}{\sqrt{2\pi}\sigma_{\Delta\phi}} e^{-\frac{(\Delta\phi)^2}{2\sigma^2_{\Delta\phi}}} \qquad (20)$$

where $\sigma^2_{\Delta\phi}$ is the variance of the phase difference. By using Equation 3.19 it can be shown that:

$$\begin{aligned}\overline{[\phi(t_a)-\phi(t_b)]^2} &= \overline{\phi^2(t_a)+\phi^2(t_b)-2\phi(t_a)\phi(t_b)} \\ &= kt_a+kt_b-2k\min(t_a,t_b) \\ &= k|\tau|\end{aligned} \tag{21}$$

where $\tau \triangleq t_a - t_b$. and k is a proportionality constant related to the laser source spectral purity. Hence the statistics of the laser light show that the mean squared phase difference is simply proportional to the time difference between the two instants of time. Using the Wiener-Khintchine theorem the power spectral density (PSD) of the field spectrum is given by the Fourier transform of the field autocorrelation. Assuming the field amplitude is constant, E_0, the autocorrelation $R_i(\tau)$ is:

$$\begin{aligned}R_i(\tau) &= \overline{\varepsilon(t+\tau)\varepsilon^*(t)} \\ &= E_0^2 e^{j\omega_0\tau}\overline{e^{j\Delta\phi(\tau)}}\end{aligned} \tag{22}$$

Now:

$$\begin{aligned}\overline{e^{j\Delta\phi(\tau)}} &= \int_{-\infty}^{\infty} e^{j\Delta\phi(\tau)} p_{\Delta\phi}(\Delta\phi)d(\Delta\phi) \\ &= e^{-\frac{1}{2}k|\tau|}\end{aligned} \tag{23}$$

Hence taking the Fourier transform of $R_i(\tau)$ using Equation 3.22 the field spectrum can be shown to be:

$$S(\nu) = \frac{2\tau_c}{1+[2\pi\tau_c(\nu-\nu_0)]^2} \tag{24}$$

where τ_c is related to the proportionality constant k by $\tau_c = 2/k$ [Moslehi]. The PSD

of the signal spectrum corresponds to a Lorentzian-shaped function centred at the laser centre frequency υ_0.

Equation 3.24 is the quantum-limited spectral density of the laser light. The quantum limit to the laser linewidth occurs when only spontaneous emissions give rise to phase fluctuations of the laser field. In this limit the Lorentzian-shaped profile will have a full width at half maximum of:

$$\Delta\nu = \frac{2\pi h\nu_0(\Delta\nu_c)^2\mu}{P} \qquad (25)$$

where $\Delta\upsilon_c$ is the passive resonator linewidth, P is the power in the laser cavity and μ is the inversion factor defined by $\mu=N_2/(N_2-N_1)_{th}$. This expression is known as the Schawlow-Townes linewidth after the co-inventors of the laser who first derived it [Schawlow].

The quantum limit would suggest that the linewidth limit for an erbium fibre laser operating at 1.55μm with a 1m cavity and output power of 1mW is of the order of 1Hz. The narrowest fibre laser spectra yet obtained are of the order 1kHz [Iwatsuki] and thus several orders of magnitude above the Schawlow-Townes limit. As will be explained in the following chapters, the long resonator lengths associated with fibre lasers make then susceptible to changes in cavity lengths due to thermal effects and acoustic vibrations, thus imposing limits on obtainable spectral widths. The measured linewidths are associated with the mechanical construction of the resonator rather than the limits imposed by spontaneous emissions.

3.6 SUMMARY

In this chapter the major factors contributing to the determination of spectral characteristics of erbium-doped fibre lasers have been described. These factors include the gain bandwidth of the erbium-doped fibre, the passive cavity mode spacing and the effects of spatial holeburning on the gain medium caused by the standing-wave pattern of a laser mode. The statistics of the laser light once single-longitudinal-mode oscillation is achieved were described. The next two chapters will describe how with the constraints imposed by these properties, erbium-doped fibre lasers can be designed to achieve narrow-linewidth and single-longitudinal-mode operation.

It is beyond the scope of this work to modify the glass host in which the active erbium ions are sited in order to modify the gain bandwidth, however Chapter 4 will describe how the multi-pass gain bandwidth can be significantly reduced by the use of a narrow-band wavelength-selective fibre grating reflector or distributed Bragg reflector (DBR) to achieve very narrow linewidth lasing. Fibre laser resonator lengths are usually quite long and with spectra hence containing many passive cavity modes, however Chapter 4 will also describe the effects of changing the length of a fibre laser resonator on the number of modes oscillating. In addition, the application of a coupled-cavity fibre laser resonator to alter the passive cavity mode structure for narrow-linewidth operation will be described.

The controlled use of spatial holeburning effects to produce single-longitudinal-mode operation in a standing-wave resonator is more suited to short laser cavities than to those utilised with erbium-doped fibre lasers. Chapter 5 describes how the elimination of spatial holeburning, the fundamental cause for multi-mode operation, by achieving travelling-wave operation is a powerful technique for achieving single-frequency operation. It will be demonstrated, in the first operation of a travelling-wave fibre laser, how this technique is viable in erbium-doped fibre lasers to achieve very

narrow linewidths. A travelling-wave resonator will be described in which lasing occurs with a linewidth less than 10kHz.

3.7 REFERENCES

Ainslie, B.J., Craig, S.P., and Davey, S.T., "The Absorption and Fluorescence Spectra of Rare Earth Ions in Silica-Based Monomode Fiber", *J. Lightwave Tech.*, **6**, 2, pp, 287-293, 1988.

Ainslie, B.J., Craig-Ryan, S.P., Davey, S.T., Armitage, J.R., Atkins, C.G. and Wyatt, R., "Optical Analysis of Erbium Doped Fibres for Efficient Lasers and Amplifiers", *Proc. IOOC,* 20A3-2, 1989.

Ainslie, B.J., Craig-Ryan, S.P., Davey, S.T., Armitage, J.R., Atkins, C.G., Massicott, J.F. and Wyatt, R., "Erbium Doped Fibres for Efficient Optical Amplifiers", *IEE Procceedings.*, **137**, Pt. J., 4, pp. 205-208, 1990.

Barnes, W.L., Poole, S.B., Townsend, J.E., Reekie, L., Taylor, D.J. and Payne, D.N., "Er^{3+}-Yb^{3+} and Er^{3+} Doped Fiber Lasers", *J. Lightwave Tech.*, **7**, 10, pp. 1461-1465, 1989.

Barnes, W.L., Laming, R.I., Tarbox, E.J. and Morkel, P.R., "Absorption and Emission Cross-sections of Er^{3+} Doped Silica Fibres," *IEEE J. Quant. Elect.*, **27**, pp. Apr. 1991.

Briançon, A-M., Jacquier, B., Gàcon, J-C., Le Sargent, C. and Marcerou, J-F., "Inhomogeneous Line Broadening of Optical Transitions in Nd^{3+} and Er^{3+} Doped Preforms and Fibers", SPIE **1373** Fiber Laser Sources and Amplifiers II, pp. 9-20, 1990.

Desurvire, E., Zyskind, J.L. and Simpson, J.R., "Spectral Gain Hole-Burning at 1.53μm in Erbium-Doped Fiber Amplifiers", *IEEE Phot. Tech. Lett.*, **2**, 4, pp. 246-248, April 1990.

Dybdal, K., Bjerre, N., Engholm Pederson, J. and Larsen, C.C., "Spectroscopic Properties of Er-doped Silica Fibers and Preforms", SPIE **1171** Fibre Laser Sources and Amplifiers, pp. 209-218, 1989.

Henry, C.H., ''Theory of the Linewidth of Semiconductor Lasers,'' *IEEE J. Quant. Elect.*, **QE-18**, 2, pp. 259- Feb. 1982.

Horiguchi, M., Shimizu, M., Yamada, M., Yoshino, K. and Hanafusa, H., ''Highly Efficient Optical Fibre Amplifier Pumped by a 0.8μm Band Laser Diode'', *El. Lett.*, **26**, pp. 1758-1759, 1990.

Giles, C.R. and Di Giovanni, D., ''Spectral Dependence of Gain and Noise in Erbium-Doped Fiber Amplifiers'', *IEEE Phot. Tech. Lett.*, **2**, 11, pp.797-800, Nov. 1990.

Goodman, J.W., *Statistical Optics*, John Wiley & Sons, New York, 1985.

Guy, S.C., Minasian, R.A., Poole, S.B. and Sceats, M.G., ''Characterisation of the Erbium Fibre Amplifier by Fluorescence Line Narrowing'', *Proc. ACOFT'90*, pp. 27-30, Sydney, Dec. 1990.

Iwatsuki, K., Okamura, H. and Saruwatari, M., ''Wavelength-tunable Single-frequency and Single-polarisation Er-doped Fibre Ring Laser with 1.4kHz Linewidth'', *El. Lett.*, **26**, p. 2033, 1990.

Kimura, Y. and Nakazawa, M., ''Lasing Characteristics of Er^{3+}-doped Silica Fibers From 1553 up to 1603nm'', *J. Appl. Phys.*, **64**, 2, pp. 516-520, July 1988.

Koechner, W.L., ''Solid State Laser Engineering'', Springer Series in Optical Sciences, 2nd Edition, Springer Verlag, Berlin, 1988.

Laming, R.I., Poole, S.B. and Tarbox, E.J., ''Pump Excited-State Absorption in Er^{3+}-Doped Fibres'', *Opt. Lett.*, **13**, pp. 1084-1086, Dec. 1988.

Laming, R.I., Farries, M.C., Morkel, P.R., Reekie, L., Payne, D.N., Scrivener, P.L., Fontana, F., and Righetti, A., ''Efficient Pump Wavelengths of Erbium-Doped Fibre Optical Amplifier'', *Electron. Lett.*, **25**, 1, pp.12-14, 1989.

Mears, R.J., Reekie, L., Poole, S.B., and Payne, D.N., ''Low Threshold Tunable CW and Q-switched Fibre Laser Operating at 1.55μm'', *Electron. Lett.*, **22**, pp884-

885, 1986.

Miniscalco, W.J., ''Erbium-Doped Glasses for Fiber Amplifiers at 1500nm'' *J. Lightwave Tech.*, **9**, 2, pp. 234-250, Feb. 1991.

Millar, C.A., Ainslie, B.J., Craig, S.P., and Armitage, J.R., ''Low-threshold CW Operation of an Erbium-doped Fibre Laser Pumped at 807nm Wavelength'', *Electron. Lett.*, **23**, pp. 865-867, 1987.

Morkel, P.R., *Active Neodymium and Erbium Fibre Devices*, Ph.D. Thesis, University of Southampton, August 1990.

Morkel, P.R., Laming, R.I., Cowle, G.J. and Payne, D.N., ''Noise Characteristics of Rare-earth-doped Fiber Sources and Amplifiers'', SPIE **1373** Fiber Laser Sources and Amplifiers II, pp. 224-233, 1990.

Moslehi, B., ''Analysis of Optical Phase Noise in Fiber-Optic Systems Employing a Laser Source with Arbitrary Coherence Time,'' *J. Lightwave Tech.*, **LT-4**, 9, pp. 1334-1351, Sept. 1986.

Sandoe, J.N., Sarkies, P.H. and Parke, S., ''Variation of Er^{3+} Cross Sections for Stimulated Emission With Glass Composition'', *J. Phys. D: Appl. Phys.*, **5**, pp. 1788-1799, 1972.

Schawlow, A.C. and Townes, C.H., *Phys. Rev.*, **112**, pp. 1940- 1958.

Shimoda, K., ''Introduction to Laser Physics'', Springer Series on Optical Sciences, 2^{nd} Edition, Springer-Verlag, Berlin, 1984.

Shinn, M.D., Sibley, W.A., Drexhage, M.G. and Brown, R.N., ''Optical Transitions of Er^{3+} ions in Fluorozirconate Glass'', *Phys. Rev. B.*, **27**, pp. 6635-6648, 1983.

Siegman, A.E., ''Lasers'', University Science Books, Mill Valley, California, 1986.

Smith, P.W, ''Mode Selection in Lasers'', *Proc. IEEE*, **60**, 4, pp. 422-440, April 1972.

Snitzer, E., Po, H., Hakimi, R., Tumminelli, R., and MaCollum, B.C., ''Erbium Fiber Laser Amplifier at 1.55μm with Pump at 1.48μm and Yb Sensitised Er Oscillator'', *OFC'88*, Paper PD2, 1988.

Tachibana, M., Laming, R.I., Morkel, P.R. and Payne, D.N., ''Spectral Gain Cross Saturation and Hole-burning in Wideband Erbium-doped Fibre Amplifiers'', *Proc. Optical Amplifiers and their Applications Topical Meeting*, pp. 104-107, Colorado, July 1991.

Wyatt, R., ''Spectroscopy of Rare Earth Doped Fibres'', SPIE **1171** Fiber Laser Sources and Amplifiers, pp. 54-64, 1989.

Yariv, A., *Optical Electronics.*, 3rd Ed., Holt, Rinehart & Winston, New York, 1985.

Zahhowski, J.J., ''The Effects of Spatial Hole Burning and Energy Diffusion on the Single-Mode Operation of Standing-Wave Lasers'', *IEEE J. Quant. Elect.*, **26**, 12, pp. 2052-2057, 1990.

Zemon, S., Lambert, G., Miniscalco, W.J., Andrews, L.J. and Hall, B.T., ''Characterisation of Er^{3+}-doped Glasses by Fluorescence Line Narrowing'', SPIE **1171** Fiber Laser Sources and Amplifiers, pp. 219-236, 1989.

Zemon, S., Lambert, G., Miniscalco, W.J., Davies, R.W., Hall, B.T., Folweiler, R.C., Wei, T., Andrews, L.J. and Singh, M.P., ''Excited State Cross Sections for Er-doped Glasses'', SPIE **1373** Fiber Laser Sources and Amplifiers II, pp. 21-32, 1990.

Zyskind, J.L., Desurvire, E., Sulhoff, J.W. and Di Giovanni, D.J., ''Determination of Homogeneous Linewidth by Spectral Gain Hole-Burning in an Erbium-Doped Fiber Amplifier with GeO_2:SiO_2 Core'', *IEEE Photon. Tech. Lett.*,**2**,12, pp. 869-871, 1990.

Chapter Four

Mode Selection Techniques - Standing-Wave Resonators

4.1 INTRODUCTION

Mode-selection techniques, often involving complex coupled-cavity resonators, are commonly implemented to achieve narrow linewidth and single-frequency operation in a variety of laser systems [Smith 1972]. These techniques are one approach to achieving single-longitudinal-mode operation in a fibre laser. Mode-selection techniques operate by ensuring that only one passive cavity mode of the laser falls within the gain bandwidth to attain threshold. Lasers in general and fibre lasers in particular have output spectra which consist of modes at a number of closely-spaced frequencies spread over a broad bandwidth, as was discussed in Chapter 3. Narrow-linewidth or single-longitudinal-mode output can be obtained in many standing-wave

laser resonators either by reducing the resonator length or by using interferometric techniques in complex laser resonators to achieve enhanced mode selectivity. The basis for these techniques were explained in Chapter 3.

This chapter describes two mode-selection techniques which have been investigated with the aim of producing single-frequency operation of erbium-doped fibre lasers, and have resulted in very narrow spectral width operation. The first technique, described in Section 4.3 is one of the simplest cavity configurations for narrow-linewidth operation, made up of a short Fabry-Perot laser incorporating a narrow-bandwidth distributed Bragg reflector to reduce the bandwidth for multi-pass gain. The second technique, described in Section 4.4, is a novel coupled-cavity resonator which operates by the interaction of orthogonal polarisations in a single-mode fibre. Prior to examining these laser resonator structures Section 4.2 describes progress towards the fabrication of very-narrow-band distributed Bragg reflectors, one of the most important devices for mode selection and wavelength selection in fibre lasers. The fabrication process is not yet complete, however once complete this reflector will also have application in fibre-based sensors and the fabrication technique for producing diffraction gratings can be adapted for linewidth narrowing of planar waveguide glass lasers.

4.2 FABRICATION OF NARROW-BAND DISTRIBUTED BRAGG REFLECTORS

4.2.1 Introduction

Distributed Bragg reflectors (DBRs) with narrow reflection bandwidths are important devices for producing narrow-line and single-longitudinal-mode operation in erbium-doped fibres. DBRs can be used to increase the resonator frequency selectivity and to set the wavelength of operation very precisely within the doped fibre gain

bandwidth. The gain curve of the Er^{3+} $^4I_{13/2}$ to $^4I_{15/2}$ transition can be very broad in silica-glass fibre lasers, therefore DBRs or other frequency selective elements are often necessary to reduce the bandwidth over which round-trip gain can occur in the laser cavity in order to achieve oscillation on a limited number of longitudinal modes. Whereas the gain bandwidth of the erbium-glass system is not significantly altered by glass composition [Sandoe] the cavity round-trip gain bandwidth can easily be narrowed by the use of a narrow-band reflector. In addition the reflection centre wavelength of the DBR can be used to set the wavelength of operation of a travelling-wave fibre laser within the broad gain curve, as will be described in Chapter 5. Fibre DBRs will also provide a route to integrated, all-fibre narrow-linewidth fibre lasers.

Fibre DBRs were first proposed as a grating coupler which was applied as a high-resolution spectrometer [Russell]. This device produced guided mode to radiation mode coupling with the direction of radiation depending on wavelength of the guided mode. An extension on this technique to produce coupling into the guided backward direction in a single-mode fibre, and thereby provide narrow-band reflection, was demonstrated by placing a metal grating in the evanescent field after side-polishing the fibre to expose the core [Sorin]. Further developments of this technique have resulted in high reflectivity ($>90\%$) narrowband DBRs. Best results to date for these evanescent field devices are produced by fabricating corrugations on the fibre core itself to achieve a surface-relief grating [Bennion] [Rowe].

Single-longitudinal-mode operation in an Nd^{3+}-doped fibre laser has been demonstrated with a short fibre laser cavity incorporating a fibre DBR [Jauncey 1988], and narrow linewidth operation has been demonstrated in an Er^{3+}-doped fibre laser [Jauncey 1987]. High erbium concentrations are required to produce low threshold operation in short resonators. Difficulties producing efficient operation at very high concentrations means that very narrow-band reflectivities are necessary to enable sufficiently low-doped fibres to be used for single-frequency operation. The fabrication techniques described in this section have been developed to provide

surface-relief DBRs with sufficient resolution for this application by improving the length and uniformity of the interaction region. This provides a very narrow-band reflection to enable long (>50cm) erbium-doped fibres to be used to achieve single-longitudinal-mode operation.

4.2.2 Device Operation

The distributed Bragg reflector operates by the interaction of the evanescent field of the single-mode fibre mode with a periodic structure. The grating is formed such that the distance between the grating and the core is small enough to allow the grating to interact with the evanescent field of the guided light. To produce the first-order Bragg reflection in the backward direction the period of the grating, Λ, should satisfy the condition:

$$\Lambda = \frac{\lambda_0}{2n_{eff}} \qquad (1)$$

where λ_0 is the free-space wavelength of the light and n_{eff} is the effective refractive index of the guided mode. Once this condition is satisfied the incident mode is coupled to a reflected guided mode via the first-order Bragg reflection.

Using the coupled-wave solution for slab waveguide gratings the DBR structure has been modelled [Rowe]. Following this analysis it can be seen that the reflection bandwidth follows the approximate relation:

$$\frac{\Delta\lambda}{\lambda} = \frac{\Lambda}{L} \qquad (2)$$

where L is the interaction length of the DBR. Hence to produce very narrowband reflections requires the fabrication of DBRs with long interaction length L. This requires both a long length of the exposed core region and a uniform grating extending over this length. This work aims to produce fibre gratings with interaction lengths ~ 1cm and reflection bandwidths < 0.1nm. This reflection bandwidth should allow a resonator length of about 30-50cm to be used to achieve single-longitudinal-mode operation. With this resonator length a fibre with sufficiently low erbium concentration should be able to be used to achieve lasing, thereby avoiding degradation of performance associated with high erbium concentrations.

4.2.3 Distributed Bragg Reflector Fabrication

The two major differences between the fabrication techniques outlined below and those employed by other workers fabricating relief gratings occur in the fibre side-polishing and holographic exposure steps. Both of these were designed in this work to improve the length and uniformity of the DBR.

4.2.3.1 Fibre Polishing

Obtaining a long even grating interaction length for efficient operation of the exposed field device is one of the limitations of previously published techniques for fabricating DBRs. In previous work the fibre has been mounted in a curved [Rowe] or straight

[Ragdale] V-groove in a silica block and the block and fibre polished to expose the fibre core. With the curved-groove technique even for a radius of curvature as large as 800mm the interaction length is only a few millimetres because the fibre is polished tangentially to the core. In addition the tangential polish results in a slight unavoidable effective chirp in the grating. Longer chirp-free lengths are possible with the flat V-groove technique but the difficulty then is to polish exactly parallel to the core axis for the polish length.

To obtain a long even interaction length a fibre polishing technique based on a rotating polishing wheel is used [Hussey]. This technique was chosen because it enables a very long interaction length to be achieved while ensuring that the polished flat is parallel to the core of the fibre, thus obtaining a long, even interaction region. The long polished flat is achieved by utilising the natural strength and concentricity of the optical fibre to aid the polishing process.

The fibre is polished by draping a section of fibre, with the outer jacket removed, over a diamond polishing wheel as illustrated in Figure 4.1. Applying tension to the fibre ends ensures the fibre is in intimate contact with the wheel. The polishing wheel is lubricated with liquid paraffin which has a refractive index matching that of the guided mode of the fibre. A signal is passed through the fibre, the signal attenuation being used to monitor the polished depth. The signal is attenuated as the polish depth approaches the core and the field interacts with the liquid paraffin. This has an index matching the index of the guided mode and hence prevents the fibre from guiding as the polished flat approaches the core. Monitoring the decrease in the transmitted signal the polishing is stopped once the transmitted signal has reduced by a level indicating that the polished depth is within a micron of the core [Minelly].

With a tension of 35g applied to the fibre end the fibre is first coarsely ground with a diamond polishing wheel to expose the fibre core until the transmitted signal reduced by 40-50dB for a polish length of 1cm, which indicates that the ground

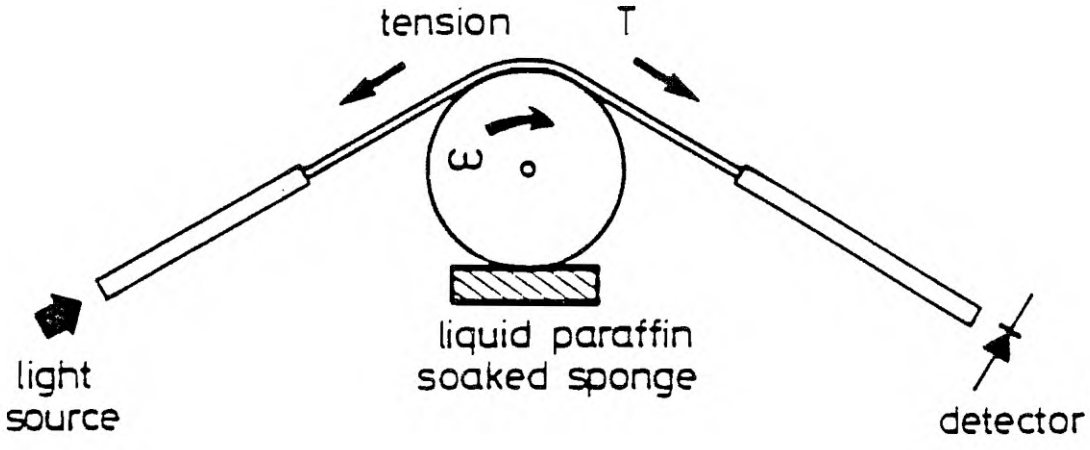

Figure 4.1 Schematic of apparatus used to produce side-polished optical fibres. [Courtesy of J.D. Minelly]

surface is approaching the fibre core. The polishing wheel is then covered with a polishing cloth soaked with a water suspension containing CeO_2, and the fibre finely polished for about 5 minutes under a tension of 5g. After polishing the fibre is cleaned and mounted on a glass slide with the polished flat facing upwards, ready for further processing. The attenuation of the signal passing through the fibre is monitored with a high index liquid (1.668) on the polished flat, in order to check the polish depth. Attenuation of 40dB with overlayer index $n=1.668$ and for a 1cm polished section indicates the polished depth is within 1 micron of the fibre core [Minelly].

4.2.3.2 Holographic Photolithography

Once the fibre core was exposed by the side-polishing process, a grating was formed in a photoresist laser on the polished flat by holographic exposure of blue/UV sensitive photoresist to an interference pattern from two laser beams. A new simple holographic exposure system was developed to expose long, even diffraction gratings in the photoresist.

To produce diffraction grating in photoresist it was first necessary to have a thin, uniform layer of photoresist on the fibre surface. The photoresist used in the process was the Shipley Microposit S1400 series which is normally exposed by light sources in the range 350-450nm. In this case exposure was by Argon-ion laser light with wavelength 457.9 nm which is slightly beyond the strongly absorbent region. As a consequence long exposure times ~ 10 minutes were necessary.

A thin layer of photoresist with thickness ~ 100nm was produced by spin coating and then baking the photoresist. Spin coating is normally employed only with flat substrates, but as in this application the polished fibre was not mounted flush with the glass slide on which it was mounted, the spin coating process had to be adapted to ensure a regular photoresist layer was formed on the polished fibre. The photoresist thickness had to be less than ~ 150nm ($<\lambda/4$) in order to avoid three-dimensional layers of gratings when exposing with interfering laser beams. In addition, because the surface was small, the photoresist had to be spun until dry in order to prevent bulging of the photoresist in the centre of the fibre when drying. Bulging on the centre of the polished flat would result from surface tension of the liquid photoresist on the 100μm fibre polished flat if the photoresist were not dry when the spinning ceased.

Taking these factors into account the following steps were followed to produce the appropriate thickness of photoresist on the polished fibre:

1. The fibre surface was thoroughly cleaned in boiling RBS 35 (made by Chemical Concentrates (RBS) Ltd.), then rinsed and dried in an oven at 100°C to evaporate any residual solvents.

2. To ensure maximum adhesion the fibre was covered with Microposit Primer for 10 seconds and spun at 4000rpm for 120 seconds until dry.

3. The fibre was covered in a Photoresist solution consisting of three parts S1400-17 Photoresist with one part Microposit Primer and spun for 360 seconds at 5000rpm until dry.

4. The photoresist and fibre were baked for 20 minutes at 90°C ready for exposure.

A diffraction grating was formed in the photoresist by holographic exposure to light from an Argon-ion laser with the system illustrated in Figure 4.2. Generally, holographic exposure of gratings requires expanded beam light delivery systems incorporating lenses and mirrors [Walpita]. The system developed in this work and illustrated in Figure 4.2 consists simply of a single-mode fibre coupler as a 50/50 beamsplitter with fibre leads used to deliver the beams. The fibre ends were cleaved to act as a beam expansion system and the fibres pointed at the interference plane to set the interference angles and grating pitch. Large areas can be exposed with this system. The limitation is how flat the wavefronts are at the substrate surface. The distance between the fibre ends and the substrate must be sufficiently large that the wavefronts are approximately flat. To prevent light reflection from the back surface of the glass slide, which would set up orthogonal standing-waves in the photoresist layer, the back surface was index-matched.

Exposure with 457.9nm light from the Argon-ion laser means that long exposure times are necessary to fully expose the photoresist with the grating pattern, as this

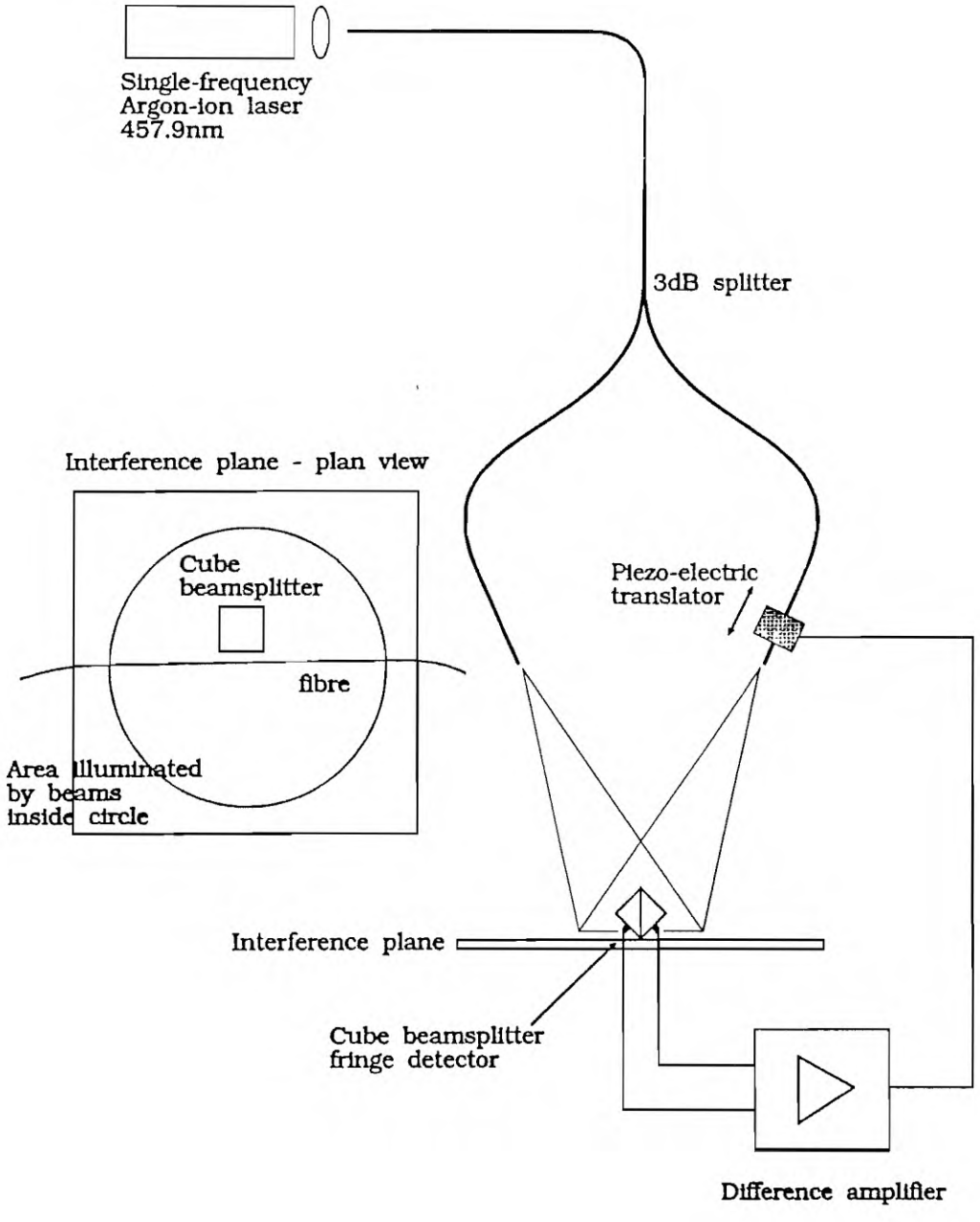

Figure 4.2 Holographic exposure system used to expose relief gratings in blue/UV sensitive photoresist. Angle between interfering beams determines grating pitch.

wavelength is beyond the strongly-absorbent region of the photoresist. Active stabilisation of the interference pattern was necessary. The stabilisation was also required to eliminate any phase differences between the optical paths arising from acoustic and temperature disturbances picked-up by the optical fibres. The stabilisation system was a closed control loop consisting of a cube beamsplitter producing a dark fringe and a light fringe on a pair of photodiodes, an amplifier to amplify the difference signal from the pair of photodiodes to monitor the movement of the interference fringes, and a piezo-electric transducer to translocate the end of one of the fibres to maintain a constant path difference.

To set up the optical paths the fibre angles were first set and the paths approximately matched to ensure that the path difference was less than the coherence length of the exposing laser. The cube beamsplitter was oriented to act as a beam combiner in a Mach-Zehnder interferometer so that one photodiode was located in a dark fringe while the photodetector on the other side of the cube beamsplitter detected a bright fringe from the interference pattern. The photodetector signals were used to derive a difference signal which was passed through an integrator and amplifier before being amplified across the piezo-electric transducer through which was mounted one of the fibre ends. This signal was used to adjust the path difference, and when in a closed loop a constant difference signal was achieved thus stabilising the interference pattern.

With this exposure system the photoresist-covered polished fibre was placed in the interference pattern at the interference plane and exposed for 9-12 minutes. Following the exposure the fibre was immersed in Shipley Microposit Developer for 5 seconds to develop the grating relief pattern, the fibre rinsed to stop the developing process and dried. At this stage a surface-relief grating has been formed on the polished flat, which will weakly interact with the fibre mode evanescent field.

4.2.3.3 DBR Evaluation

Two measurement techniques were used to evaluate the DBRs formed with the photoresist gratings. The first measurement, to measure diffraction of light out of the fibre by the grating was performed as an initial observation of diffraction from the grating, to ensure that the grating was present on the polished fibre and that the pitch was approximately correct. The second measurement was a direct measurement of the grating reflectivity and reflection bandwidth.

The first measurement used the fibre grating as it was first proposed, as an in-line single-mode fibre-optic spectrometer [Russell]. Light was launched into the fibre and through the DBR. Some of the light passing through the DBR is diffracted out of the fibre and emerges into free space above the grating as a half-cone of light, with the angle of the cone to the fibre axis, θ_λ, depending on the wavelength as:

$$\cos\theta_\lambda = n + \frac{k\lambda}{\Lambda} \qquad (3)$$

where n is the effective index of the mode, λ is the wavelength of the light, Λ is the grating pitch and k (integer) is the order of the diffraction (see Figure 4.3). Passing light from an argon-ion laser through the fibre and measuring the angle of the diffraction out of the fibre was a quick method of checking the strength of the grating and of estimating the grating pitch, Λ.

After ensuring that the grating was present with the measurement described above, the reflection bandwidth was measured directly by the system shown in Figure 4.4. An ELED was used to generate a broad-band signal in the 1.55μm region and was launched into a 3dB or 50:50 coupler. The DBR was spliced onto one of the coupler ports and the reflection bandwidth determined with monochromator. A sample reflection spectrum from a photoresist grating is shown in Figure 4.5. The strength

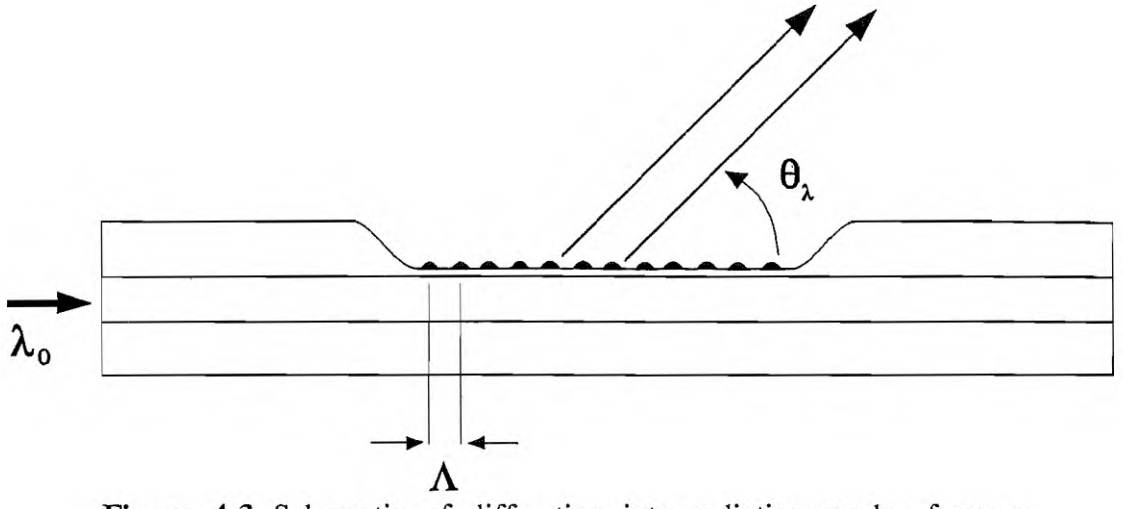

Figure 4.3 Schematic of diffraction into radiation modes from a distributed Bragg reflector.

of the grating with only photoresist on the polished flat was weak, typically $<2\%$, however the reflection bandwidth was resolution limited to <0.2nm, indicating that a long interaction region was achieved.

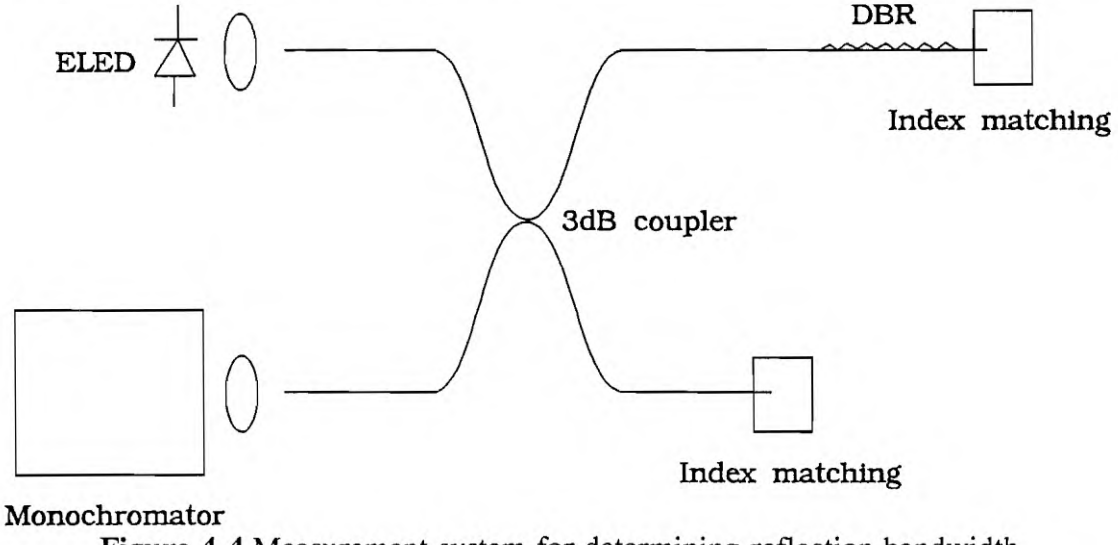

Figure 4.4 Measurement system for determining reflection bandwidth of DBRs. Resolution of monochromator 0.1nm.

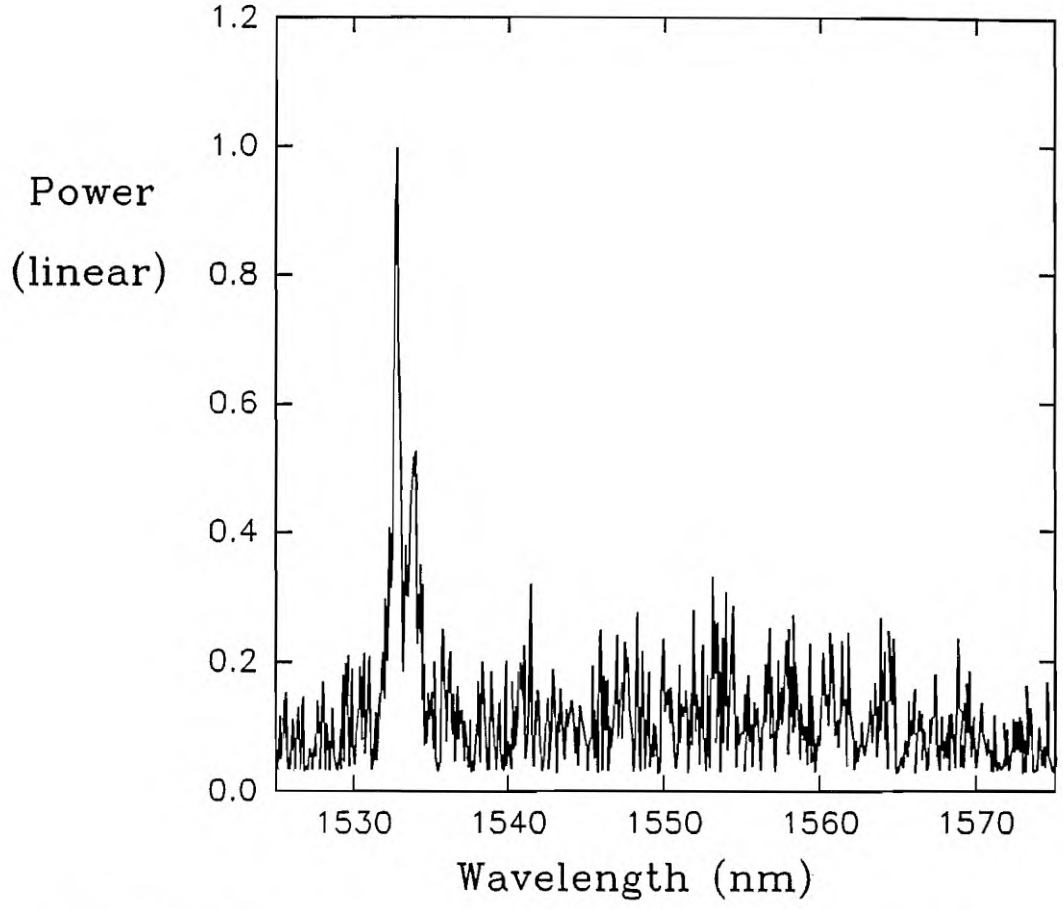

Figure 4.5 Reflection spectrum from photoresist DBR. Reflectivity 1.5%, Resolution 0.2nm.

4.2.3.4 Ion-beam Etching of DBR

The polishing and grating exposure steps as developed appear to be capable providing the required narrow-band reflection. In order to complete the device and enhance the reflectivity and durability, the corrugations in the photoresist are required to be transferred to the glass of the optical fibre. The development of this process has commenced, the technique being employed is reactive ion-beam etching (RIBE).

Reactive ion-beam etching is a dry, directional etching process by which a pattern photolithographically produced in photoresist can be transferred to a glass or other

similar material. In RIBE, surface atoms are removed by momentum transfer from directed ions and chemical reactions, with the photoresist acting as a mask. A glow-discharge plasma generates the etching environment consisting of positive and negative ions, electrons and radicals from a feed gas, in this case CHF_3. The material to be etched is placed on a high-frequency driven and dc-biased electrode. Chemical reactions occur at the silica surface with radicals from the freon gas to produce volatile species. Positive ions are accelerated across the plasma to remove material by sputtering. The combination of chemical reactions and the directionality of ion-beam sputtering result in high, anisotropic material erosion rates make this technique appropriate for etching the photoresist pattern into or close to a fibre core while achieving the appropriate resolution to etch patterns with $<0.5\mu$m features. In comparison, wet chemical etching tends to degrade the geometry of sub-micron features by undercutting and solution saturation effects [Darbyshire].

An etching process is being developed with an Oxford Instruments ion-beam etcher to transfer the photoresist grating close to the fibre core. An etch depth of 0.5-1μm is required. Once the grating has been transferred to the fibre, a thin high-index overlayer material will be deposited on the grating and an index-matching oil with index close to the cladding value used in top of the grating. With no overlayer material the field strength will be low at the core boundary containing the surface-relief grating. The overlayers will enhance the reflectivity, pulling the fibre mode up towards the grating [Rowe]. This process is currently being developed. Development of the process was initially stopped because attempts to perform reactive ion etching in a modified plasma sputtering machine failed to achieve sufficient etch resolution. Steps have started to re-characterise the process now that the Oxford Instruments ion-beam etcher has been delivered, and progress is expected shortly.

A schematic diagram of the DBR fabrication process is illustrated in Figure 4.6. Steps (a)-(e) have been completed, while step (f) is still under development.

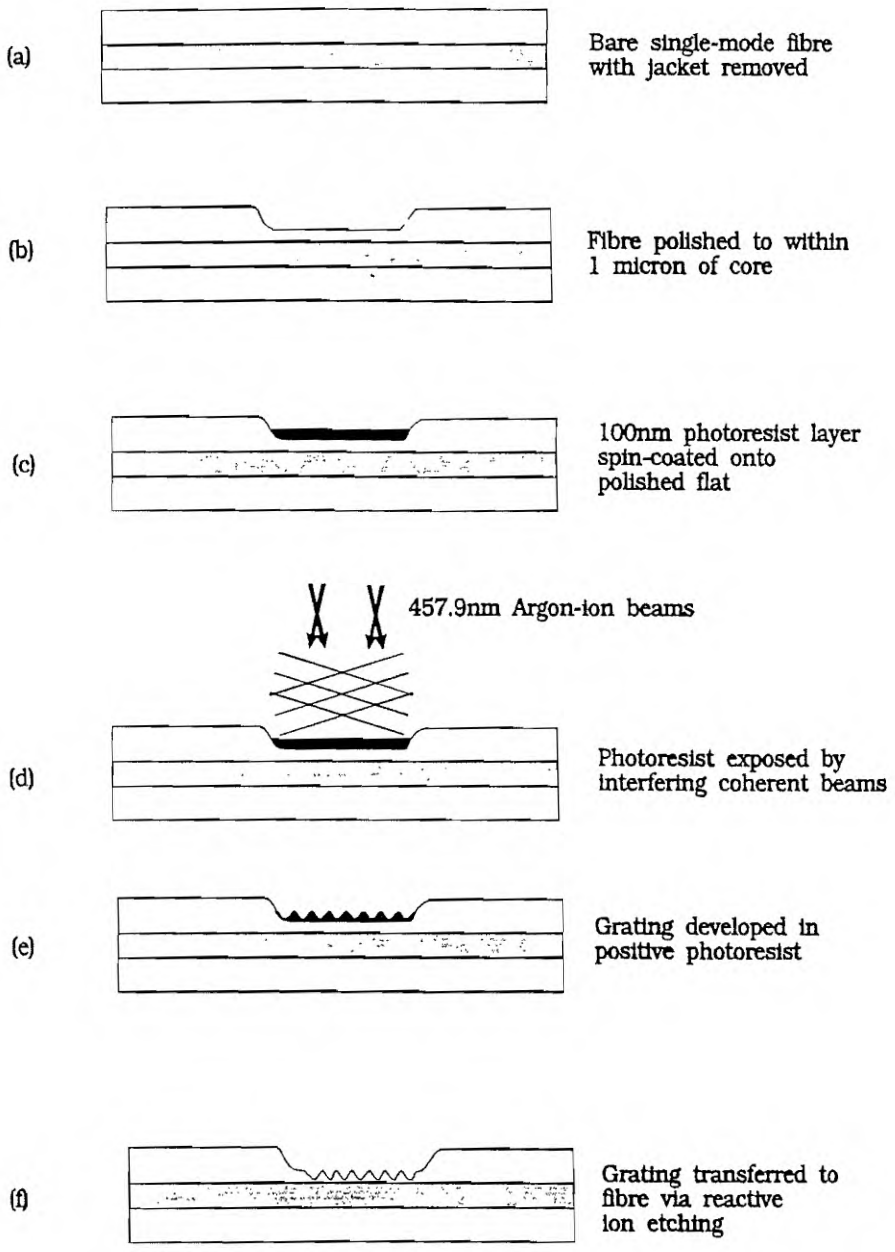

Figure 4.6 Process diagram of techniques used to fabricate narrow bandwidth distributed Bragg reflectors.

4.2.3.5 Summary

Narrow-bandwidth fibre DBRs are important devices for use in narrow-linewidth and single-longitudinal-mode erbium-doped fibre lasers. Section 4.2 has described progress towards the fabrication of narrow-bandwidth surface relief gratings with reflection bandwidths < 0.2nm. Towards this end, new fibre side-polishing techniques and actively-stabilised holographic exposure techniques have been developed to enable long, even interaction lengths required for narrow-bandwidth reflections. The development of the processes are not fully complete, the final step, which is still being developed, being reactive ion-beam etching of the photoresist pattern into the polished fibre surface.

Once complete these devices will enable single-frequency operation of erbium-doped fibre lasers, as described in Section 4.3. This type of resonator will provide selectable wavelength of operation via the grating pitch and stable wavelength operation. Other applications are likely to include wavelength selection in fibre lasers around 1.55μm and other wavelengths, and wavelength selectivity for wavelength division multiplexed communication systems and sensors. In addition the fabrication technology could easily be adapted for producing diffraction gratings on planar waveguide lasers, which may be of interest for active integrated optics devices [Mwaranai].

A comparison must be made between this technology for fabricating DBRs and the alternative technology of photorefractive DBRs [Meltz]. To fabricate photorefractive DBRs a refractive index grating is directly formed in a germania-doped fibre core by transverse holographic exposure to UV light. These devices may well supersede surface relief gratings for many applications, particularly a comparison of the fabrication techniques makes surface-relief gratings complex compared to photorefractive gratings. In contrast to the fabrication techniques previously outlined, photorefractive gratings can be produced noninvasively. Similar reflection properties are achievable in each technology [Ball]. One benefit to be gained from the surface-relief

grating is the resulting polarisation sensitivity which may be useful in laser resonators to produce single-frequency single-polarisation devices. The fabrication technology of surface-relief DBRs is applicable to alumino-silica, phospho-silica, phosphate and other multi-component glass fibres. Long term tests are required to determine whether photorefractive gratings are resilient to optical bleaching and will not degrade with time or temperature. Surface-relief gratings should remain robust without any degradation.

4.3 SHORT FIBRE LASERS WITH DBR REFLECTORS

4.3.1 Introduction

The simplest form of standing-wave single-longitudinal-mode laser is a short laser cavity in which the inter-mode spacing is large enough such that only one cavity mode can reach lasing threshold. This technique has been used effectively in many lasers systems, for example He-Ne gas lasers and many crystal lasers [Smith 1972]. These lasers, particularly gas lasers, have narrow gain bandwidths to make this technique viable. The width of the gain bandwidth and the long lengths normally required for efficient operation of fibre lasers mean that this simple technique is not feasible for single-frequency erbium-doped fibre lasers. Although a small degree of variation in gain bandwidth can be achieved by variation of the glass composition, it is not expected that a sufficiently small gain bandwidth could be achieved to enable efficient operation using a simple short fibre laser resonator. In order to make the technique feasible a filter needs to be incorporated into the laser to limit the bandwidth for which gain is possible, and one of the simplest forms this can take is the use of a frequency-selective reflector in the form of a DBR. The bandwidth of the laser is then limited to being within the reflection bandwidth of the Bragg reflector. The actual linewidth in the case of single-longitudinal-mode operation is much less

than that of the grating reflectivity, typically related to the Schawlow-Townes limit. This technique was demonstrated in a neodymium-doped fibre laser in 1988 by Jauncey et. al. [Jauncey 1988]. To demonstrate single-longitudinal-mode operation a very short length of doped fibre was used (5cm) in conjunction with a DBR with reflection bandwidth 0.8nm to achieve lasing with linewidth 1.3MHz FWHM at 1082nm.

In principle the technique of using a short cavity with a DBR can be directly applied to the Er^{3+}-doped fibre laser scheme, although in practice it is more difficult to achieve in the erbium system. The reasons for this, as explained in detail in previous chapters, are because of the difficulty in obtaining efficient erbium-doped fibres with high dopant concentrations. Consequently it is an exacting task to achieve a short erbium laser. Demonstrating this technique requires far greater selectivity from the DBR than was required from the DBR in the neodymium-doped laser with a 1.3MHz spectral width [Jauncey 1988]. The requirement for a longer laser in the erbium-doped fibre case will result in passive cavity modes with larger spacing. For these reasons the narrow-band DBRs as described in Section 4.2 are under development, to allow long(>50cm) fibre lengths to be used to achieve single-frequency operation.

4.3.2 Experimental Results

This section describes experiments carried out to characterise the performance of short erbium-doped fibre lasers incorporating DBRs. The DBR used in these experiments was fabricated by Plessey Research Caswell Ltd. The techniques described in section 4.2 were not sufficiently developed to enable fabrication of a suitable grating at the time these experiments were performed. The grating was manufactured by side-polishing a single-mode optical fibre mounted in a flat V-groove in a silica block and forming a relief grating on the polished flat so that the

evanescent field of the mode in the fibre interacts with the grating [Bennion]. The transmission characteristic of the grating is shown in Figure 4.7. The transmission characteristic was measured by passing a white-light signal through the grating and scanning the transmitted signal with a monochromator. The ripples in the transmission characteristic at wavelengths shorter than the reflection centre, as observed in Figure 4.7, are caused by coupling to leaky modes. Corresponding peaks in the reflection characteristic do not occur [Bennion]. Being an exposed-field device the reflection characteristics of this type of DBR are sensitive to the refractive index of the overlayer. The measurement was taken while the grating had an overlayer of index matching oil with index 1.416. The DBR with this overlayer exhibited a reflection centred at 1.5533μm with half power width $\sim$0.3nm.

In order to determine the modal characteristics and linewidth of a fibre laser incorporating the DBR, the grating was butt-joined to an erbium-doped fibre laser and a laser cavity formed with a dielectric mirror as indicated in Figure 4.8. The doped fibre used in these first measurements was a phospho-alumino-silicate fibre characterised by an Er^{3+} concentration of 800ppm, a NA of 0.15 and cut-off wavelength of λ_c=950nm. The fibre laser was pumped at 980nm by a Ti:sapphire laser and the fibre laser output measurements were taken from the signal transmitted through the DBR.

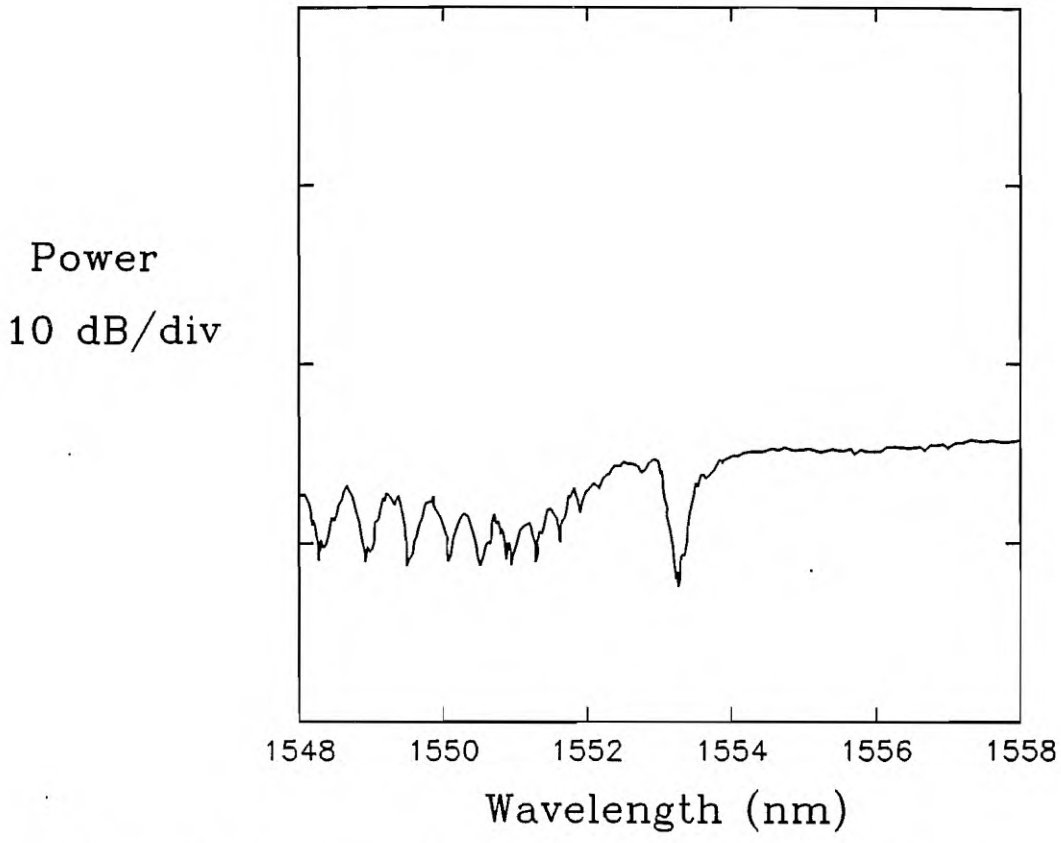

Figure 4.7 Transmission characteristic of DBR fabricated by Plessey Research Caswell Ltd. Reflection bandwidth 0.3nm FWHM, reflectivity 70%. (Resolution 0.1nm).

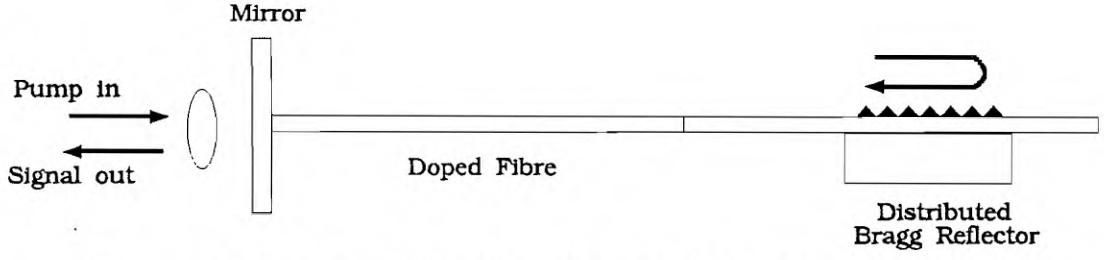

Figure 4.8 Experimental configuration of short erbium-doped fibre laser incorporating distributed Bragg reflector.

The modal behaviour and bandwidth of the laser were investigated for this resonator configuration. Initially a long length of doped fibre was used, and the length was progressively cut back, while monitoring the spectral characteristics. The laser length was thus decreased and the mode spacing increased. In reducing the length of doped fibre the gain and threshold behaviour of the laser are expected to change due to different population inversion properties arising from the three-level nature of the transition. Nevertheless the reflection bandwidth of the DBR will dominate in determining the bandwidth over which net gain will occur in the laser cavity and hence this technique should reveal useful information on the laser spectral width.

With an initial cavity length of 112cm, of which 25cm was the undoped fibre containing the DBR, the laser oscillated at the peak of the grating reflection as illustrated from the monochromator output illustrated in Figure 4.9. Passing the signal through a Fabry-Perot spectrum analyser, it was possible to resolve the number of modes in the cavity, spaced by 89MHz, illustrated in Figures 4.10 and 4.11. With 112cm cavity length the laser output consisted of about five modes with overall spectral width of 450MHz. Assuming the passive cavity spectral width is determined by the reflection characteristics of the DBR the spectral width of the laser is a reduction in the passive cavity width by a factor of about 100.

As the spectral width of the laser is dominated by the reflection response of the DBR, reducing the cavity length should result in fewer modes oscillating. To verify this behaviour the cavity length was progressively cut back in steps of about 90mm. In each measurement the length of the undoped fibre remained constant at 25cm. The mode spacing and the number of modes oscillating was observed to change. The behaviour is summarised in Table 4.I. Also shown in Table 4.I is the total width of the laser spectrum determined from the number of modes oscillating and the mode spacing. The total spectral width varies through the measurements by up to 25%, but this is explained by the precise spacing of the modes which depends on the cavity length. To a lesser extent variations in spectral width were due to variations in laser

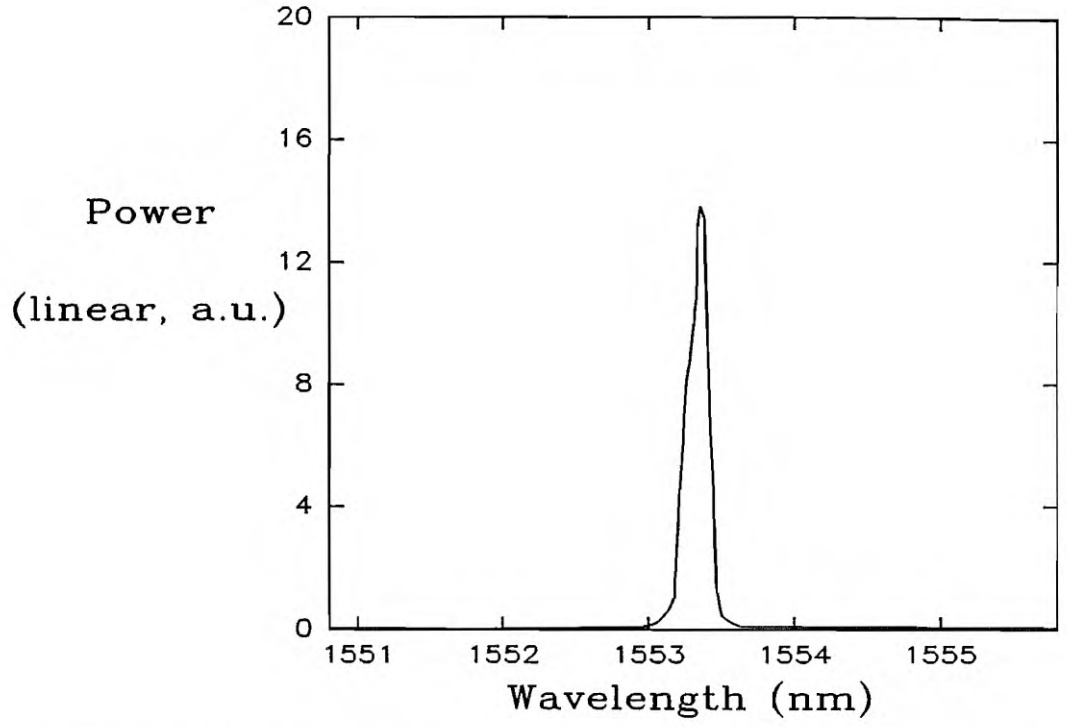

Figure 4.9 Narrow linewidth spectrum of DBR fibre laser, resonator length 112cm. (Resolution 0.1nm).

power due to gain reduction with decreasing doped fibre length. From this information it is possible to estimate the cavity length required for the laser to oscillate on only one longitudinal mode. Using this DBR with 0.3nm reflection bandwidth, a total cavity length of no more than 20cm is required.

In a three-level end-pumped laser there is an optimum cavity length to achieve minimum threshold, and as the cavity length decreases from the optimum length the threshold increases. The above measurements were performed with an Er^{3+}-doped fibre with a concentration of 800ppm for which the optimum length for minimum threshold was approximately 1 metre. The final measurement in the above set used a doped fibre length of 21cm and with the available pump power it was not possible to achieve threshold with a shorter length of this particular fibre. Consequently it was necessary to use a more highly-doped fibre as the lasing medium to achieve threshold

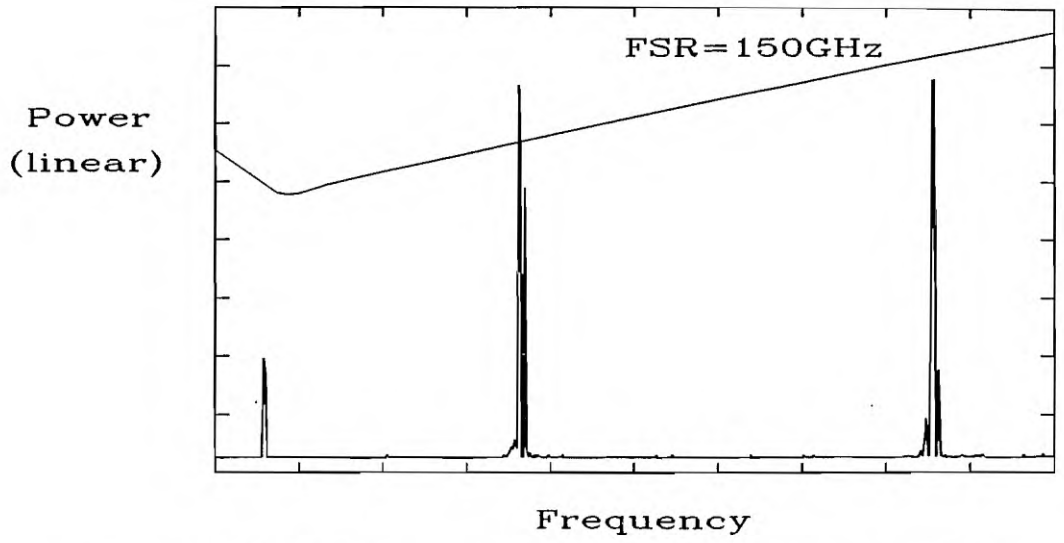

Figure 4.10 Modal structure of 112cm DBR fibre laser, determined from scanning Fabry-Perot spectrum analyzer,showing two free spectral ranges.

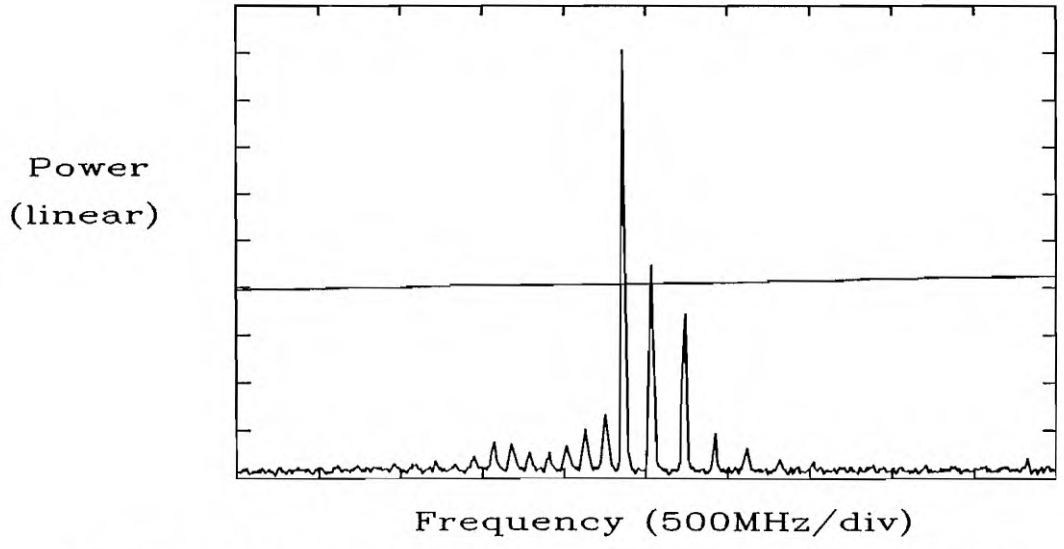

Figure 4.11 Detailed structure of one FSR of short DBR laser with 112cm resonator length.

with a shorter laser cavity length, the shorter length being expected to result in single-longitudinal-mode operation. The drawback from increasing the dopant concentration

doped fibre length (cm)	undoped fibre length (cm)	mode spacing (MHz)	number of modes	laser spectral width (MHz)
87	25	89	5	445
79	25	96	5	480
70	25	105	4	468
61	25	117	4	585
51	25	131	4	524
45	25	150	3	450
40	25	154	3	460
21	25	220	2	440
Er^{3+} conc	800ppm	NA 0.13	λ_c 950nm	

Table I Variation of modal behaviour for DBR laser as in Figure 4.5.

was, however, a reduction in efficiency, as discussed in Chapter 3.

In order to construct a shorter laser, a set of measurements were performed with several erbium-doped fibres with Er^{3+} concentrations of around 2000ppm. The first of these fibres, a phospho-alumino-silicate fibre with Er^{3+} concentration 2200ppm and NA 0.13, exhibited low-threshold operation for a doped fibre length of 12-15cm. With a 10cm length of this fibre butt-joined to the DBR as in Figure 4.8 and with a total resonator length of 15cm lasing was achieved with only one mode evident on the Fabry-Perot spectrum analyser. Single-frequency operation was realised as predicted by the cut-back measurements described above. However the laser output was not CW but instead exhibited undamped spiking behaviour.

To investigate the nature of this pulsing or spiking behaviour which became evident

only on short erbium fibre lasers with highly-doped fibre, measurements were performed using a variety of highly-doped fibres. One such fibre with Er^{3+} concentration of 2000ppm exhibited spiking behaviour for lengths less than about 30cm when a laser cavity was formed simply by butting the fibre ends against high-reflectivity dielectric mirrors. This behaviour indicated that the pulsing was not related to the use of a narrow-band reflector. It was also verified by placing an isolator on the laser output that the pulsing was not caused by non-linear feedback from the detector. The fibre length was progressively cut back and the behaviour monitored. The results of the measurements are illustrated in Figures 4.12-4.15. Figure 4.12 shows the periodic behaviour for constant pump power. The behaviour is characteristic of undamped relaxation oscillations. Rather than damped sinusoidal behaviour normally observed in erbium-doped fibre lasers, the pulsing is periodic with the intensity dropping to zero between pulses. The threshold for the onset of lasing in this pulsed operation is a function of the fibre length as would be expected for a three-level laser system. Figure 4.13 shows threshold behaviour for this fibre as a function of length. The peak power of the pulses increases with the length of the doped fibre as illustrated in Figure 4.13. This figure indicates that high peak powers are observed, significantly higher than normally observed with relaxation oscillations in erbium-doped fibre lasers in which the peak power during relaxation oscillations is typically less than twice the CW power. The peak powers observed are however much less than are observed in Q-switched or mode-locked operation. Figure 4.15 shows the variation of the maximum pulsation frequency with the doped fibre length, maximum frequency of pulsing occurring for the length showing minimum threshold.

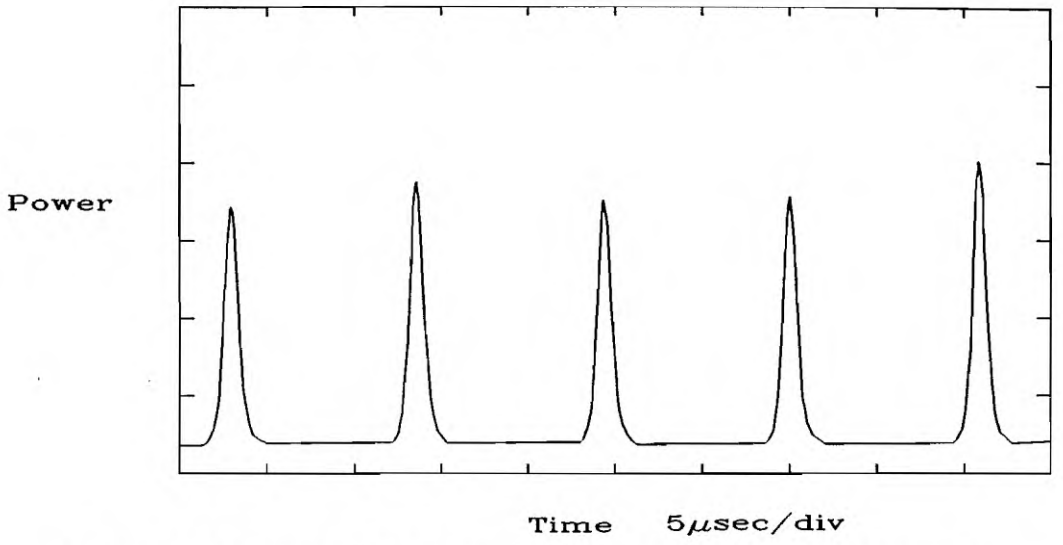

Figure 4.12 Temporal behaviour of short fibre laser spiking for cavity length 25cm. Note the sharp rise and fall of the pulses and that the power becomes zero between pulses.

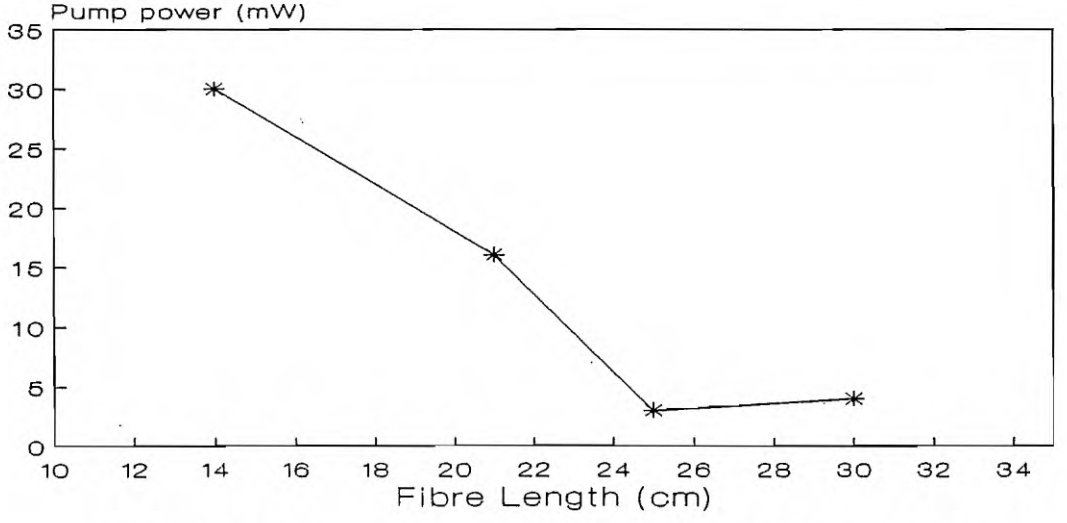

Figure 4.13 Variation of threshold for short laser spiking with fibre laser length. Dopant concentration 2000ppm.

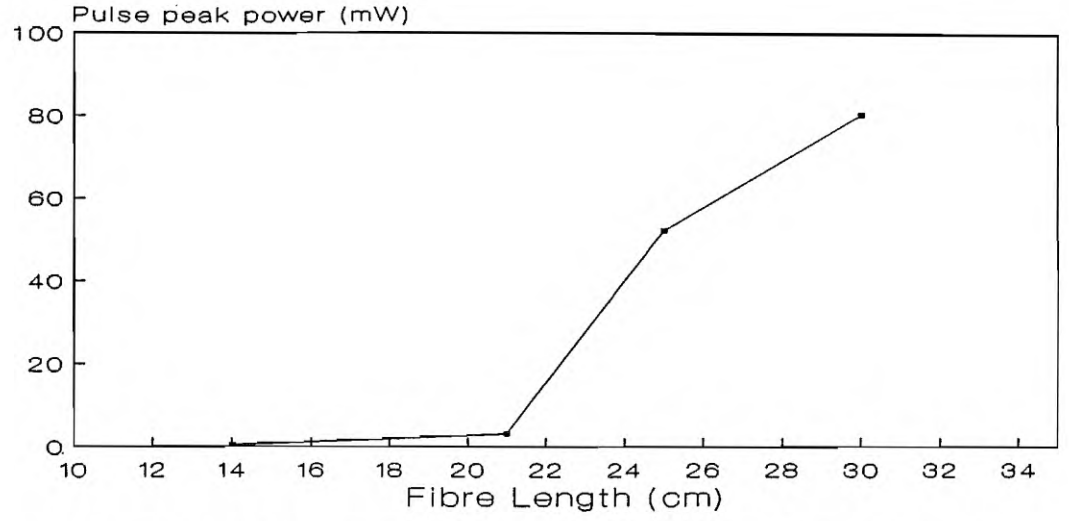

Figure 4.14 Variation of peak pulse power of short laser with cavity length. Mirror reflectivities 100% and 70%, Er^{3+} concentration 2000ppm.

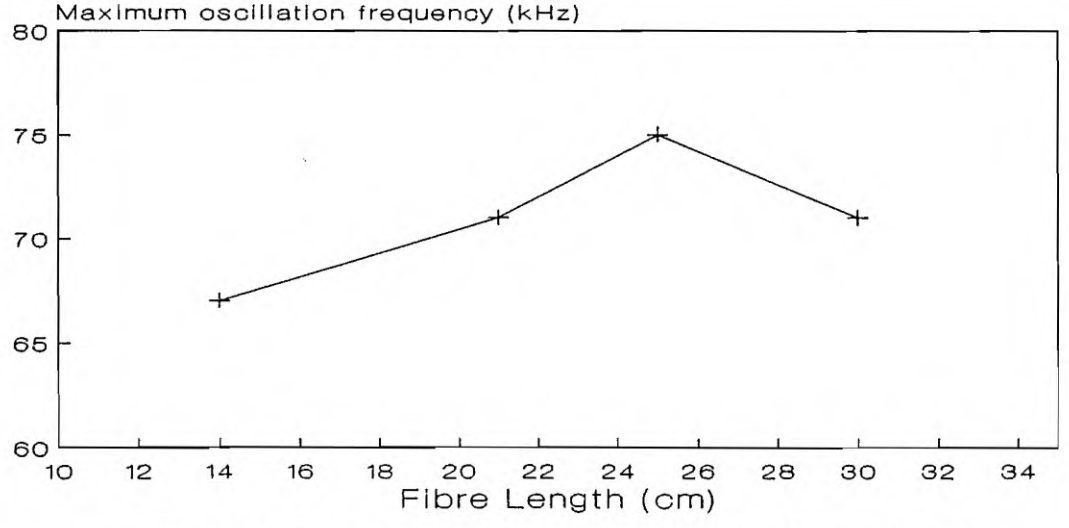

Figure 4.15 Variation of pulse repetition frequency of short fibre laser with resonator length. Mirror reflectivities 100%, 70%, Er^{3+} concentration 2000ppm.

The pulsing behaviour is thought to be spiking or undamped relaxation oscillations. Such behaviour has been observed in a variety of laser and maser systems, from early

in their development [Statz]. Further investigation is required to determine the exact cause of the observed behaviour, however the behaviour was only observed for very short fibre laser resonators which were pumped at 980nm.

Spiking is not a new phenomenon, being observed in the first ruby laser. In the ruby laser case however, the spiking was not regular as in the situation observed with the short fibre laser. Spiking or relaxation oscillations normally damp down in a decaying quasi-sinusoidal fashion [Siegman]. Spiking is normally observed only if the decay time of the population inversion is substantially longer than the cavity decay time, as is the case for the short Er^{3+}-doped fibre laser. Spiking can also be triggered by changes in the pump rate or changes in cavity losses. Strong spiking as observed with Er^{3+}-doped fibre lasers is consistent with the fluorescence decay being much slower than the cavity decay time.

Damped oscillations are normally observed because neither the cavity photon number or the population inversion drops to zero following a spike. The observed temporal behaviour of the short fibre laser resonator as illustrated in Figure 4.12 indicates that the photon number was zero, or very close to zero between pulses.

Although the undamped relaxation oscillations in the short fibre laser are not yet fully understood, the characteristics of the behaviour are that, firstly such behaviour only normally occurs for short resonator lengths, secondly the pulsing is undamped, and thirdly for short resonator length the behaviour is always exhibited even at low pump powers, although the pulse duration increases as the pump power is reduced.

With this evidence it is likely that the undamped behaviour is associated with the cavity decay time, which decreases as the cavity length is reduced. Spiking is also sensitive to pump modulation, and it is possible that as the population inversion is varied modulation in pump absorption occurs, leading to feedback in the pulsing cycle which drives the pulsing.

4.3.3 Summary

Single-frequency operation has been achieved using a short-resonator arrangement, however CW operation was not obtained due to operation in a regime of undamped relaxation oscillations. The short fibre with DBR reflector technique requires very narrow-band selectivity from the DBR. The 0.3nm reflection bandwidth used in these measurements was not sufficient. It is expected that once the DBRs described in Section 4.2 are fully developed, the short laser technique will result in single-frequency CW operation. It has recently been demonstrated with photorefractive DBRs that once sufficient wavelength selectivity is achieved this technique will result in single-frequency operation [Ball].

It is difficult to calculate the gain/loss differential between adjacent passive cavity modes required to ensure single-longitudinal-mode operation. The magnitude of the gain/loss differential is extremely small. However, empirical observations have been made on the amount of spectral filtering required to produce single-longitudinal-mode fibre laser operation. The results presented above and other reported results on single-frequency and narrow linewidth operation [Jauncey] [Jauncey 1988] [Reekie] indicate that to achieve single-frequency operation in a standing-wave resonator the passive cavity mode spacing must be such that less than 100 passive cavity modes fall within the passive cavity bandwidth. This will normally ensure that the gain/loss differential between adjacent modes is sufficient for the resonator to support only one mode above threshold. An empirical design rule to ensure single-longitudinal-mode operation would be for the resonator to be such that only 50 passive cavity modes fall within the passive cavity bandwidth.

4.4 COUPLED-CAVITY FIBRE LASERS

Complex resonator structures, often known as coupled-cavity lasers or multiple-mirror lasers, have been investigated in many types of laser systems. The resonance properties of such structures can be useful for several purposes, including spectral line-narrowing. Fibre Fox-Smith devices have been demonstrated as a method of producing narrow-line and single-longitudinal-mode oscillation in fibre lasers [Barnsley]. The use of a Fox-Smith resonator is a very well established technique for experimental laser configurations [Fox][Smith 1965]. The resonator increases the passive cavity mode spacing by using a coupled-cavity arrangement which requires phase matching for all coupled cavities for a resonance condition. As a result, the inter-mode spacing increases over that expected for a simple resonator of the same length. The mode spacing of the coupled cavity Fox-Smith resonator is determined by the difference in the individual cavity lengths. In principle, if the final cavity mode spacing is large enough, single-longitudinal-mode operation can be achieved. In a fibre laser however, because of the broad gain bandwidth, single-longitudinal-mode operation is difficult to achieve. By incorporating a diffraction grating as a reflector in a Fox-Smith cavity Barnsley et. al. demonstrated single-longitudinal-mode operation from a Fox-Smith fibre laser made with Er^{3+}-doped fibre. The laser, pumped by an Argon-ion laser, has a threshold of 175mW, slope efficiency 0.04% and linewidth <8.5MHz, in a resonator with coupled cavities with length almost one metre.

A characteristic of this laser configuration is that the two degenerate polarisation states exist in the single-mode fibre which constitutes the laser cavity and hence the laser can operate in two modes, orthogonally polarised. The following section describes a coupled-cavity configuration which operates by the interaction of orthogonally-polarised modes to produce single-polarisation narrow-line operation, and which with modification could eventually result in single-longitudinal-mode operation.

4.4.1 Polarimetric Coupled-Cavity Fibre Laser

Many applications of single-longitudinal-mode lasers require a single linear polarisation output, which a laser of the fibre Fox-Smith type demonstrated by Barnsley et. al. [Barnsley], does not, in general, produce. The fibre laser shown schematically in Figure 4.16 was designed in an attempt to produce a narrow-linewidth, single-polarisation output. The cavity is a Michelson-type resonator which utilises the birefringence of a high-birefringence (hi-bi) single-mode fibre to produce a cavity for which the two orthogonal polarisations have different optical path lengths. The two polarisations are mixed to produce an interferometric cavity by an intra-cavity polariser aligned at 45° to the polarisation axes if the hi-bi fibre.

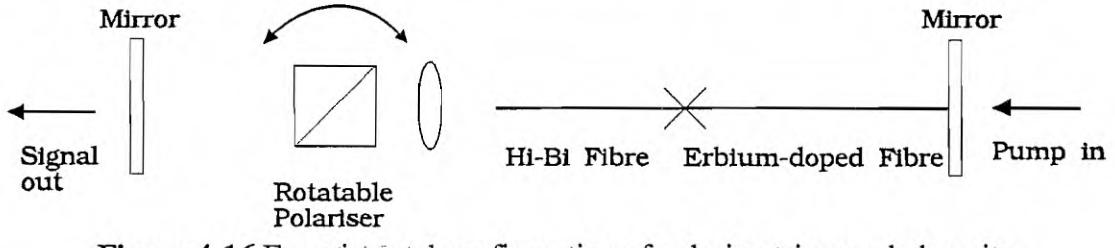

Figure 4.16 Experimental configuration of polarimetric coupled-cavity erbium-doped fibre laser.

4.4.2 Experimental Results

Experiments were performed with the system illustrated in Figure 4.16 to determine the spectral properties of the laser. The doped fibre had an Er^{3+} concentration of 800ppm and length 1.1 metres, while the undoped high-birefringence fibre, which was used in several lengths from 1.5 metres to 25 centimetres, had a beat length of 2mm. The beat length l_b is the fibre length such that $\delta\beta \times l_b = 2\pi$, where $\delta\beta$ is the difference in propagation constant between the fast and slow birefringence axes. The

fibre laser was pumped at 980nm from a Ti:sapphire laser. Observing the laser output with the use of a monochromator, narrow-line operation could be achieved by rotating the intra-cavity polariser to certain angles, which were at 45° to the birefringence axes. Narrow-line operation is illustrated in Figure 4.17 for the case when the length of hi-bi fibre was approximately 1 metre. As the intra-cavity polariser was rotated with respect to the hi-bi fibre axes, angles of the polariser at which single-line operation occurred were separated by 90°, confirming the operation of the polarimetric coupled-cavity. Between the angles at which single-line operation was observed, multi-line operation was evident. A sample of such a multi-line spectrum is illustrated in Figure 4.18. In this case, with the polariser misaligned for narrow-line operation, the spectral width is in excess of 2.5nm as distinct from the resolution limited (<0.1nm) spectrum observed with the polariser aligned for narrow-line operation. Observation of the spectrum within the single line of Figure 4.17 with a scanning Fabry-Perot spectrum analyser revealed fine structure, illustrated in Figure 4.19, illustrating that although the operation was narrow-linewidth it was nevertheless multi-longitudinal-mode. The spectral width in this case was less than 5GHz or 0.04nm. The spectral properties were investigated as the length of hi-bi fibre was shortened. The narrow-line behaviour was observed for several long lengths of high-birefringence fibre, but once the length became too short (<25cm) in became impossible to obtain narrow line operation using this resonator configuration. As will be seen in Section 4.4.3 where the resonator is modelled, the wavelength response has a longer period and less sharp filtering as the length of hi-bi fibre is reduced. The experimental observation was that eventually narrow-linewidth operation is not obtained with a short length of hi-bi fibre in the resonator.

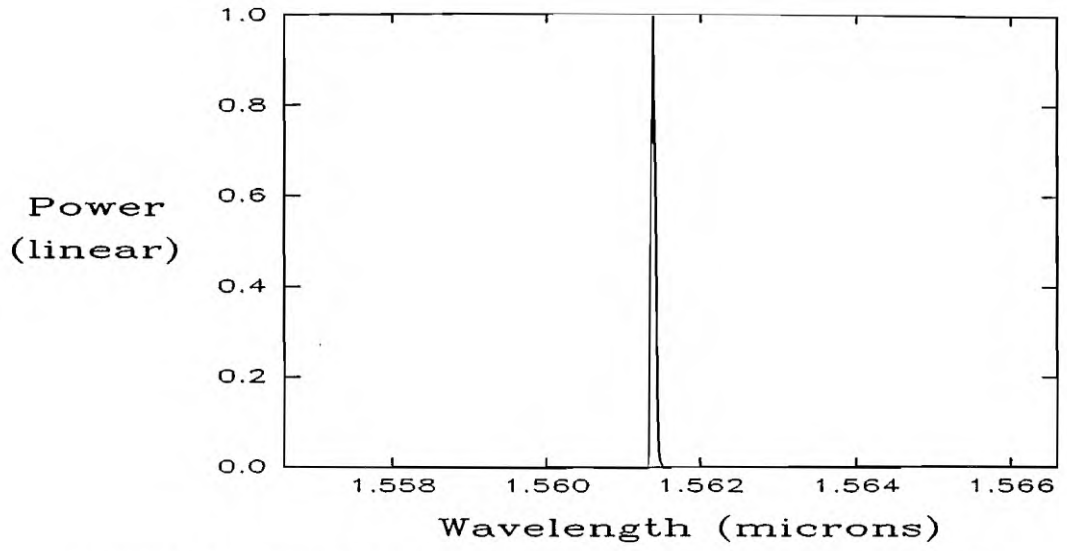

Figure 4.17 Narrow-linewidth operation of polarimetric coupled-cavity laser with intra-cavity polariser at 45° to hi-bi axes. Resolution 0.1nm.

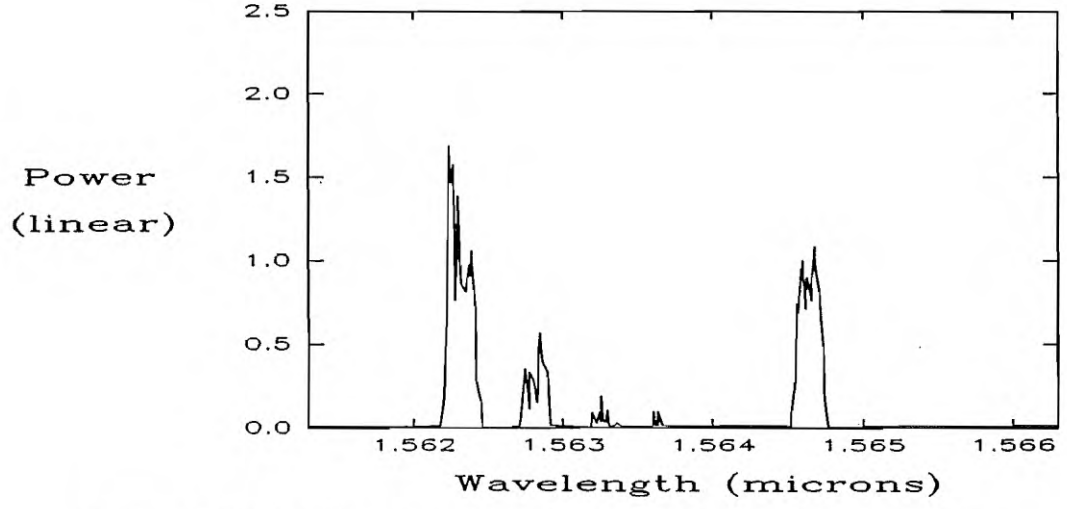

Figure 4.18 Multi-line operation of polarimetric coupled-cavity fibre laser with intra-cavity polariser misaligned for single-line operation. Resolution 0.1nm.

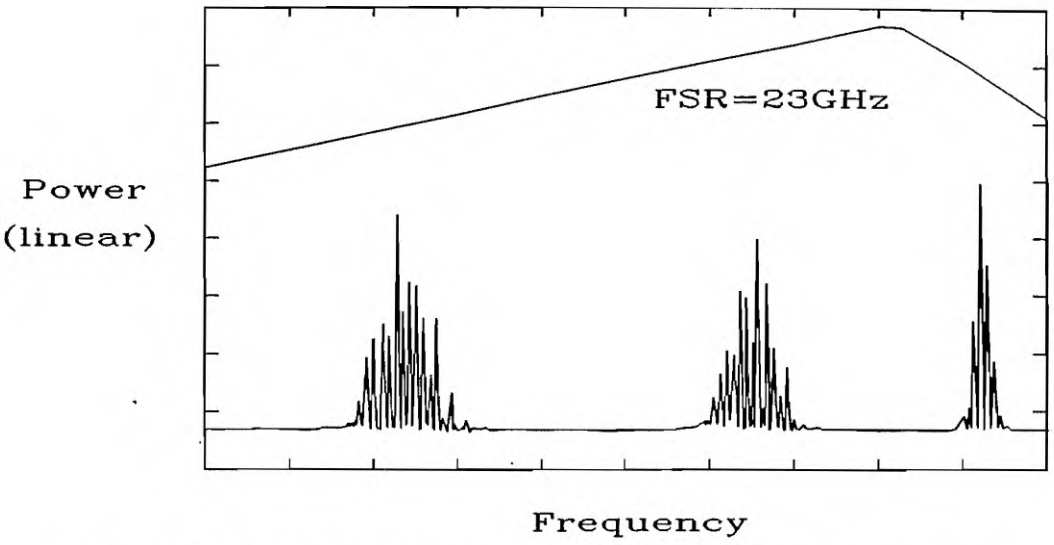

Figure 4.19 Polarimetric coupled-cavity fibre laser mode structure measured with Fabry-Perot spectrum analyzer, showing two free spectral ranges.

The polarimetric coupled-cavity erbium fibre laser can thus be seen to be an effective method of achieving narrow-linewidth operation, although single-frequency operation was not observed. Section 4.4.3 will model the resonator in order to determine whether this type of resonator is capable of achieving single-longitudinal-mode operation in erbium-doped fibre lasers.

4.4.3 Resonator Modelling

The wavelength selective action of the polarimetric resonator can be calculated by modelling the cavity with reference to the model illustrated in Figure 4.20. The cavity consists of a free-space path with length l_1, loss coefficient α_1 and propagation constant β_1, a length of fibre l_2 with loss coefficient α_2 and propagation constant β_2 (doped fibre in the experimental configuration) and a length l_3 of high-birefringence fibre with loss coefficient α_3 and propagation constants β_{3x} and β_{3y} in the X- and Y-

directions respectively. The resonator is completed by mirrors with reflectivities r_1 and r_2, with the input mirror having transmittance t_1.

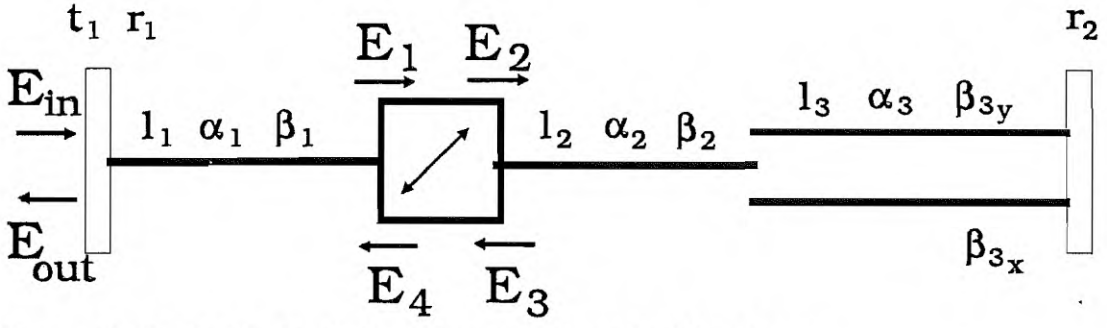

Figure 4.20 Model of polarimetric coupled-cavity fibre laser.

The electric fields of the light are represented by Jones vectors with basis vectors aligned with the orthogonal birefringence axes of the hi-bi fibre. The polariser is aligned at 45° to the orthogonal birefringence axes. The wavelength selectivity of the hi-bi fibre can be seen in single-pass operation by ignoring the effect of the input reflectance r_1, that is, $r_1=0$.

To simplify the calculations, the input signal E_{in} is assumed to be aligned with the polariser which is set 45° to the birefringence axes. In Jones vector notation [Azzam] [Shircliff] the two components are hence of equal strength:

$$\underline{E_{in}} = \begin{bmatrix} E_{in} \\ E_{in} \end{bmatrix} \tag{4}$$

The fields are calculated entering and leaving the intra-cavity polariser. The field at the polariser after passing through the air path is:

$$\underline{E_1} = \begin{bmatrix} e^{(-\alpha_1+j\beta_1)l_1} & 0 \\ 0 & e^{-\alpha_1+j\beta_1)l_1} \end{bmatrix} \begin{bmatrix} E_{in} \\ E_{in} \end{bmatrix} = \begin{bmatrix} E_{in}e^{(-\alpha_1+j\beta_1)l_1} \\ E_{in}e^{(-\alpha_1+j\beta_1)l_1} \end{bmatrix} \quad (5)$$

The Jones matrix representation of a polariser oriented at an angle α to the X axis is:

$$T = \begin{bmatrix} \cos^2\alpha & \sin\alpha\cos\alpha \\ \sin\alpha\cos\alpha & \sin^2\alpha \end{bmatrix} \quad (6)$$

Hence with the polariser aligned such that $\alpha=45°$ the field after passing through the polariser is:

$$\underline{E_2} = \begin{bmatrix} 0.5 & 0.5 \\ 0.5 & 0.5 \end{bmatrix} \begin{bmatrix} E_{in}e^{(-\alpha_1+j\beta_1)l_1} \\ E_{in}e^{(-\alpha_1+j\beta_1)l_1} \end{bmatrix} = \begin{bmatrix} E_{in}e^{(-\alpha_1+j\beta_1)l_1} \\ E_{in}e^{(-\alpha_1+j\beta_1)l_1} \end{bmatrix} \quad (7)$$

After passing through the length l_2 of fibre with propagation constant β_2 the field becomes:

$$\underline{E_{2'}} = \begin{bmatrix} E_{in}e^{(-\alpha_1+j\beta_1)l_1+(-\alpha_2+j\beta_2)l_2} \\ E_{in}e^{(-\alpha_1+j\beta_1)l_1+(-\alpha_2+j\beta_2)l_2} \end{bmatrix} \quad (8)$$

The field then twice traverses a hi-bi fibre with propagation constants β_{3x}, β_{3y} in the X,Y directions respectively and with length l_3. The field is then:

$$\underline{E_{2//}} = \begin{bmatrix} r_2 E_{in} e^{(-\alpha_1 + j\beta_1)l_1 + (-\alpha_2 + j\beta_2)l_2 + (-\alpha_3 + j\beta_{3y})2l_3} \\ r_2 E_{in} e^{(-\alpha_1 + j\beta_1)l_1 + (-\alpha_2 + j\beta_2)l_2 + (-\alpha_3 + j\beta_{3x})2l_3} \end{bmatrix} \quad (9)$$

The field returning to the polariser passes again through the undoped fibre and is of the form:

$$\underline{E_3} = \begin{bmatrix} r_2 E_{in} e^{(-\alpha_1 + j\beta_1)l_1 + (-\alpha_2 + j\beta_2)2l_2 + (-\alpha_3 + j\beta_{3y})2l_3} \\ r_2 E_{in} e^{(-\alpha_1 + j\beta_1)L_1 + (-\alpha_2 + j\beta_2)2l_2 + (-\alpha_3 + j\beta_{3x})2l_3} \end{bmatrix} \quad (10)$$

The field passed by the polariser becomes:

$$\begin{aligned} \underline{E_4} &= \begin{bmatrix} 0.5 & 0.5 \\ 0.5 & 0.5 \end{bmatrix} \begin{bmatrix} r_2 E_{in} e^{(-\alpha_1 + j\beta_1)l_1 + (-\alpha_2 + j\beta_2)2l_2 + (-\alpha_3 + j\beta_{3y})2l_3} \\ r_2 E_{in} e^{(-\alpha_1 + j\beta_1)l_1 + (-\alpha_2 + j\beta_2)2l_2 + (-\alpha_3 + j\beta_{3x})2l_3} \end{bmatrix} \\ &= \begin{bmatrix} 0.5 r_2 E_{in} \left(e^{(-\alpha_1 + j\beta_1)l_1 + (-\alpha_2 + j\beta_2)2l_2}\right)\left(e^{(-\alpha_3 + j\beta_{3y})2l_3} + e^{(-\alpha_3 + j\beta_{3x})2l_3}\right) \\ 0.5 r_2 E_{in} \left(e^{(-\alpha_1 + j\beta_1)l_1 + (-\alpha_2 + j\beta_2)2l_2}\right)\left(e^{(-\alpha_3 + j\beta_{3y})2l_3} + e^{(-\alpha_3 + j\beta_{3x})2l_3}\right) \end{bmatrix} \end{aligned} \quad (11)$$

The output field thus takes the form:

$$\underline{E_{out}} = \begin{bmatrix} 0.5 r_2 t_1 E_{in} \left(e^{(-\alpha_1 + j\beta_1)2l_1 + (-\alpha_2 + j\beta_2)2l_2}\right)\left(e^{(-\alpha_3 + j\beta_{3y})2l_3} + e^{(-\alpha_3 + j\beta_{3x})2l_3}\right) \\ 0.5 r_2 t_1 E_{in} \left(e^{(-\alpha_1 + j\beta_1)2l_1 + (-\alpha_2 + j\beta_2)2l_2}\right)\left(e^{(-\alpha_3 + j\beta_{3y})2l_3} + e^{(-\alpha_3 + j\beta_{3x})2l_3}\right) \end{bmatrix} \quad (12)$$

The output field is, as would be expected, linearly polarised at 45° to the X-axis, the angle of the polariser. The output intensity I_{out} of this linearly polarised beam can be calculated to be:

$$
\begin{aligned}
I_{out} &= E_{out}^{*} E_{out} \\
&= e^{-4(\alpha_1 l_1 + \alpha_2 l_2 + \alpha_3 l_3)} \left(2 + 2\cos 2 l_3 (\beta_{3x} - \beta_{3y})\right) \\
&= 2e^{-4(\alpha_1 l_1 + \alpha_2 l_2 + \alpha_3 l_3)} \left(1 + \cos\left(\frac{4\pi l_3}{\lambda_0}(n_x - n_y)\right)\right)
\end{aligned}
\tag{13}
$$

where λ_0 is the free-space wavelength and n_x, n_y are the effective refractive indices if the X- and Y-polarisation states.

From Equation 4.13 it can be seen that at a given wavelength of operation the wavelength selectivity of the response depends only on the length of the hi-bi fibre and the birefringence on the fibre. The wavelength filtering is periodic with wavelength, with the period becoming shorter with increasing length of the hi-bi fibre or increasing birefringence. The behaviour is illustrated in Figures 4.21 and 4.22 for parameters approximately matching the experimental conditions. Figure 4.21 shows the wavelength selectivity for a given value of birefringence and for three values of hi-bi fibre length. As illustrated the response becomes sharper as the length increases. This illustrates an experimental observation that once the length of hi-bi fibre became too short the response was no longer seen to be 'narrow-line'. Although only a fixed birefringence was possible in the experimental configuration, Figure 4.22, in which the filtering response is plotted for a fixed fibre length and for different values of birefringence, illustrates the sharpening of the filter response which could be achieved if it were possible to increase the birefringence in the hi-bi fibre. The values of birefringence in Figure 4.22 correspond to beat lengths of approximately 2mm, 1mm and 0.4mm.

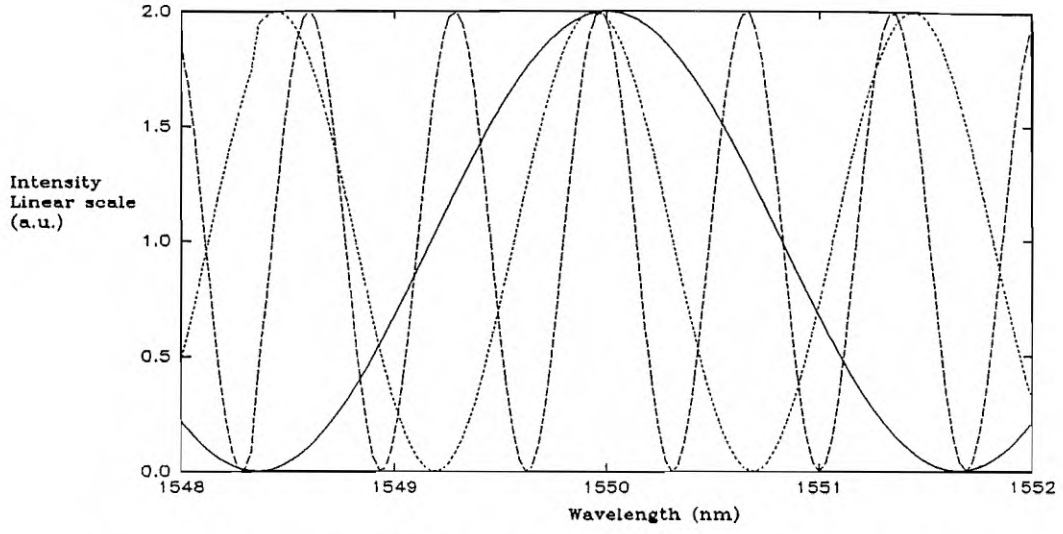

Figure 4.21 Wavelength filtering of polarimetric coupled cavity laser as hi-bi fibre length varied. $n_y=1.001n_x$, $l_3=0.25$m(solid),0.55m(dotted),1,2m(dashed).

The preceding calculations give the wavelength response without taking into account the individual modal structure. That is, the wavelength filtering was calculated from a double-pass analysis. In order to determine the cavity response including the modal behaviour of the resonator the complex amplitudes of the cavity fields must be equated with the incorporation of round-trip feedback. Using the model illustrated in Figure 4.20 the complex amplitudes of the resonator fields can be set up by taking $0<r_1<1$. The input field $\underline{E}_{in}$ is again modelled as a Jones vector linearly polarised at 45° to the birefringence axes:

$$\underline{E_{in}} = \begin{bmatrix} E_{in_y} \\ E_{in_x} \end{bmatrix} \tag{14}$$

with basis vectors aligned to the polarisation axes of the hi-bi fibre. The polariser is again assumed to be aligned at 45° to the axes of the hi-bi fibre. The complex amplitude equations of the fields entering and leaving the polariser can be written:

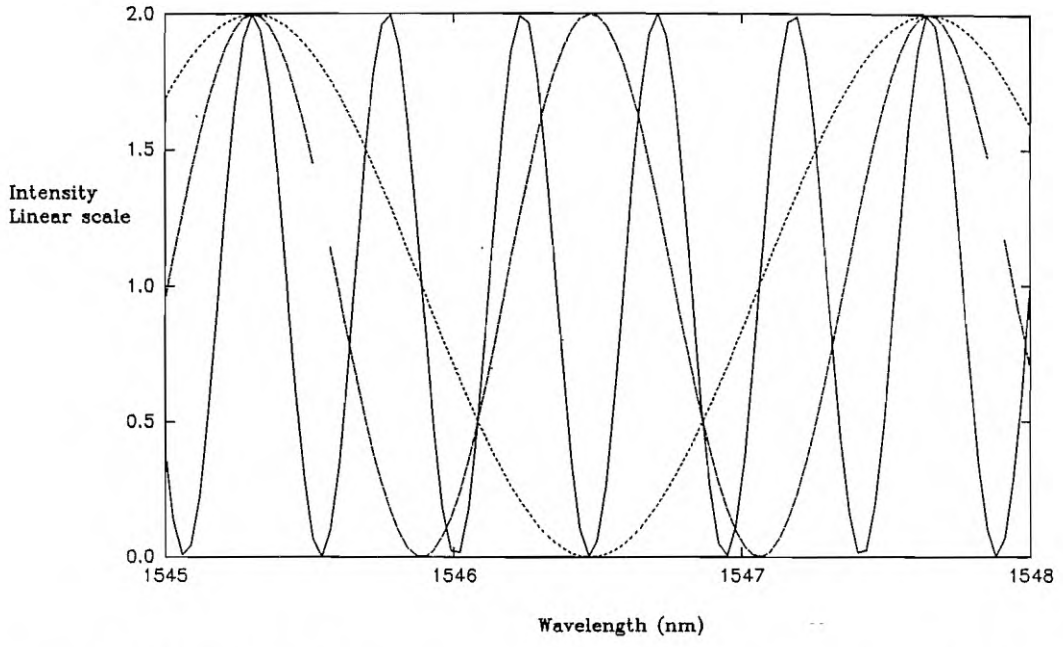

Figure 4.22 Wavelength filtering action of polarimetric coupled cavity fibre laser as birefringence varies. l_3=0.35m, n_y=1.001n_x(dotted),1.002n_x(dash),1,005n_x(solid).

$$\underline{E_1} = t_1 e^{(-\alpha_1+j\beta_1)l_1}\underline{E_{in}} + r_1 e^{(-\alpha_1+j\beta_1)2l_1}\underline{E_4} = \begin{bmatrix} E_{1_y} \\ E_{1_x} \end{bmatrix} \tag{15}$$

$$\underline{E_2} = \begin{bmatrix} 0.5 & 0.5 \\ 0.5 & 0.5 \end{bmatrix}\underline{E_1} = \begin{bmatrix} E_{2_y} \\ E_{2_x} \end{bmatrix} \tag{16}$$

$$\underline{E_3} = \begin{bmatrix} r_2 e^{(-\alpha_2+j\beta_2)2l_2} e^{(-\alpha_3+j\beta_{3_y})2l_3} & 0 \\ 0 & r_2 e^{(-\alpha_2+j\beta_2)2l_2} e^{(-\alpha_3+j\beta_{3_x})2l_3} \end{bmatrix}\begin{bmatrix} E_{2_y} \\ E_{2_x} \end{bmatrix} = \begin{bmatrix} E_{3_y} \\ E_{3_x} \end{bmatrix} \tag{17}$$

$$\underline{E_4} = \begin{bmatrix} 0.5 & 0.5 \\ 0.5 & 0.5 \end{bmatrix} \begin{bmatrix} \underline{E_3} \end{bmatrix} = \begin{bmatrix} E_{4_y} \\ E_{4_x} \end{bmatrix} \tag{18}$$

while the output $\underline{E}_{out}$ is related to $\underline{E}_4$ by:

$$\underline{E_{out}} = t_1 e^{j\beta_1 l_1} \begin{bmatrix} \underline{E_4} \end{bmatrix} \tag{19}$$

The analysis can be simplified by dropping the α_i loss terms and by noting that if the input signal is aligned with the polariser, which is aligned at 45° to the birefringence axes, the amplitudes of the fields in each birefringence axis will be identical. With these assumptions $\underline{E}_4$ can be expressed as:

$$\underline{E_4} = \begin{bmatrix} \frac{1}{2} r_2 e^{j\beta_2 2l_2} e^{j\beta_1 l_1} \left(t_1 E_{in} + r_1 e^{j\beta_1 l_1} E_4 \right) \left(e^{j\beta_{3_y} 2l_3} + e^{j\beta_{3_x} 2l_3} \right) \\ \frac{1}{2} r_2 e^{j\beta_2 2l_3} e^{j\beta_1 l_1} \left(t_1 E_{in} + r_1 e^{j\beta_1 l_1} E_4 \right) \left(e^{j\beta_{3_y} 2l_3} + e^{j\beta_{3_x} 2l_3} \right) \end{bmatrix} \tag{20}$$

Thus the transfer function of the electric field of the resonator, polarised at 45° to the hi-bi fibre axes, becomes:

$$\frac{E_{out}}{E_{in}} = \frac{\frac{1}{2} r_2 t_1^2 e^{j\beta_1 2l_1} e^{j\beta_2 2l_2} \left(e^{j\beta_{3_y} 2l_3} + e^{j\beta_{3_x} 2l_3} \right)}{1 - \frac{1}{2} r_2 r_1 e^{j\beta_2 2l_2} e^{j\beta_1 2l_1} \left(e^{j\beta_{3_y} 2l_3} + e^{j\beta_{3_x} 2l_3} \right)} \tag{21}$$

The intensity of the transfer function is obtained by the usual method of multiplying the complex conjugate of the transfer function of Equation 4.21 by the transfer function itself to obtain:

$$\frac{I_{out}}{I_{in}} \propto \frac{\frac{1}{2}r_2^2 t_1^4\left(1+\cos\frac{4\pi l_3}{\lambda_0}(n_x-n_y)\right)}{1+\frac{1}{2}r_1^2r_2^2-r_2r_1\left(\cos\frac{4\pi}{\lambda_0}(l_1+nl_2+n_yl_3)+\cos\frac{4\pi}{\lambda_0}(l_1+nl_2+n_xl_3)\right)+\frac{1}{2}r_1^2r_2^2\cos\frac{4\pi l_3}{\lambda_0}(n_x-n_y)} \quad (22)$$

The numerator of Equation 4.22 represents the wavelength selectivity of the resonator and is identical to Equation 4.13 (ignoring the loss term) while the denominator describes the modal structure of the transfer function spectrum.

The modal structure calculated from Equation 4.22 for the passive resonator is illustrated in Figure 4.23 with constants approximating the experimental conditions. The modal structure contains the periodic wavelength filtering into which fits the modal structure. Each wavelength peak contains many passive cavity modes. The actual passive cavity mode spacing is narrower than that indicated in Figure 4.23, the 'mode spacing' indicated in Figure 4.23 results from aliasing between the actual mode spacing and the wavelength steps used when calculating the response. The envelope of the cavity response is however correct. On a finer wavelength scale the actual mode spacing can be plotted as illustrated in Figure 4.24, where the wavelength range corresponds to one of the peaks in the wavelength response shown in Figure 4.23.

Figure 4.23 does however serve to illustrate the problems which occur in trying to extend the polarimetric coupled-cavity laser from narrow line operation to single-frequency operation. The wavelength peaks could be sharpened by increasing the length of hi-bi fibre, but the passive cavity mode spacing is proportional to the cavity length and hence increasing the length of high-birefringence fibre would also result in closer mode spacing. The wavelength selectivity would be improved by sharpening the response but the number of modes oscillating not significantly altered because of their closer spacing. A solution would be to use a material with more birefringence, but significantly increased birefringence would not be possible using hi-bi fibre. A

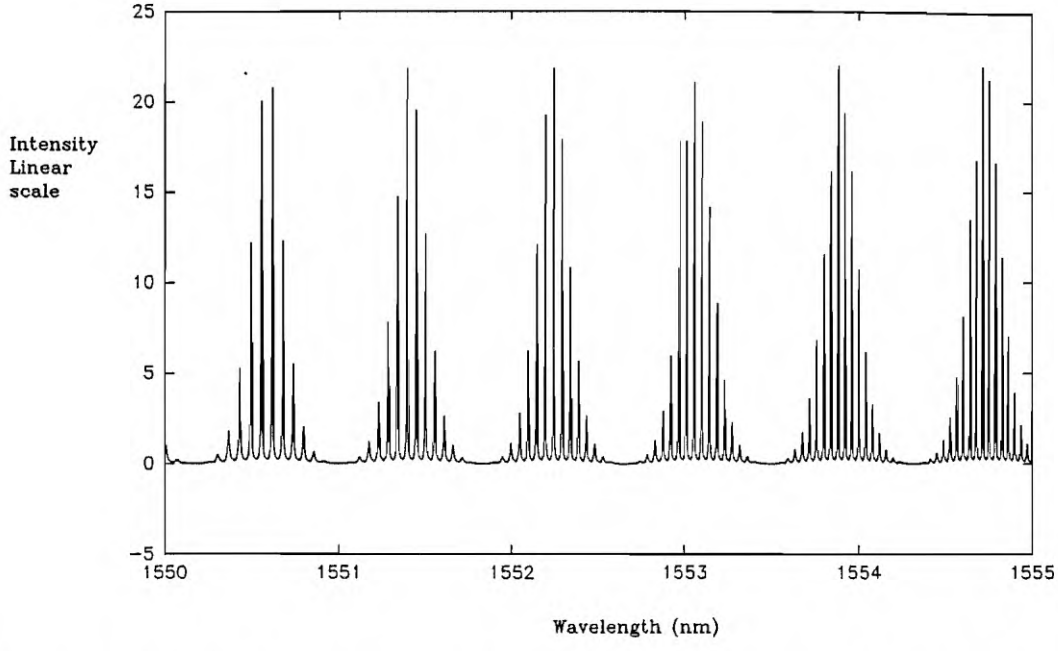

Figure 4.23 Modal structure of polarimetric coupled-cavity laser. Simulation constants: $n_2=n_{3x}=1.456$, $n_{3y}=n_{3x}\times 1.001$, $r_1=r_2=0.9$, $l_1=0.2$m, $l_2=0.5$m, $l_3=1$m.

bulk material such as calcite could be used in the resonator to improve the modal structure, however this would be at the expense of the fibre-based resonator.

4.5 SUMMARY AND CONCLUSIONS

This chapter has been concerned with the experimental development and characterisation of standing-wave fibre lasers, and devices for narrow-linewidth operation. Section 4.2 detailed the development of narrow-bandwidth distributed Bragg reflectors, important devices for line-narrowing the spectral width of fibre lasers. Although the development of these devices is not fully complete, significant progress has been made to demonstrate very narrow bandwidth reflections (<0.2nm) from weak DBRs. Narrow-bandwidth reflections have been achieved by producing

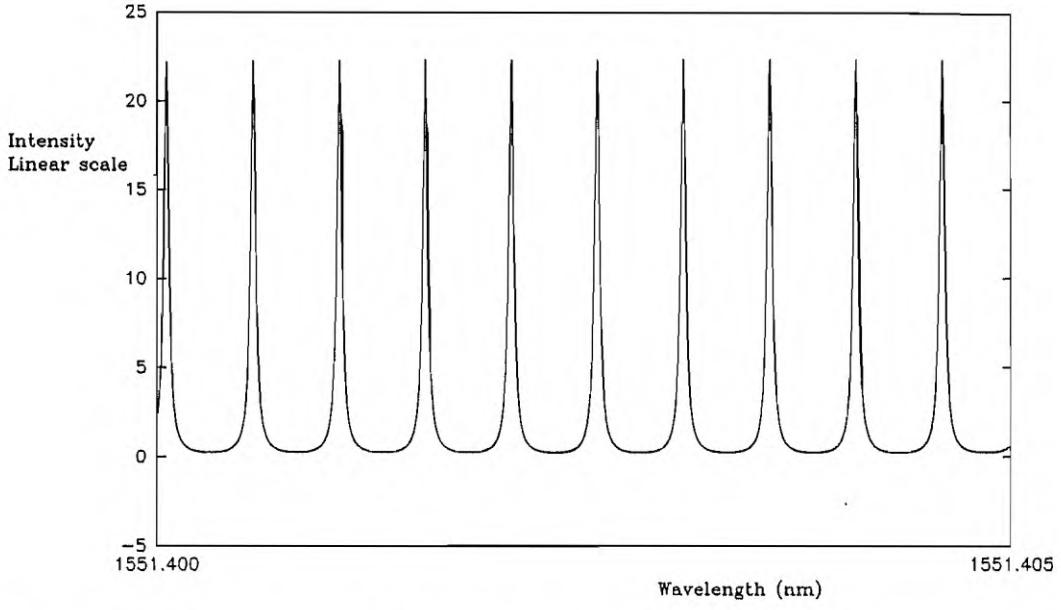

Figure 4.24 Individual mode structure at peak of wavelength transmission of polarimetric coupled-cavity laser. Simulation values as in Figure 4.23.

a long interaction region and an even grating. Details of fibre side-polishing and holographic photolithography were described. It is expected that ion-beam etching of the photoresist grating will enhance the reflectivity of the DBR, and further work is continuing to improve the reflectivity of the devices via reactive ion-beam etching of the grating into or close to the fibre core.

Section 4.3 characterised the modal properties of short fibre lasers incorporating DBRs for narrow-bandwidth feedback. Although single-longitudinal-mode operation was achieved, a problem with undamped relaxation oscillations was identified, which prevented CW lasing. Various techniques for overcoming this problem were identified, including pumping the laser into a different pump level and utilising a Yb/Er co-doped fibre. This technique of a short resonator with DBR requires highly-selective DBRs and will become viable once the DBRs detailed in Section 4.2 are available. Empirical observations have been made as to the spectral filtering required to produce single-longitudinal-mode operation in standing-wave resonators. As a

design consideration for single-frequency operation the passive cavity mode spacing must be such that only about 50 passive cavity modes fall within the passive cavity bandwidth.

Section 4.4 described and characterised an novel coupled-cavity arrangement for realising narrow-linewidth operation in the 1.5μm region. The Michelson resonator was arranged to have coupled cavities by the interaction of orthogonal polarisations in a high-birefringence single-mode fibre. Although multi-mode, a spectral width of less than 5GHz or 0.04nm was achieved.

Many of the problems associated with standing-wave resonators and their application to single-frequency erbium-doped fibre lasers arise from the long resonator lengths which are necessary for good efficiency from the erbium-doped fibres. The long resonator length required for good efficiency leads to close mode spacing, thus requiring very selective standing-wave resonators to achieve single-longitudinal-mode operation. Chapter 5 presents successful techniques for overcoming this length and efficiency problem, by operating the resonator as a travelling-wave resonator instead of a standing-wave resonator. Once travelling-wave operation is achieved the length of the resonator is not important for mode selection and does not affect modal properties.

Two useful results which have been demonstrated recently for standing-wave erbium-doped fibre lasers are a complex coupled-cavity arrangement [Gilbert] and a standing-wave resonator incorporating photorefractive DBRs [Ball]. In the standing-wave arrangement demonstrated by Gilbert, multiple coupled cavities and a grating set for Littrow conditions were used to achieve single-frequency operation with linewidth less than 1.6MHz. The complex nature of this arrangement illustrates the type of resonator often required to achieve single-frequency operation in the erbium-doped fibre system. The second important result [Ball] achieved single frequency operation in a short (50cm) erbium-doped fibre onto both ends of which was incorporated very narrow-

band photorefractive DBRs. A linewidth less than 47kHz was achieved. This result illustrates the long interaction length from gratings required for this application, the target lengths were in Ball's case 12.5mm.

4.6 REFERENCES

Azzam, R.M. and Bachara, N.M., *Ellipsometry and Polarised Light*, North-Holland Publishing Company, Amsterdam, 1977.

Ball, G.A., Morey, W.W. and Glenn, W.H., "Standing-Wave Monomode Erbium Fiber Laser," *IEEE Phot. Tech. Lett.*, **3**, 7, pp. 613-615, July 1991.

Barnsley, P., Urquhart, P., Millar, C. and Brierley, M., "Fiber Fox-Smith Resonators: Application to Single-Longitudinal-Mode Operation of Fiber Lasers," *J. Opt. Soc. Am. A.*, **5**, 8, pp. 1339-1346, Aug. 1988.

Bennion, I., Reid, D.C.J., Rowe, C.J. and Stewart, W.J., "High-reflectivity Monomode Fibre Grating Filters," *El. Lett.*, **22**, pp. 341-343, 1986.

Darbyshire, D.A., Overbury, A.P. and Pitt, C.W., "Ion and Plasma Assisted Etching of Holographic Gratings", Vacuum, **36**, pp. 55-60, 1986.

Fox, A.G., "Optical maser mode selector," U.S. Patent 3 504 299.

Gilbert, S.L., "Frequency Stabilisation of a Tunable Erbium-doped Fiber Laser," *Opt. Lett.*, **16**, 3, pp. 150-152, Feb. 1991.

Goodman, J.W., *Statistical Optics*, John Wiley & Sons, New York, 1985.

Hussey, C.D. and Minelly, J.D., "Optical Fibre Polishing with a Motor-driven Polishing Wheel," *El. Lett.*, **24**, pp. 805-807, June 1988.

Jauncey, I.M., Reekie, L., Mears, R.J. and Rowe, C.J., "Narrow-linewidth Fibre Laser Operating at 1.55μm," *Opt. Lett.*, **12**, pp. 164- Mar. 1987.

Jauncey, I,M., Reekie, L., Townsend, J.E., Payne, D.N. and Rowe, C.J., "Single-longitudinal-mode Operation of an Nd^{3+}-doped Fibre Laser." *El. Lett.*, **24**, 1, Jan. 1988.

Meltz, G., Morey, W.W. and Glenn, W.H., "Formation of Bragg Gratings in Optical Fibres by a Transverse Holographic Method," *Opt. Lett.*, **14**, Aug. 1989.

Minelly, J.D., *Field Access Techniques for Single-Mode Fibres*, Ph.D Thesis, University of Southampton, 1990.

Mwaranai, E.K, Reekie, L., Wang, J. and Wilkinson, J.S., "Low-threshold Monomode Ion-exchanged Waveguide Lasers in Neodymium-doped BK-7 Glass", *El. Lett.*, **26**, 16, pp. 1317-1318, Aug. 1990.

Ragdale, C.M., Reid, D., Robbins, D.J., Buus, J. and Bennion, I., "Narrowband Fiber Grating Filters," *IEEE J. Sel. Areas in Comms.*, **8**, 6, pp. 1146-1150, Aug. 1990.

Reekie, L., Mears, R.J., Poole, S.B. and Payne, D.N., "Tunable Single-Mode Fibre Lasers", *J. Lightwave Tech.*, **LT-4**, 7, pp. 956-966, July 1986.

Rowe, C.J., Bennion, I., and Reid, D.C.J., "High-Reflectivity Surface-Relief Gratings in Single-Mode Optical Fibres," *IEE Proc. J*, **134**, 3, June 1987.

Russell. P. St. J. and Ulrich, R., "Grating-fiber Coupler as a High-Resolution Spectrometer," *Opt. Lett.*, **10**, 6, pp. 291-293, June 1987.

Sandoe, J.N., Sarkies, P.H. and Parke, S., "Variation of Er^{3+} Cross Section for Stimulated Emission With Glass Composition", *J. Phys. D: Appl. Phys.*, **5**, pp. 1788-1798, 1972.

Shircliff, W.A., *Polarised Light*, Harvard University Press, Cambridge, Massachusetts, 1962.

Smith. P.W., "Stabilised, Single-frequency Output From a Long Laser Cavity," *IEEE J. Quantum. Electron.*, **QE-1**, pp. 343-348, Nov. 1985.

Smith, P.W., "Mode Selection in Lasers", *Proc. IEEE*, **60**, 4, pp. 422-440, Apr. 1972.

Sorin. W.V. and Shaw, H.J., "A Single-Mode Fiber Evanescent Grating Reflector," *J. Lightwave Tech.*, **3**, 5, pp. 1041-1043, Oct. 1985.

Statz, H. and deMars, G., "Transients and Oscillation Pulses in Masers" in *Quantum Electronics*, Townes, C.H., Ed., Columbia University Press, New York, 1960.

Townsend, J.E., *Private communications.*

Urquhart, P., "Transversely Coupled Fiber Fabry-Perot Resonator: Theory," *Appl. Opt.*, **26**, 3, pp. 456-463, Feb. 1987.

Urquhart, P., "Compound Optical-fiber-based Resonators," *J. Opt. Soc. Am. A*, **5**, 6, pp. 803-812, June 1988.

Walpita, L.M. and Pitt, C.W., "Fabrication and Evaluation of Linear Constant Period Beam Expander Gratings," *Opt. Comms*, **52**, 4, pp. 241-246, Dec. 1984.

Chapter Five

Travelling-Wave Resonators

5.1 INTRODUCTION

The approaches adopted for obtaining narrow-linewidth and single-longitudinal-mode operation described in the previous chapter relied on minimising the number of modes oscillating in a standing-wave resonator. This was achieved by utilising cavity designs allowing only one or a few modes to experience multi-pass gain and reach lasing threshold. An alternative approach towards narrow linewidth operation is to eliminate the cause of multi-mode operation, namely spatial holeburning, some of the consequences of which were described on Chapter 3. It will be shown in this chapter that eliminating spatial holeburning by operating in a travelling-wave mode is an

effective technique of achieving single-longitudinal-mode operation in erbium-doped fibre lasers. Travelling-wave operation allows higher single-mode power to be obtained than would be achieved in a similar resonator with a standing-wave, because standing-wave lasers will eventually become multi-mode because of spatial holeburning if the pump power is increased sufficiently. This work represents the first time that travelling-wave operation has been demonstrated in fibre lasers.

It was shown in Chapter 3 how spatial holeburning due to the standing-wave pattern of a laser mode is the primary factor leading to multi-mode laser oscillation. Elimination of spatial holeburning has been demonstrated to be a viable technique for achieving single-longitudinal-mode operation in a variety of solid-state lasers [Koechner], and often the elimination of spatial holeburning is all that is required to obtain single-frequency operation [P.W. Smith]. Various techniques have been demonstrated for eliminating the effects of spatial holeburning both for travelling-wave operation in a ring laser and for standing-wave operation in a Fabry-Perot resonator. As early as 1963 it was described how uni-directional operation of a ruby laser led to single-frequency output [Tang] by suppression of the standing-wave in the resonator. Other techniques of preventing multi-mode operation involve smearing or physically moving the standing-wave pattern of the optical intensity, at a rate which prevents the creation of spatial variations of the population inversion, which would allow multi-mode operation. In homogeneously-broadened lasers these techniques result in automatic single-longitudinal-mode output [Danielmeyer]. Recent results have demonstrated the operation of this type of technique to achieve single-longitudinal-mode operation of neodymium-doped fibre lasers [Sabert]. Similar results from preventing standing-waves have been achieved in various laser systems by obtaining different polarisations for the forward and backward travelling waves via $\lambda/4$ plates or 45° rotators [Evtuhov] [Bowness], and by introducing asymmetry in a ring laser via an acousto-optic modulator [Neev].

Techniques which eliminate the effects of spatial holeburning have certain advantages over fixed standing-wave resonators for single-longitudinal-mode operation. These

advantages include that they can be used with long laser cavities, and that very small gain discriminations can determine the operating wavelength of the laser, leading to the possibility of easily tunable operation. The fact that long laser cavities can be used is particularly important for the realisation of single-longitudinal-mode erbium-doped fibre lasers due to the necessity for using a particular doped fibre length for low threshold and efficient operation. This necessity arises because the gain medium is a three-level system and end-pumped, and also because the efficiency of erbium-doped fibres has been demonstrated to decrease with increasing erbium concentration (see Chapter 3).

It is shown in this chapter that eliminating the standing-wave pattern of a laser mode leads to single-longitudinal-mode operation in erbium-doped fibre lasers. In the first demonstration of a travelling-wave fibre ring laser single-longitudinal-mode operation of an erbium-doped fibre ring laser was realised with less than 60kHz linewidth. In addition, a novel Sagnac-like laser resonator, with no direct analogies in other laser technologies, is described. This laser configuration has resulted in linewidths less than 10kHz. The small pump powers required to achieve threshold mean that single-frequency fibre lasers can be produced pumped by diode lasers for compact, efficient and potentially reliable solid-state sources.

5.2 TRAVELLING-WAVE FIBRE RING LASER

Fibre ring lasers have been investigated by several authors. They are attractive configurations for fibre laser sources by virtue of their simplicity in all-fibre form. Utilising fibre couplers, and their characteristics such as wavelength selectivity and tunability, allows for the fabrication of all-fibre resonators. This takes away the need to incorporate reflectors on fibre end-faces and results in a robust resonator [Chaoyu] [Scrivener]. Although narrow linewidth operation has been demonstrated, all fibre

ring lasers previously investigated have been bi-directional, multi-mode devices. Bi-directional operation allows for the build-up of a standing-wave pattern leading to spatial holeburning in the gain medium and multi-longitudinal-mode operation. By operating a fibre ring laser as a uni-directional device and preventing this standing-wave pattern from arising, single-frequency operation can be achieved, as described in this chapter.

5.2.1 Fibre Ring Laser Experimental Configuration

Uni-directional operation in a fibre laser requires a substantial degree of differential loss to be introduced between modes travelling in opposite directions. Since the development of compact pig-tailed optical isolators, this can be achieved in a fibre-coupled device. The experimental laser configuration of the uni-directional fibre ring laser, utilising such an optical isolator, developed to achieve single-longitudinal-mode operation in the 1.55μm region, is shown in Figure 5.1. With the exception of the incorporation of the optical isolator, the ring is as a conventional bi-directional ring laser. A dichroic coupler was used to introduce the pump light, to form the resonant ring, and to serve as the laser output coupler. The coupler used introduced 95% of the pump light at 980nm into the loop and coupling out 15% of the signal light in the 1.55μm region. The active fibre was a 1 metre length of phospho-alumino-silicate fibre with NA=0.15, λ_c=1250nm, and Er^{3+} concentration 800ppm, which was uniformly doped throughout the core. The fibre resonator was formed to ensure no unwanted reflections by low-loss fusion splicing the fibre coupler ports, doped fibre and the pigtails of the optical isolator. The isolator was specified to provide isolation $>$40dB, return loss fibre coupled 60dB and polarisation sensitivity $<$0.1dB. The total resonator length was minimised to around 4m to maximise the intermode spacing.

The high gain of the erbium system means that small reflections can easily set up

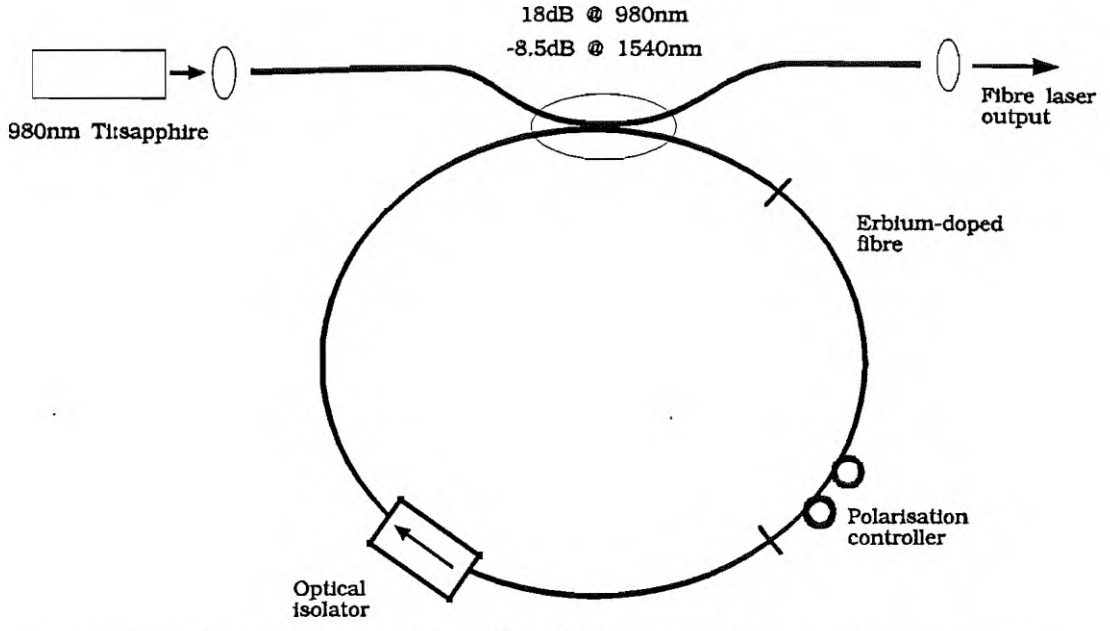

Figure 5.1 Experimental configuration of erbium-doped fibre ring laser. Doped fibre parameters: NA=0.15, λ_c=1250nm, Er^{3+} conc.=800ppm.

standing-wave effects in the gain medium, resulting in multi-mode operation. Initial efforts towards travelling-wave operation in the ring configuration were by collimating a beam through a bulk isolator. Single-frequency operation was not possible due to additional reflections involved in collimating the output from the fibre and the use of non-anti-reflection-coated lenses, leading to standing-wave effects in the gain medium.

5.2.2 Fibre Ring Laser Power Characteristics

The ring laser was pumped at 980nm by an Argon-ion pumped Ti:sapphire laser with the pump light being introduced to the ring via the dichroic coupler. The fibre laser attained threshold for 6mW pump power launched into the ring. The laser power

characteristic, measured at the signal output port of the dichroic coupler, is shown in Figure 5.2, illustrating the laser slope efficiency of 2.3%.

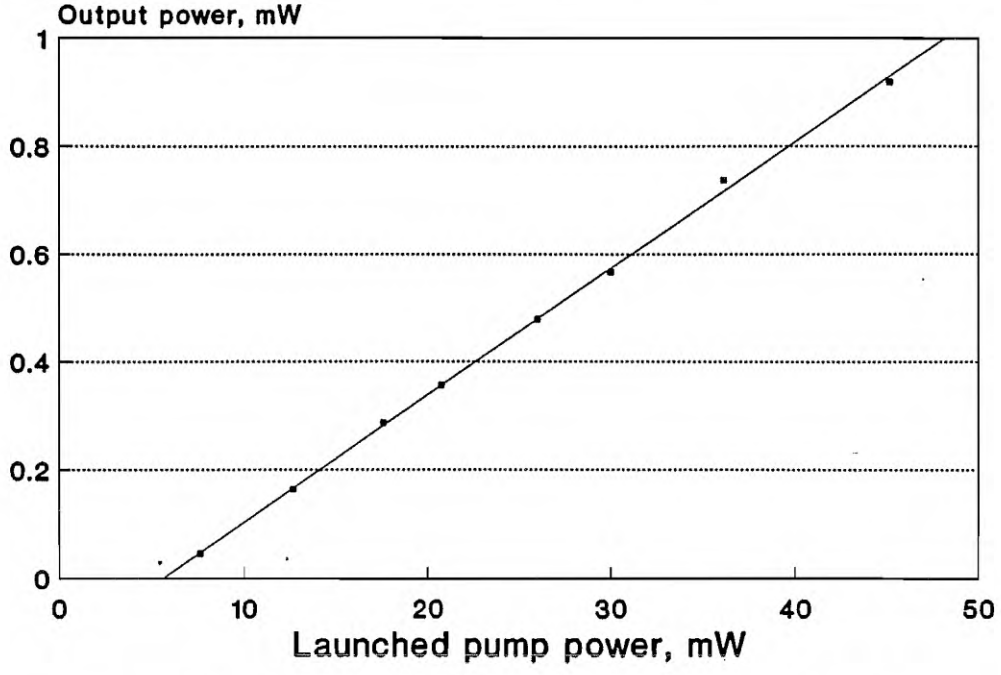

Figure 5.2 Power characteristic of single-frequency fibre ring laser. Pump power from 980nm Ti:sapphire laser, threshold 6mW, slope efficiency 2.3%.

The laser performance under steady state conditions can be compared with predicted performance by considering the single-pass fibre amplifier within the fibre ring as a lumped element with a given saturated gain. The gain and loss elements within the ring can then be modelled as in the diagram in Figure 5.3 where G represents the saturated gain under steady state conditions produced by the section of doped fibre, T represents the percentage transmission through the isolator, the coupler is characterised by an excess loss resulting in transmission E% and splitting ratio s:1-s. Any additional loss within the loop (splice loss, bend loss from polarisation controllers, etc.) is accounted for by signal power transmission of A% through the lumped loss element.

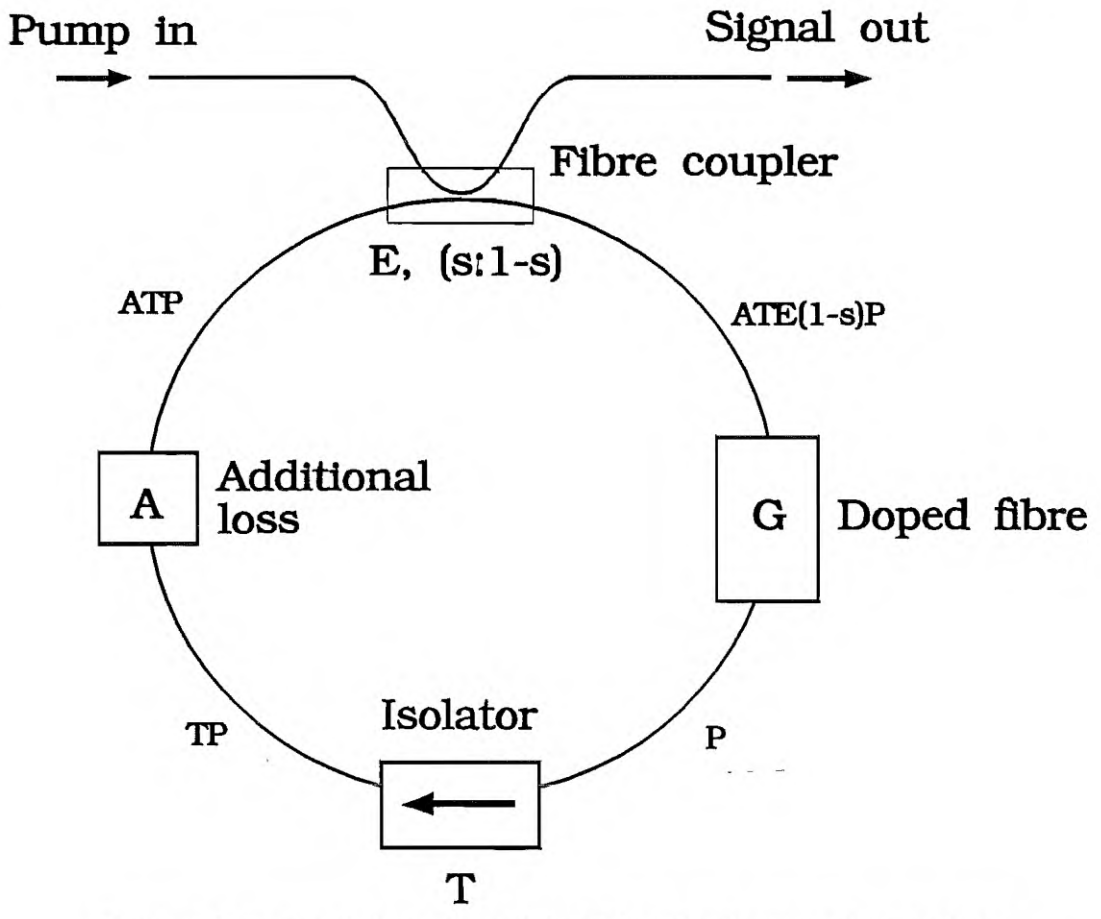

Figure 5.3 Lumped element model of fibre ring laser used to evaluate laser power characteristics. Each cavity element is modelled by a lumped element representing distributed gain or loss.

By considering the steady state situation and following the evolution of the signal power P in a cavity round trip, the gain required to achieve lasing threshold is:

$$G_{th} = \frac{1}{A\ E\ (1-s)T} \qquad (1)$$

while the slope efficiency, output signal power to launched pump power is approximately:

$$eff = \frac{\lambda_p}{\lambda_s} A\ E\ s\ T \qquad (2)$$

Using the known parameters of the intracavity components, s ~ 14%, T ~ 83%, E ~ 90%, the additional cavity losses can be estimated to be ~ 3dB, this value of loss being required to result in the experimentally measured slope efficiency of 2.3%. This loss is the result of splice losses due to fibre mismatches, bend loss induced by the loop polarisation controller and the conversion efficiency of pump to signal light.

5.2.3 Fibre Ring Laser Spectral Characteristics

The spectral characteristics of the fibre ring laser were determined using several instruments with different wavelength/frequency ranges in order to fully characterise the linewidth and spectral characteristics of the laser. The spectrum of the fibre ring laser measured with a grating monochromator is shown in Figure 5.4. Single-line operation on the scale of this instrument with resolution 0.1nm was obtainable by appropriate adjustment of the intra-cavity coil polarisation controller, with the lasing wavelength being 1.5553μm. In the travelling-wave ring laser configuration with no explicit wavelength selection, the operating wavelength is simply that at which most multi-pass gain occurs. The operating wavelength is thus determined not only by the gain spectrum and length of the doped fibre gain medium but also by the wavelength dependence of loss of the intra-cavity components such as the isolator and fibre coupler.

Single-longitudinal-mode operation was confirmed by analysing the laser output signal with a scanning Fabry-Perot spectrum analyser. The output spectrum when measured with a free spectral range of 1GHz is shown in Figure 5.5. The parallel-plate Fabry-

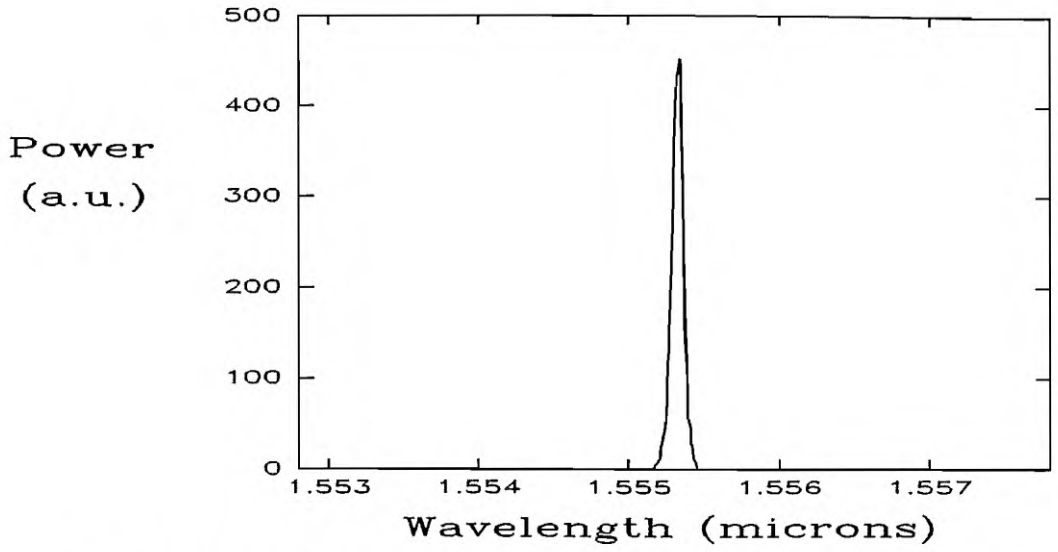

Figure 5.4 Spectrum of Er^{3+}-doped travelling-wave fibre ring laser measured by monochromator with resolution 0.1nm.

Perot spectrum analyser had a finesse >100, sufficient with a free spectral range of 1GHz to resolve adjacent longitudinal modes which would be spaced by 50MHz. A single line was resolvable, resolution limited in width to approximately 10MHz on the Fabry-Perot. A degree of instability was observed in the laser output leading to mode-hopping and occasional multi-mode operation as illustrated by the spectrum shown in Figure 5.6, however single-frequency operation could be achieved by adjusting the polarisation controller to align the state of polarisation for a round-trip of the ring. The operating wavelength of the laser was also influenced by the settings of the loop polarisation controller. The polarisation states of the laser will be elliptical, and this, together with a degree of polarisation gain anisotropy and residual polarisation anisotropy of the optical isolator and fibre coupler will result in a degree of mode selection via birefringence. Adjustment of the polarisation controller could compensate for the residual birefringence in the resonator components to achieve optimum orientation of the polarisation within the ring. No attempts were made to isolate the resonator from environmental disturbances, however the laser could be maintained on a single mode for periods of the order of 10 seconds, after which time ambient variations would often cause it to drift. Single-mode operation could be

restored by adjusting the polarisation control coils.

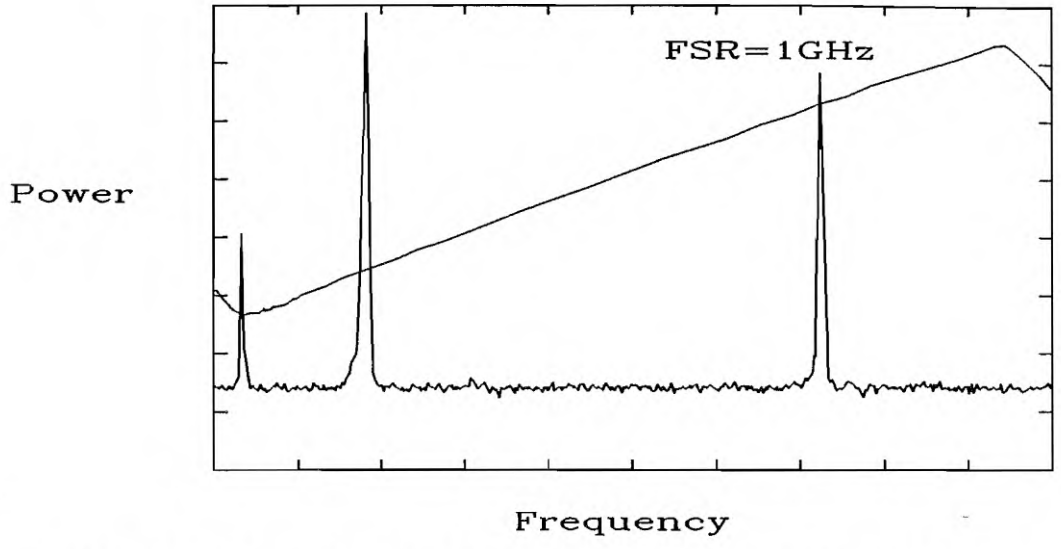

Figure 5.5 Travelling-wave fibre ring laser spectrum measured with Fabry-Perot spectrum analyzer, showing two free spectral ranges. Upper trace ramp voltage, lower trace optical signal.

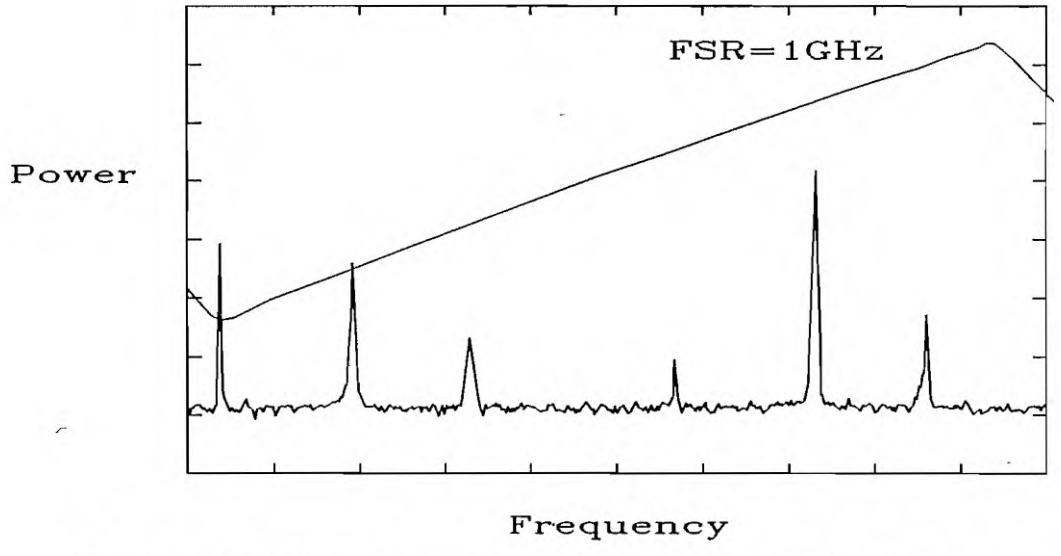

Figure 5.6 Multi-mode operation of travelling-wave ring laser as observed with scanning Fabry-Perot spectrum analyzer. Upper trace ramp voltage, lower trace optical signal.

Clearly the travelling-wave ring method of achieving single-longitudinal-mode operation, by the elimination of spatial holeburning, is an extremely powerful technique. The gain difference between adjacent cavity modes is very small and yet single-longitudinal-mode operation is achievable in a cavity which, except for the inclusion of the optical isolator, would be likely to result in a linewidth of typically >1nm [Scrivener] [Chaoyu]. The small gain differential between adjacent modes required in this technique for single-longitudinal-mode operation would also indicate that setting the wavelength of operation would only require weak wavelength filtering within the laser resonator.

The instantaneous linewidth of the laser was determined by a delayed self-heterodyne interferometer (described in Appendix A.1). Using a 25km fibre delay line, capable of resolving without ambiguity a laser line width of 4kHz, and a piezo-electric fibre stretcher in the reference arm driven at 500kHz to give rise to a phase shift and frequency sidebands, the linewidth was measured to be less than 60kHz. A typical RF spectrum is illustrated in Figure 5.7. The additional structure in the RF spectrum rather than the expected laser Lorentzian line, as evident in Figure 5.7, is due to beating of the laser signal with the relaxation oscillation frequency. The presence of the relaxation oscillations is due to mode-hopping, although the spectrum is instantaneously single-longitudinal mode. The relaxation oscillation frequency was also measured in a homodyne beat signal and determined to be $\sim$30kHz. Although likely to be significantly less, the linewidth estimate was less than 60kHz full width at half maximum.

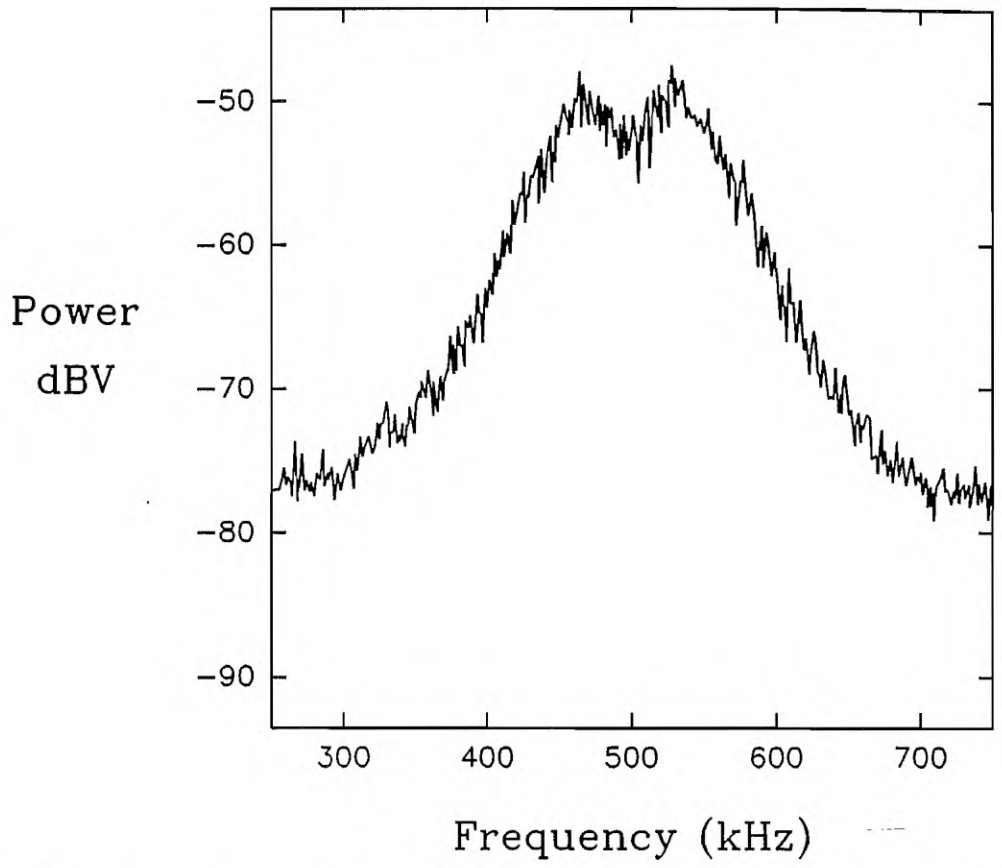

Figure 5.7 Instantaneous self-heterodyne beat spectrum of travelling-wave fibre ring laser measured with self-heterodyne interferometer with 25km delay line.

5.2.4 Discussion

It is perhaps slightly surprising that the travelling-wave method of achieving single-longitudinal-mode operation achieves single-frequency operation in an erbium-doped silica fibre laser in which the gain medium is not simply an ideally homogeneously-broadened transition, but rather the energy levels of the Er^{3+} ion are split by the random structure of the silica field. However single-frequency operation indicates that the gain medium acts here as a homogeneous medium. The homogeneous and inhomogeneous widths are similar for alumino-silicate fibres and hence spectral holeburning does not occur, spectral holeburning only occurring if inhomogeneous broadening dominates [Guy]. Elimination of spatial holeburning by smearing of a

standing-wave has also been demonstrated to result in single-frequency operation in a neodymium-doped silica fibre laser [Sabert]. As was indicated in Section 3.2, site-to-site variations are of the same order as the Stark splitting in the erbium-silica system, the strong spectral overlap between emission from different sites results in homogeneous broadening being a good approximation for room temperature operation [Zyskind].

With the results described in Section 5.2.3, although single-frequency operation was achieved, the wavelength of operation of the could not easily be set. The wavelength of operation is that at which the gain first overcomes the cavity losses, after which the gain will be clamped. Typical cavity loss in the ring cavity is about 3dB, which although high for other laser systems is small compared to the gain available from the doped fibre. Operation was observed at the long-wavelength or quasi-4-level part of the gain medium with no wavelength selectivity in the resonator. Operation in this part of the spectrum was also observed for the travelling-wave loop laser in the next section when operating without wavelength selectivity. As the gain medium is pumped the small amount of gain required for threshold occurs at longer wavelengths (1.55μm) before the shorter wavelengths. In a more lossy resonator the laser would operate at shorter wavelengths. Although erbium-doped fibres exhibit most gain in the 1.535μm region, at low pump powers more gain will exist at longer wavelengths [Kimura]. The wavelength selectivity with cavity losses occurs because the unpumped parts of the fibre act as an absorber, particularly for shorter wavelengths where the system acts more as a 3-level system while the field splitting makes longer wavelength parts of the transition a quasi-4-level system. When the travelling-wave fibre is pumped, gain overcomes loss at the long-wavelength part of the gain first thus determining the lasing wavelength. To achieve free-running wavelengths in the 1.535μm region would require a more lossy cavity for a given doped fibre length so that the gain required was higher than could be achieved in the 1.55μm region.

The broad width of the $^4I_{13/2}$ to $^4I_{15/2}$ transition of Er^{3+} in glass, means that broad

tuning of the lasing wavelength is possible, and desirable for many applications. Tunable operation can be achieved by incorporating a filter into the ring to introduce loss and thereby set the wavelength at which there is minimum loss and most multi-pass gain. Since the publication of the above results, the extension of this technique to tunable single-frequency operations has been demonstrated by several authors using filters within the travelling-wave ring. Based on the travelling-wave ring laser described above, a variety of tuning elements have been incorporated including interference filters [Iwatsuki], acousto-optic filters [Smith], liquid crystal filters [Smith 1991a] and fibre Fabry-Perot filters [Zyskind 1991], with tuning ranges exceeding 60nm being demonstrated. In each case a filter is used in conjunction with an optical isolator, the isolator ensuring single-frequency operation and the filter providing wavelength selectivity.

5.3 TRAVELLING-WAVE FIBRE LOOP LASER

The travelling-wave erbium fibre ring laser described in Section 5.2 clearly demonstrates the effectiveness of the travelling-wave approach to achieving very narrow linewidths from an erbium fibre laser operating in the in the 1.5μm telecommunications window. However, an important consideration for many applications of narrow-linewidth lasers in this wavelength region, such as coherent communication systems, is precise setting of the operating wavelength of the laser. For accurate absolute wavelength control the most attractive type of wavelength selection device is a diffraction grating or DBR reflector. However, it is not possible to incorporate such a device in a travelling-wave ring laser. The travelling-wave fibre laser described in this section uses a novel cavity configuration which allows the incorporation of a frequency-selective distributed Bragg reflector. The resonator configuration permits very precise control over the operating wavelength, while obtaining single-longitudinal-mode operation with less than 10kHz linewidth.

The resonator configuration of the fibre loop laser is illustrated in Figure 5.8. The resonator is based on a single four-port coupler with two output ports joined to form a fibre loop in a Sagnac-like arrangement [Siegman] [Mortimore] by a length of erbium-doped fibre. The interferometric operation of the loop is prevented by the inclusion of an optical isolator in the loop which establishes uni-directional operation in the fibre loop. The two remaining coupler ports are used to introduce pump light and to incorporate a reflector to form a resonant cavity. The reflector can be of several forms, a dielectric mirror and distributed Bragg reflector will be discussed.

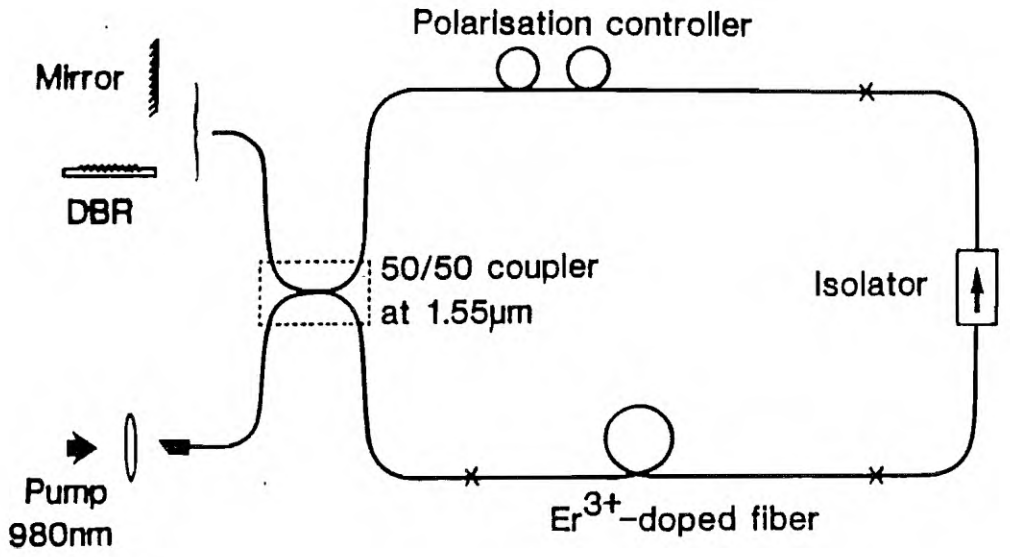

Figure 5.8 Experimental configuration of travelling-wave Er^{3+}-doped fibre loop laser.

5.3.1 Fibre Loop Laser Experimental Configuration

The fibre loop laser schematically illustrated in Figure 5.8 was formed by joining two output ports of a 1.55μm 3dB fused fibre coupler by a length of phospho-alumino-silicate erbium-doped fibre (Er^{3+} conc. =800ppm, λ_c=1525nm, NA=0.15) and a pig-tailed, polarisation-independent isolator. The isolator provided isolation of 45.2dB with insertion loss $<$0.4dB, return loss $>$60dB, and polarisation sensitivity of only 0.02dB. Pump light was introduced into the resonator via port A as indicated in Figure 5.8, with the fibre end angle polished at $\sim 15°$ to minimise Fresnel reflections. The coupler used was a standard telecommunications 3dB coupler which had the favourable characteristic of coupling 95% of the pump wavelength light launched through port A into the section of doped fibre.

To form a resonant cavity, a reflector was arranged at the end of port B. The reflector for fixed-wavelength operation took the form of either a dielectric mirror (70% reflectivity @ 1.5μm) or a distributed Bragg reflector (DBR) capable of accurate wavelength selection. The DBR used in the experiments had a reflectivity of 70% and half-power bandwidth of 0.3nm, centred at 1.552μm. The grating was fabricated by Plessey Research Caswell, by side-polishing a single-mode fibre mounted in a flat silica V-groove and holographically exposing a diffraction grating in a thin photoresist layer which was spin-coated onto the surface. To enhance the reflectivity the grating was etched into the fibre and a layer of high-index material sputtered on the surface [Bennion] [Rowe] [Ragdale]. A polarisation controller was used in the loop to overcome the polarisation sensitivity to reflection of the DBR. The use of the controller enabled the light in the loop to be optimised for maximum reflection. The round-trip laser cavity length was 9.5m, corresponding to an adjacent passive cavity mode spacing of 21MHz. For convenience the fibre laser was pumped at 980nm by a Ti:sapphire laser.

By virtue of the isolator and the location of the doped fibre *within* the fibre loop, the

signal in the 1.55μm region generated by the Er^{3+}-doped fibre travels in only one direction in the fibre loop, consequently preventing the build-up of a standing-wave in the gain medium and eliminating spatial hole-burning in the gain medium. The single-mode fibre coupler acts as the output coupler of the laser and couples half of the signal which passes through the isolator to the reflector on port B. Half of the signal returned from the reflector is fed back into the active fibre thus forming a resonant structure. The laser resonator is travelling-wave in the doped fibre gain medium, and hence the manner of achieving single-longitudinal-mode operation is thus similar to the travelling-wave ring laser, but because this laser cavity incorporates a reflector, accurate wavelength selection is possible by the use of a wavelength selective DBR.

5.3.2 Loop Laser Spectral Characteristics

The fibre loop laser was first operated with the dielectric mirror reflector on port B, as indicated in Figure 5.8. This resonator arrangement is a more rigorous test of single-longitudinal-mode operation than operation with a frequency-selective reflector, which will provide a narrow-band cavity response. When pumped by the Ti:sapphire laser operating at 980nm, narrow-linewidth operation of the fibre laser was observed centred at 1.5577μm, as indicated in the monochromator-generated spectrum shown in Figure 5.9, with the monochromator resolution being 0.1nm. As in the case of the travelling-wave ring laser, the wavelength of operation is that wavelength at which the gain first overcomes the intra-cavity losses. Single-frequency operation was verified using a scanning Fabry-Perot spectrum analyser with free spectral range 1.3GHz and finesse in excess of 100. As additional proof of single-longitudinal-mode operation, no intermodal beat signal was detectable at multiples of the passive cavity mode spacing when the current from a photodiode upon which the laser signal was incident was analysed by an RF spectrum analyser.

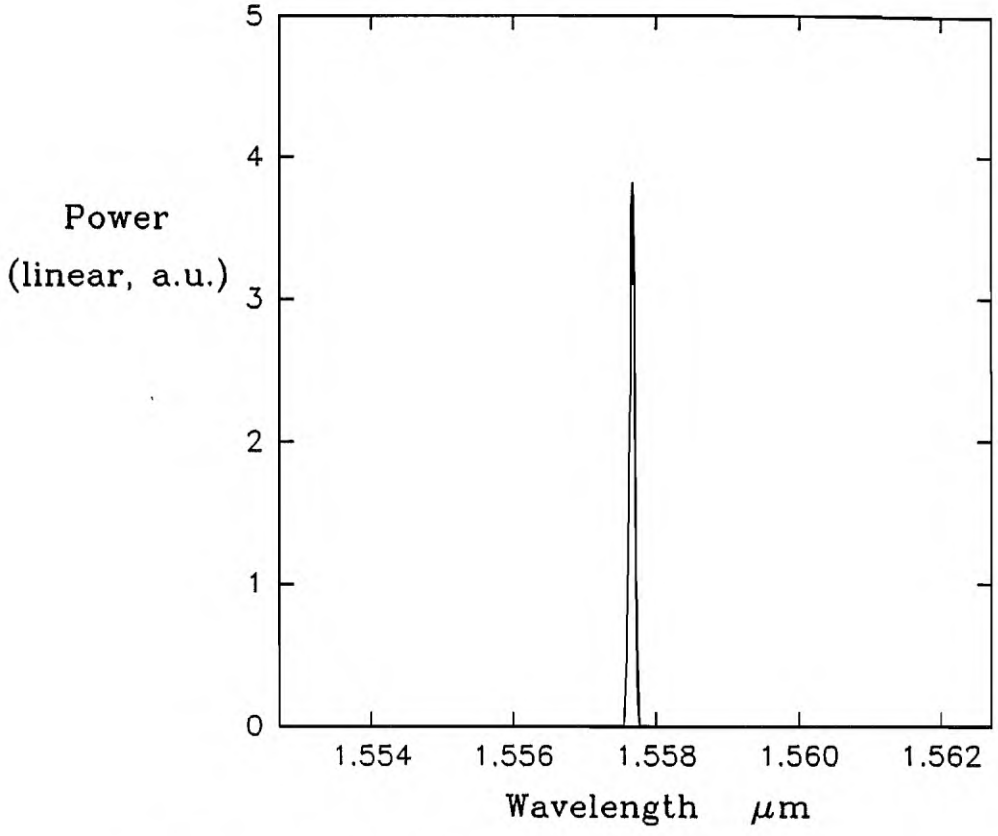

Figure 5.9 Spectrum of fibre loop laser with 70% mirror reflector, measured with monochromator with 0.1nm resolution.

Operating the laser with a mirror reflector offers no significant advantage over the travelling-wave ring technique, notwithstanding the experimental verification of single-longitudinal-mode operation of the novel cavity configuration under demanding conditions in which the resonator has no explicit wavelength selectivity to narrow the lasing bandwidth. The advantage of the loop laser configuration lies in the ability to accurately determine the operating wavelength when incorporating a frequency-selective reflector. This was demonstrated when the mirror on port B was replaced with the DBR with maximum reflectivity at 1.552μm. With this reflector, the lasing wavelength shifted to 1.552μm, as illustrated by the monochromator spectrum reproduced in Figure 5.10. Analysing the spectrum with a scanning Fabry-Perot

whose free spectral range was sufficient to resolve adjacent modes spaced by 21MHz, only one mode was evident as illustrated in Figure 5.11. Moreover, no intermodal beat signal was detectable.

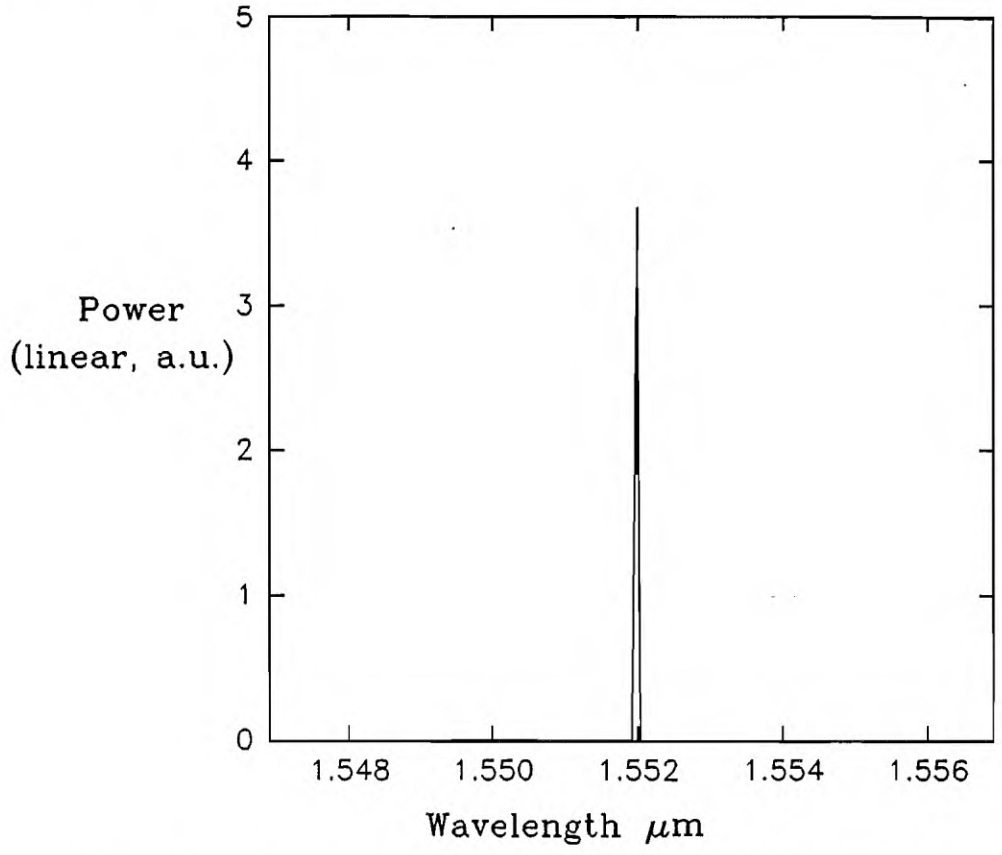

Figure 5.10 Spectrum of loop laser incorporating DBR reflector measured with a monochromator with 0.1nm resolution.

The linewidth of the loop laser was determined by the delayed self-heterodyne technique using a 25km delay line. The RF spectrum from such a measurement is illustrated in Figure 5.12, and corresponds to a full width at half maximum of about 9.5kHz, fully resolvable by a 25km delay line. Variation of the laser linewidth when the laser power was varied was not significant or quantifiable, implying that the linewidth may be determined by the stability of the laser cavity with respect to

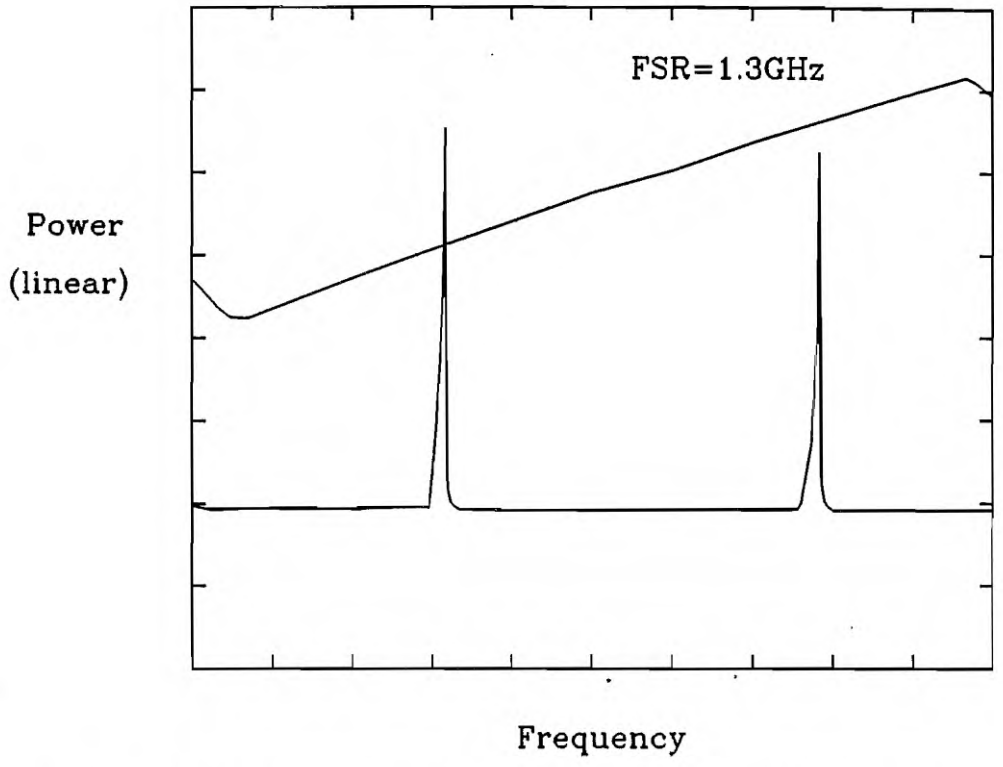

Figure 5.11 Spectrum of loop laser incorporating DBR reflector measured with Fabry-Perot spectrum analyzer, showing two free spectral ranges with FSR=1.3GHz.

temperature effects and vibrations. Certainly the measured linewidth was far larger than would be expected from the Schawlow-Townes limit ($\sim$ 1Hz).

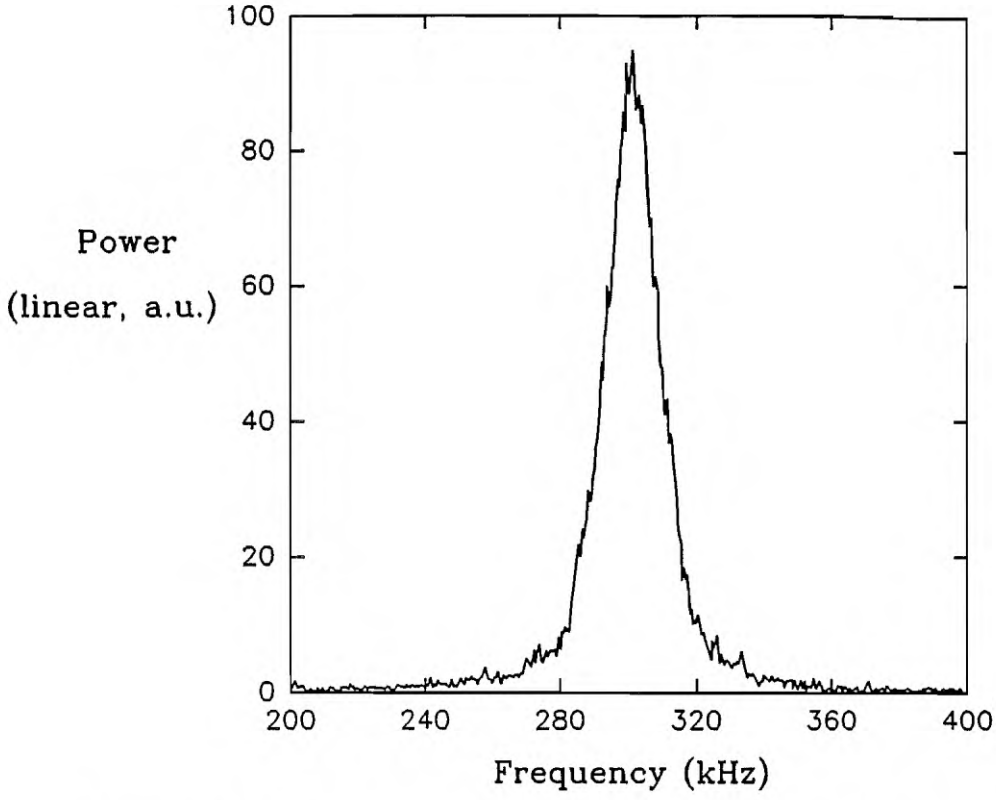

Figure 5.12 Instantaneous self-heterodyne beat spectrum of fibre loop laser, measured with self-heterodyne interferometer with 25km delay line and 300kHz frequency shift.

5.3.3 Loop Laser Power Characteristics

The laser power characteristic was determined for the signal output from port A and is illustrated in Figure 5.13. Lasing threshold was measured to be 6mW launched pump power at 980nm, while the slope efficiency with respect to launched pump power was 29%. Taking into account the loss associated with the isolator and coupler, this slope efficiency translates to a conversion efficiency within the doped fibre of at least 95%, which is the result of the negligible excited state absorption for pumping at 980nm.

The presence of the 3dB coupler in the cavity results in a laser which is inherently lossy, as half of the reflected power from the mirror or DBR is lost. However the

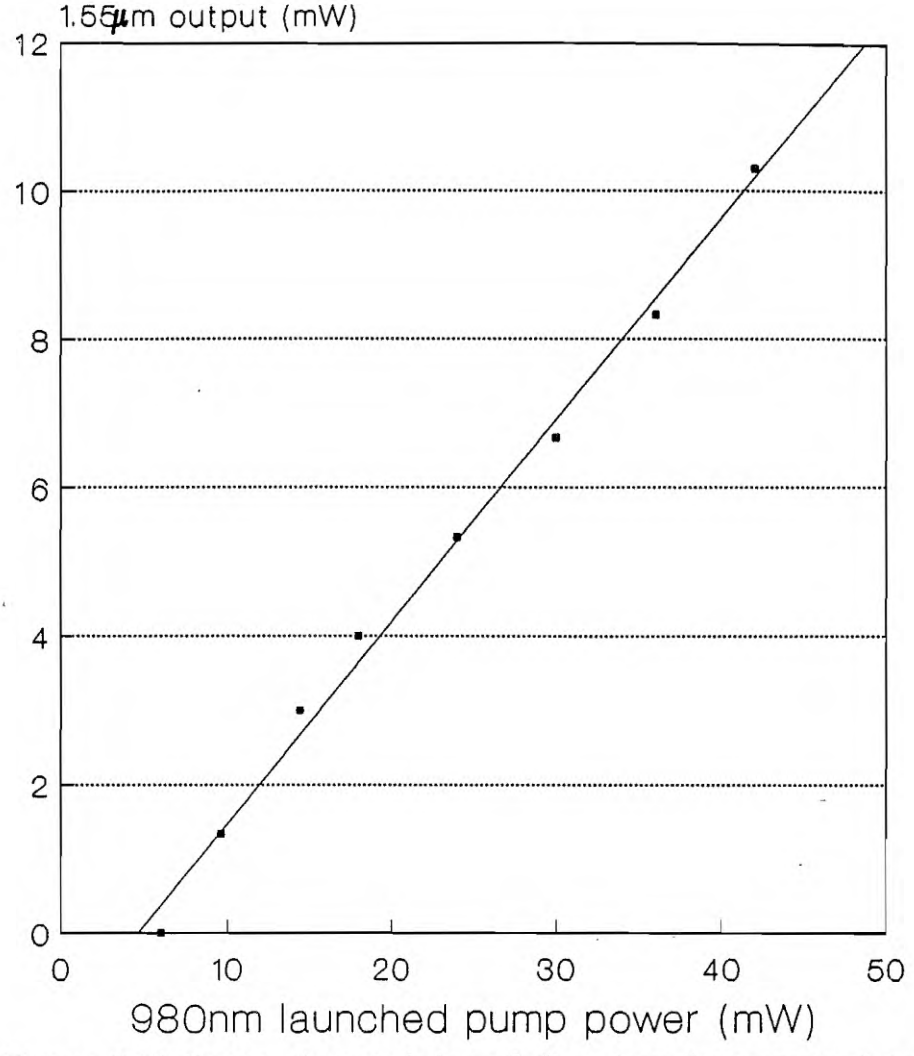

Figure 5.13 Power characteristics of fibre loop laser pumped by Ti:sapphire laser.

laser characteristic illustrates that good performance can still be obtained. This results from the large output coupling where the intra-cavity power is greatest, before the signal reaches the lossy cavity element. The laser configuration has not been demonstrated in other types of lasers, therefore it is important to examine the properties of the resonator. The resonator can be modelled for steady state conditions as shown in Figure 5.14. The coupler is characterised by coupling ratio α:1-α ($\alpha \leq 1$) and excess loss which results in transmission E% through the coupler, the doped fibre is modelled simply by the saturated gain G for steady state conditions, the isolator

passes T% of the light in the low-loss direction while passing 0% in the opposite direction, transmission of A% accounts for excess loss due to splices and the loop polarisation controller, and the reflectivity of the grating or mirror is R%.

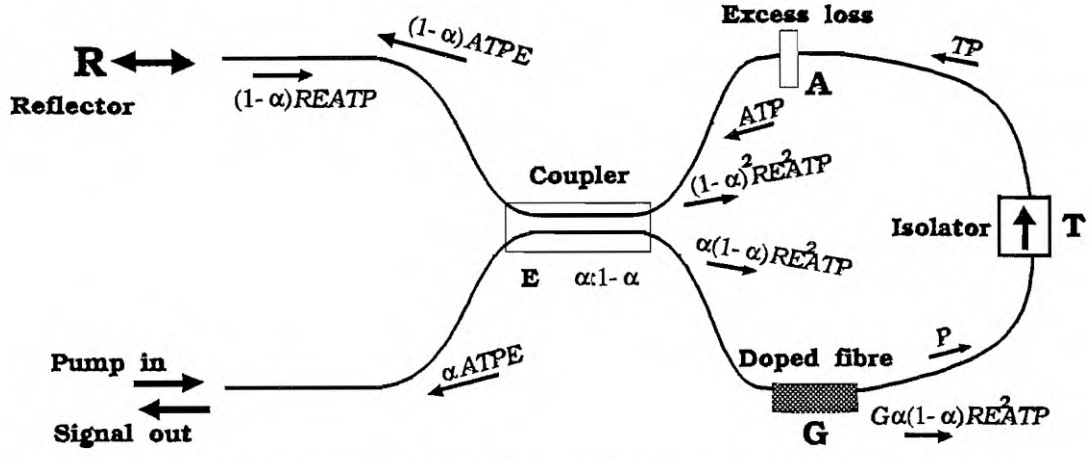

Figure 5.14 Schematic description of fibre loop laser lumped-element model used for power and efficiency considerations.

The conditions for lasing threshold can be considered from power conservation considerations. Maximum signal power occurs in the resonator at the output of the single-pass doped fibre amplifier. If this power is denoted P, then by energy conservation of the signal travelling around a single pass of the resonator we require:

$$G\ \alpha(1-\alpha)RE^2ATP = P \tag{3}$$

Therefore the gain required to achieve threshold is:

$$G = \frac{1}{\alpha(1-\alpha)RE^2AT} \tag{4}$$

To calculate the coupling ratio α required to achieve minimum threshold, equation 5.4 is differentiated with respect to α to give:

$$\frac{dG}{d\alpha} = 0 \qquad when \qquad \alpha = 0.5 \tag{5}$$

This confirms that the choice of a 3dB coupler is the optimum choice for low threshold operation.

The two cavity parameters most easily controlled in the loop laser are the coupler splitting ratio and the reflectivity of the mirror or grating completing the cavity. It is of interest to see how variation of these parameters will affect the expected laser performance. The variation of the gain required to reach threshold as a function of the coupler splitting ratio for R = 25%, 50%, 70%, 99% is shown in Figure 5.15, assuming for the sake of these calculations T=98%, E=98% and A=100%. From Figure 5.15 it can be seen that the gain required to achieve threshold is symmetrical about the minimum at $\alpha = 0.5$. The resonator is inherently lossy as illustrated by a minimum gain of about 4 being required for threshold with a 99% reflector rising to gain of 17 with a 25% reflector. However as the erbium-doped fibre is capable of very high gain (>40dB) and >10dB/mW, lasing threshold is still easily achievable in these cases. This illustrates one of the benefits of a high gain lasing medium for complex resonator designs, i.e., that it allows the incorporation of lossy intra-cavity elements in order to achieve desired spectral qualities while still achieving threshold for reasonable pump levels.

As the resonator is lossy it is useful to examine the efficiency of the resonator with a view towards optimising the resonator. Using the steady state model of Figure 5.14 the output power can be expressed in terms of the maximum power in the loop as:

$$P_{out} = \alpha ATEP \tag{6}$$

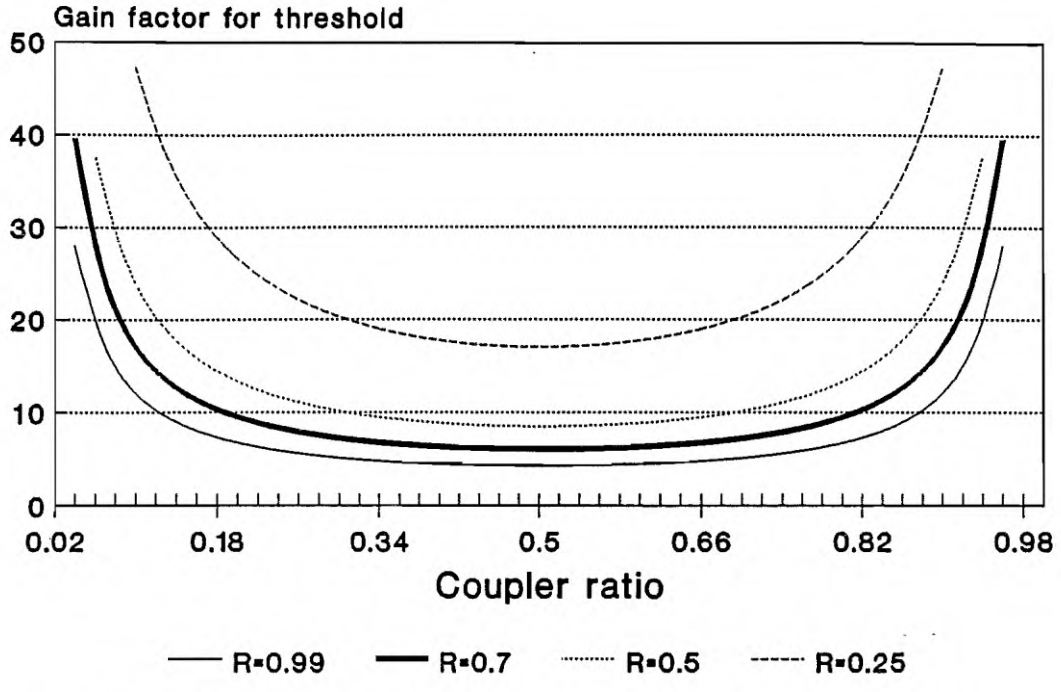

Figure 5.15 Gain required for threshold in fibre loop laser plotted as a function of coupler ratio for R=0.25,0.5,0.7,0.99. E=98%, T=98%.

while the intrinsic power losses are:

$$P_{loss} = (1-\alpha)(1-R)AETP + (1-\alpha)^2AE^2RTP + (1-T)P + (1-A)TP + \alpha(1-E)ATEP \quad (7)$$

The resonator efficiency η_r is defined by:

$$\eta_r = \frac{P_{out}}{P_{out}+P_{loss}} \quad (8)$$

with P_{out} and P_{loss} as given in equations 5.6 and 5.7 respectively. The resonator efficiency is plotted in Figure 5.16 for R = 25%, 50%, 70%, 99%, as a function of the coupler splitting ratio. Figure 5.16 indicates that the resonator efficiency is a monotonically increasing function with respect to increasing percentage of power split

out of the resonator by the fibre coupler. With $\alpha = 0.5$, the condition for minimum threshold operation the resonator efficiency is only about 55% for a 70% reflector, but would increase to >85% if the coupler splitting ratio were 0.2:0.8. Returning to Figure 5.15 it can be seen that with $\alpha = 0.8$ and R = 70% the gain required to reach threshold is a factor of about 13, easily achievable with the erbium-doped fibre system. Thus depending on whether threshold or output power is the most important characteristic the fibre loop laser can be optimised to achieve the desired characteristic. Obviously higher resonator efficiency is at the expense of low threshold operation but if high powers are required and sufficient pump power is available, this tradeoff could be made.

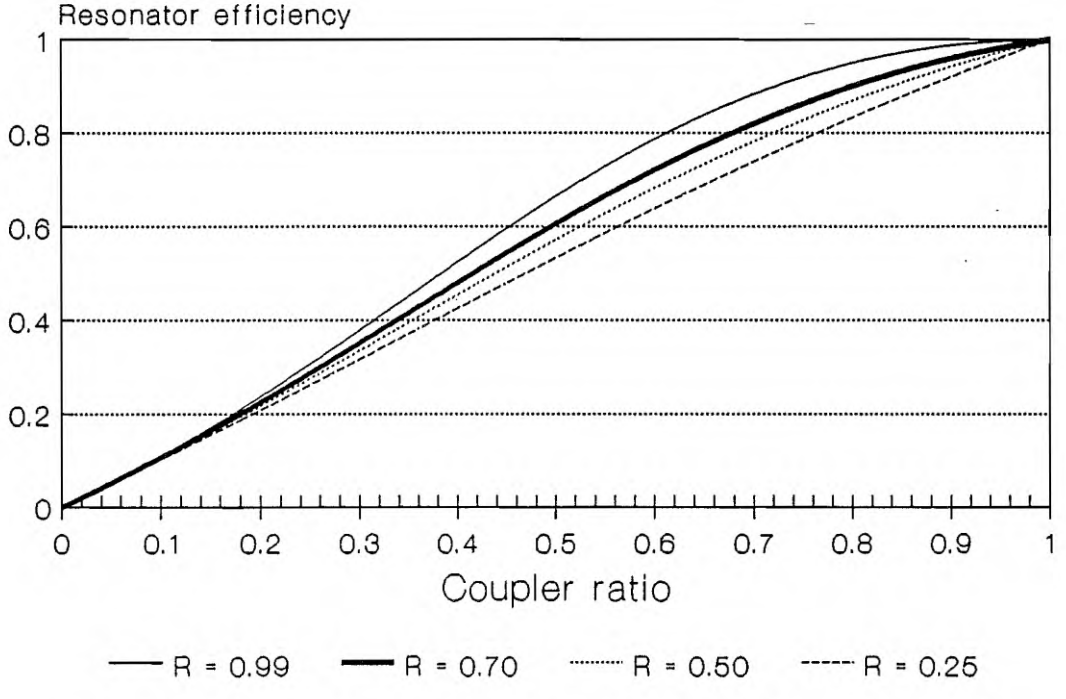

Figure 5.16 Resonator efficiency as a function of coupler splitting ratio for R=0.25,0.5,0.7,0.99.

5.3.4 Single-frequency Tunable Fibre Laser

The results presented thus far have been concerned with single-longitudinal-mode operation at a fixed wavelength, with little scope for tuning the operating wavelength. A small degree of tuning would be possible however by changing the refractive index of the index-matching oil overlayer on the etched DBR [Ragdale]. By using a different type of grating reflector, a bulk grating, a large tuning range can be obtained as described in this sub-section.

The tunable loop laser was realised by replacing the DBR with a bulk diffraction grating in the Littrow or autocollimation mount, as illustrated in Figure 5.17. The grating used was an aluminium-coated 600line/mm grating blazed at 1.25μm. To couple light to the grating the fibre end was angle-polished to minimise extraneous reflections and the light was either collimated or focused onto the grating with a $\times 10$ microscope objective which had high transmission in the 1.5μm region. The distance between the grating and the fibre was typically 25cm. The range of wavelengths reflected into the fibre can be calculated from [Hecht]:

$$\frac{\Delta\lambda}{\Delta x} = \frac{10^6\lambda}{2\tan\beta F} \qquad nm/mm \qquad (9)$$

where F is the focal length of the collimating lens, β is the angle of the grating and x is the distance over which diffraction occurs. With the experimental parameters as given $\Delta\lambda$ = 0.012nm. This technique clearly will give sufficient wavelength discrimination to allow tuning, although the overall reflectivity is only estimated at about 10%, which will result in increased threshold over the previous results. However the high gain available because of the ability in this gain medium to produce complete population inversion allows high-loss components to be incorporated in the resonator. Rotating angle of the grating with respect to the direction of the collimated beam (β in Equation 5.9) will alter the centre frequency of the light fed back into the

laser to tune the lasing wavelength.

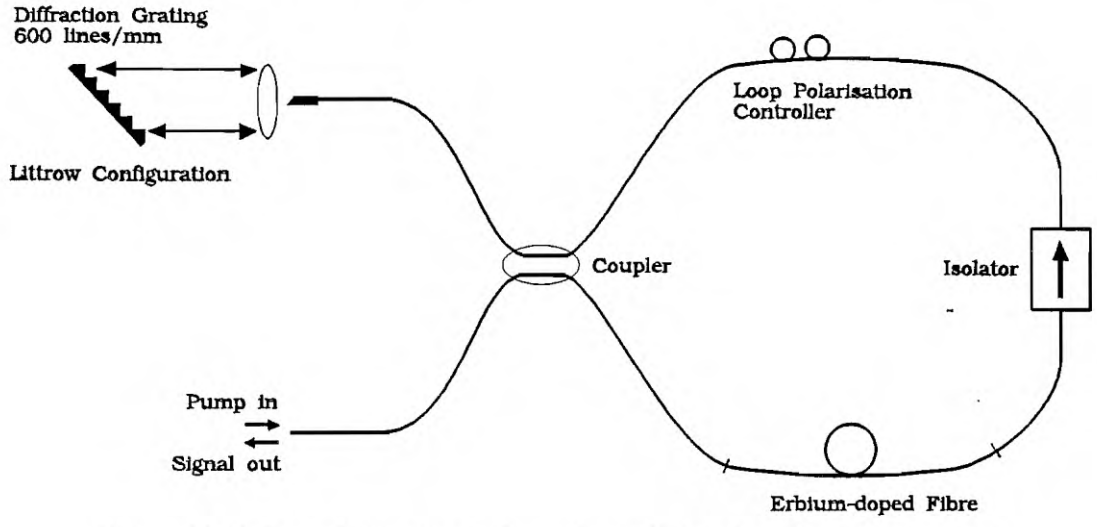

Figure 5.17 Experimental configuration of fibre loop laser incorporating a diffraction grating in the Littrow configuration for wavelength-selective feedback.

When pumped at 980mn from a Ti:sapphire laser the fibre laser was observed to lase once the grating was adjusted to provide feedback into the resonator. Rotating the angle of the grating, without requiring adjustment of the loop polarisation controller, the lasing wavelength was observed to change as indicated in Figure 5.18. Measurements with a Fabry-Perot spectrum analyser and the absence of any inter-modal beat signal indicated that the laser was instantaneously single-frequency across the tuning range, which is plotted in Figure 5.19 for constant pump power, close to the threshold power. The laser was tunable from 1525nm to 1565nm, a tuning range of 40nm. Some variation in the output power across the tuning range is evident, in particular the 3dB dip in the 1.54μm region, the result of the low-Q cavity due to the small reflectivity into the fibre from the grating in combination with the lossy cavity due to the 3dB coupler. The doped fibre used in this experiment did not have a flat fluorescence spectrum, but exhibited a dip in the 1.54μm region. It should be noted that until this work was performed very few [Wyatt] tunable erbium fibre lasers exhibited continuous tuning without a break in the tuning range in the 1.54μm region.

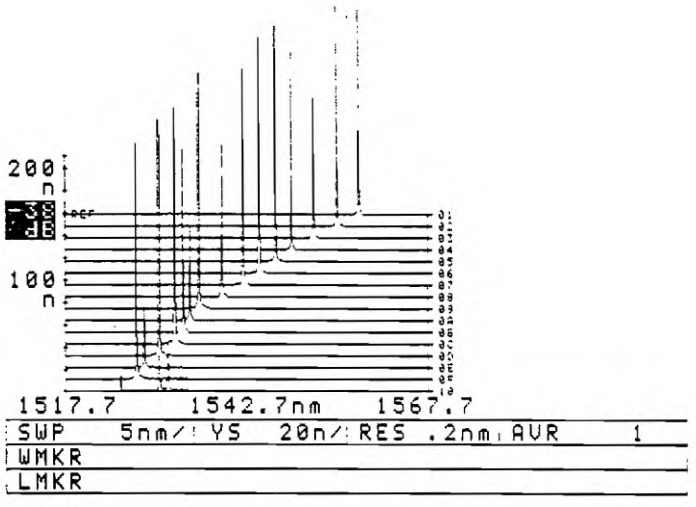

Figure 5.18 Tuning of fibre loop laser with Littrow grating reflector, achieved by rotating grating.

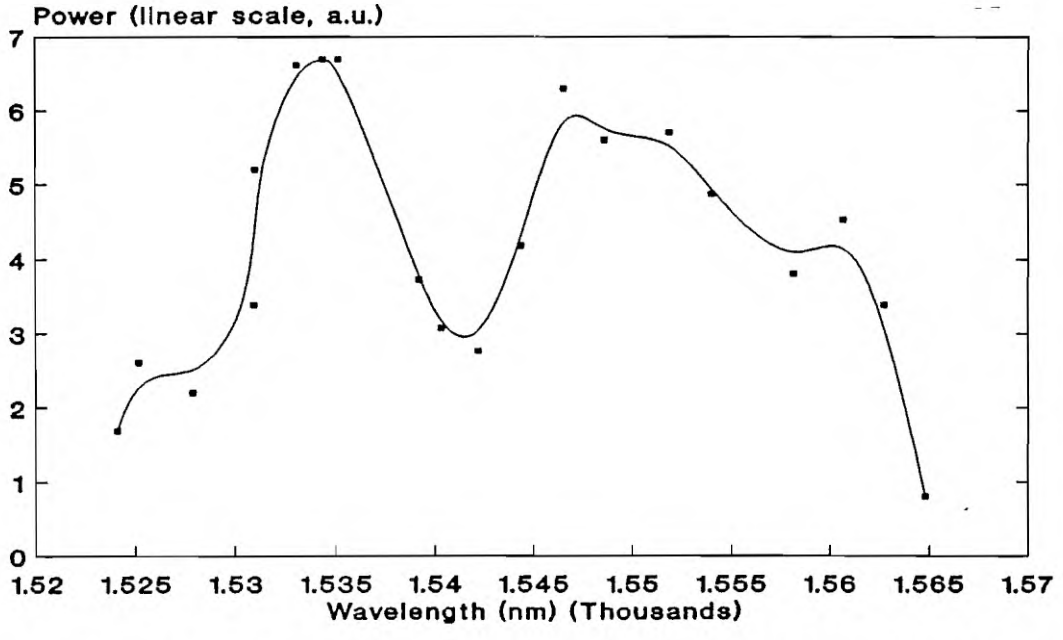

Figure 5.19 Tuning range of fibre loop laser with Littrow grating reflector achieved by rotating the grating. Fixed pump power, close to threshold.

5.3.5 Diode Pumped Loop Laser

The laser characteristic of the fibre loop laser shown in Figure 5.13 indicates that low threshold operation is possible in the loop laser configuration. To take advantage of the low pump power requirement and to realise a potentially cheap and reliable single-frequency source at 1.55μm, it is of interest to pump the fibre laser with a diode laser. This pumping scheme was realised with the set-up indicated in Figure 5.20 in which a 980nm laser diode was used as the pump source. Where as in previous measurements the signal was taken from a beamsplitter at the pump input, this arrangement introduces the pump signal and taps off the fibre laser output using a wavelength division multiplexing (WDM) 980nm/1550nm fibre coupler. Although in this case the diode laser was not fibre pigtailed, this pumping scheme would be most attractive with a pigtailed pump diode to result in a all-fibre scheme with resulting launch stability and overall reliability.

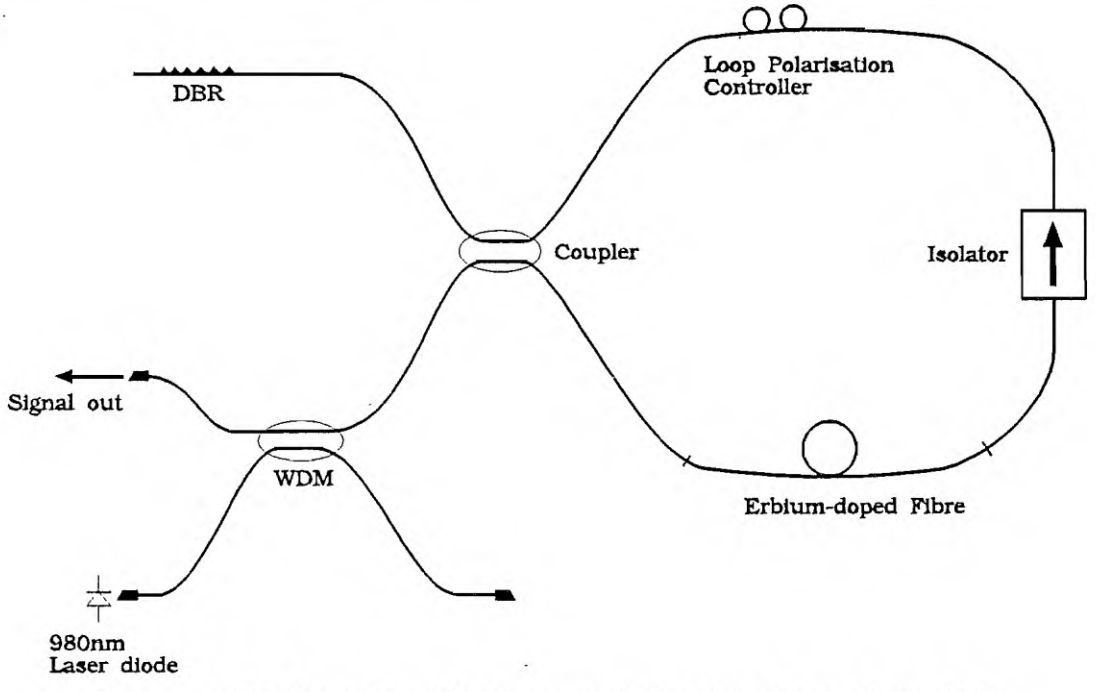

Figure 5.20 Schematic of diode-pumped fibre loop laser. Pump light is introduced via WDM coupler for 'all-fibre' arrangement.

The laser characteristic and the spectrum (via monochromator) of the diode pumped loop laser are shown in Figures 5.21 and 5.22 respectively. The launched power in this case refers to the pump signal launched into the 980/1550 WDM coupler. The threshold is higher than in the Ti:sapphire-pumped case illustrated in Figure 5.13 for three reasons; the 3dB coupler used in this experiment had high loss (25%) at the pump wavelength, there was also 10% loss of the pump signal due to the WDM coupler and the spectral characteristics of the pump laser were such that only about 50% of the pump signal was at the peak of the erbium absorption band, with the remainder in two lines about 4nm on either side of the absorption peak. Nevertheless a diode pumped single-frequency source was demonstrated at 1.55μm with over 1mW output power.

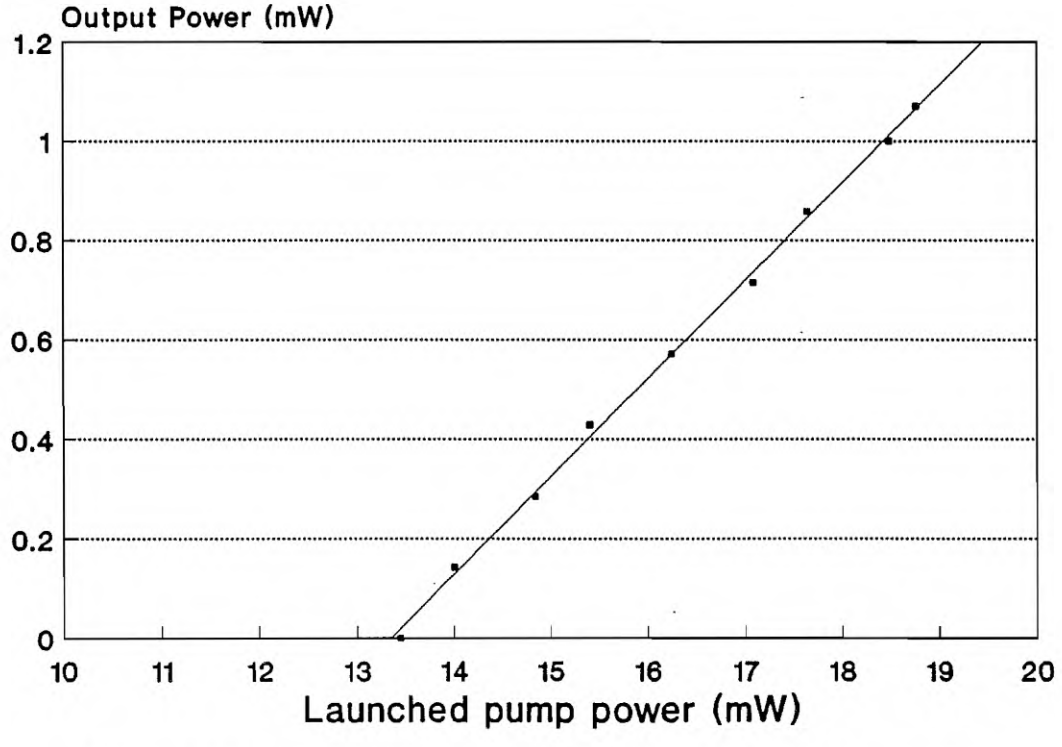

Figure 5.21 Power characteristic of diode-pumped single-frequency loop laser.

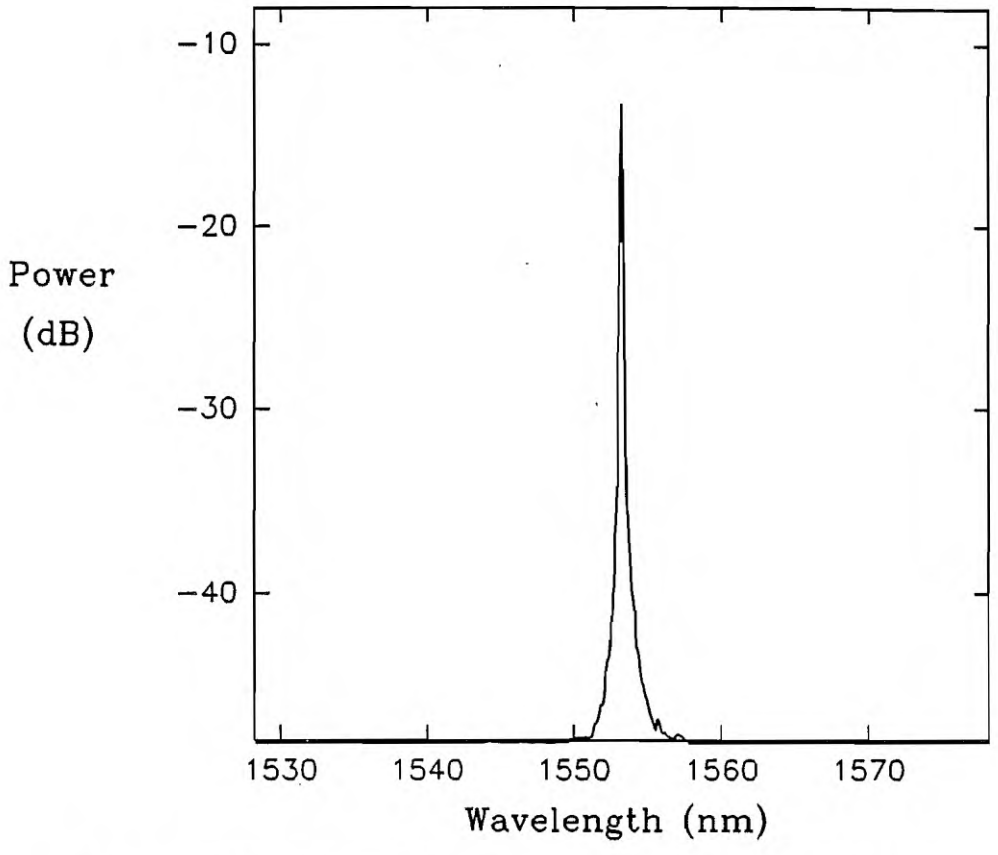

Figure 5.22 Spectrum of diode pumped fibre loop laser taken with monochromator with resolution 0.1nm

5.3.6 Discussion

The fibre loop laser is a novel fibre laser configuration which operates on a single-longitudinal-mode by the elimination of spatial holeburning due to travelling-wave operation in the gain medium. A linewidth of less than 10kHz in the 1.5μm telecommunications window has been demonstrated, with 6mW threshold and 29% slope efficiency. By suitable choice of reflector fixed wavelength operation or tunable operation is possible. A tuning range of 40nm has been demonstrated, however this cavity configuration is most suited to fixed wavelength operation taking advantage of

the wavelength stability furnished by a grating reflector. Although such a cavity configuration will always contain an intrinsic loss, it has been shown that suitable choice of coupler ratio enables efficient energy extraction to be obtained. Low threshold operation is possible, allowing for the use of diode lasers as pump sources, resulting in the possibility of stable and compact single-frequency fibre laser sources.

5.4 LINEWIDTH LIMITS

The measured linewidth of both the travelling-wave fibre ring laser and the travelling-wave fibre loop laser are several orders of magnitude larger than the linewidth predicted by the Schawlow-Townes expression (see Chapter 3), from which linewidths $\sim$ 1Hz would be expected. In addition, no significant amount of linewidth variation was measurable when the laser power was varied as would be expected from the Schawlow-Townes expression. However the Schawlow-Townes expression only takes into account noise fluctuations arising from spontaneous emission. As variations in linewidth according to the Schawlow-Townes expression do not occur, such as variations in linewidth with lasers power, other noise mechanisms must be dominant. It is believed that the measured linewidths arise from instabilities in the resonator. These instabilities may be due in part to refractive index changes arising from changes in temperature and from cavity length and hence phase variations due to acoustic disturbances. In this manner it is the cavity stability rather than spontaneous emissions giving rise to the measured linewidth. The measured linewidth thus appears to be limited by thermal and mechanical design parameters. To date the Schawlow-Townes limit has most successfully been approached using mechanically stable monolithic minature solid-state lasers such as nonplanar ring oscillators [Day] [Fan].

The temporal variation of the laser mode frequency, $\Delta\nu(t)$, which occurs as a consequence of fluctuations in the cavity length, $\Delta L(t)$, and fluctuations in the

refractive index, $\Delta n(t)$, can be expressed as:

$$\Delta \nu(t) = -\frac{\nu_0}{n_0 L_0}(n_0 \Delta L(t) + \Delta n(t) L_0) \qquad (10)$$

where L_0 represents the average resonator length and n_0 represents the average refractive index [Hall].

It is not surprising that fibre lasers should be sensitive to temperature and pressure, single-mode fibres are used in sensing external stimuli such as temperature, pressure, strain and acoustic waves. Silica has a refractive index thermo-optic coefficient of the order of $-10^{-5}/°C$ [Jeunhomme]. This sensitivity will lead to a frequency shift of a few gigahertz in a 1.5μm laser for a degree celsius temperature change. A 10kHz variation at 1.5μm will result from temperature variations of the order of 5μ°C. To minimise the laser linewidth will hence require accurate stabilisation and isolation of the fibre laser cavity.

The magnitude of any disturbances will determine the nature of the effect on the laser spectrum. Small cavity length or refractive index changes will result in a continuous drift of the laser frequency, contributing to the laser mode's intrinsic linewidth, but only if these disturbances are small and result in changes of the same order as the linewidth. Larger variations will result in frequency drifts which cannot be tracked by the laser, resulting in mode-hopping. Both types of variation, as well as full noise measurements require further characterisation.

5.5 SUMMARY AND CONCLUSIONS

In this chapter several novel travelling-wave erbium-doped fibre laser structures have been described which operate in a single-longitudinal-mode by virtue of the elimination of the prime cause of multi-mode operation, spatial holeburning in the gain medium. They offer single-frequency operation in the 1.5μm telecommunications window with linewidths of the order of tens of kilohertz.

The travelling-wave ring laser represents the first operation of a fibre laser as a travelling-wave laser. This first demonstration, with a linewidth of less than 60kHz, illustrates the strength of the technique which can result in single-frequency operation without the need for a strongly frequency-selective resonator as required in standing-wave resonators.

The travelling-wave loop laser is a novel laser configuration which has not been demonstrated in other types of lasers, which also eliminates spatial holeburning within the gain medium. This configuration allows for the incorporation of an wavelength selective element in the form of a diffraction grating to determine the wavelength of operation. Single-frequency operation was demonstrated with a linewidth less than 10kHz. The use of a distributed Bragg reflector permits stable operation at the reflection centre of the DBR, while the use of a bulk grating in the Littrow configuration was used to demonstrate a tuning range of 40nm. Although an inherently lossy cavity, high resonator efficiency can be achieved, allowing for the demonstration of diode-pumped operation of the laser.

5.6 REFERENCES

Barnes, W.L., Laming, R.I., Tarbox, E.J. and Morkel, P.R., "Absorption and Emission Cross-sections of Er^{3+} Doped Silica Fibres," *IEEE J. Quant. Elect.*, **27**, pp. Apr. 1991.

Bennion, I., Reid, D.C.J., Rowe, C.J. and W.J Stewart, "High-Reflectivity Monomode-Fibre Grating Filters", *Elect. Lett.*, **22**, 6, pp.341-343, Mar. 1986.

Bowness, C., "Single Mode Laser," U.S. Patent 3 409 843, Apr. 2, 1964.

Chaoyu, Y., Jiangde, P. and Bingkun, Z., "Tunable Nd^{3+}-doped Fibre Ring Laser," *Elect. Lett.*, **25**, 2, pp. 101-102, Jan. 1989.

Danielmeyer, H.G., and Turner, E.H., "Electro-optic Elimination of Spatial Hole Burning in Lasers", Appl. Phys. Lett., 17, 12, pp.519-521, Dec. 1970.

Day, T., Gustafson, E.K. and Byer, R.L., "Active Frequency Stabilization of a 1.062μm, Nd:GGG, Diode-laser-pumped Nonplanar Ring Oscillator To Less Than 3Hz of Relative Linewidth" *Opt. Lett.*, **15**, 4, pp. 221-223, Feb. 1990.

Evtuhov, V., and Siegman, A.E., "A "Twisted-Mode" Technique for Obtaining Axially Uniform Energy Density in a Laser Cavity", Appl. Opt., 4, 1, Jan. 1965.

Fan, T.S. and Byer, R.L., "Diode Laser-Pumped Solid-State Lasers", *IEEE J. Quant. El.*, **24**, 6, pp. 895-912, June 1988.

Guy, S.C., Minasian, R.A., Poole, S.B. and Sceats, M.G., "Characterisation of the Erbium Fibre Amplifier by Fluorescence Line Narrowing", *Proc. 15th ACOFT*, pp. 27-30, Sydney, Dec. 1990.

Hall, D.R. and Jackson, P.E. (eds) *The Physics and Technology of Laser Resonators.*, Adam Hilger, Bristol, England, 1989.

Hecht, E. and Zajac, A., *Optics.*, Addison-Wesley publishing Company, Reading Massachusetts, 1974.

Iwatsuki, K., Okamura, H. and Saruwatari, M., "Wavelength-tunable Single-frequency and Single-polarisation Er-doped Fibre Ring Laser with 1.4kHz Linewidth", *El. Lett.*, **26**, p. 2033, 1990

Jeunhomme, L.C., *Single-mode Fiber Optics.*, Marcel Dekker, Inc., New York, 1983.

Kimura, Y. and Nakazawa, M., "Lasing Characteristics of Er^{3+}-doped Silica Fibers From 1553 Up To 1603nm", *J. Appl. Phys.*, **64**, 2, pp. 516-520, July 1988.

Kittel, C., *Introduction to Solid State Physics.*, 5th Edition, John Wiley & Sons, New York, 1976.

Koechner, W.L., *Solid State Laser Engineering*, Springer Series in Optical Sciences, 2nd Edition, Springer Verlag, Berlin, 1988.

Morkel, P.R., Cowle, G.J. and Payne, D.N., "Travelling-wave Erbium Fibre Ring Laser with 60kHz Linewidth," *Elect. Lett.*, **26**, 10, pp. 632-634, May 1990.

Morkel, P.R., *Active Neodymium and Erbium Doped Fibre Devices*, Ph.D. Thesis, University of Southampton, Aug. 1990.

Mortimore, D.B., "Fiber Loop reflectors", *J. Lightwave Tech.*, **6**, 7, pp. 1217-1224, July 1988.

Neev, J. and Kowalski, F.V., "Unidirectional Device for a Ring Laser Using an Acousto-optic Modulator", *Opt. Lett.*, **13**, 5, pp. 375-377, May 1988.

Okamura, H. and Iwatsuki, K., "Spectral Linewidth Broadening in Er^{3+}-doped-fibre Amplifiers Measured With Less Than 1.4kHz Linewidth Light Source," *Elect. Lett.*, **26**, 23, pp. 1965-1967, Nov. 1990.

Ragdale, C.M., Reid, D., Robbins, D.J., Buus, J. and Bennoin, I., "Narrowband

Fiber Grating Filters,'' *IEEE J. Sel. Areas in Comms.*, **88**, 6, pp. 1146-1150, Aug. 1990.

Rigrod, W.W., ''Saturation Effects in High-gain Lasers,'' *J. Appl. Phys.*, **36**, pp. 2487-2490, Aug. 1965.

Rowe, C.J., Bennion, I. and Reid, D.C.J., ''High-Reflectivity Surface-Relief Gratings in Single-Mode Optical Fibres'', *IEE Proc. J*, **134**, 3, pp. 197-202, June 1987.

Sabert, H. and Ulrich, R., ''Single Longitudinal Mode Operation of Nd^{3+}-Fibre Laser,'' *Proc. ACOFT 15.*, pp. 31-34, Dec. 1990.

Scrivener, P.L., Tarbox, E.J. and Maton, P.D., ''Narrow Linewidth Tunable Operation of Er^{3+}-doped Single-mode Fibre Laser,'' *Elect. Lett.*, **25**, 8, pp. 549-550, April 1989.

Siegman, A.E., *Lasers*, University Science Books, Mill Valley, California, 1986.

Smith, D.A., Maeda, M.W., Johnson, J.J., Patel, J.S., Saifi, M.A. and Von Lehman, A., ''Acoustically Tuned Erbium-doped Fiber Ring Laser,'' *Opt. Lett.*, **16**, 6, pp. 387-389, March 1991.

Smith, D.A., Maeda, M.W., Patel, J.S., Johnson, J.J., Saifi, M.A. and Chinlon Lin, ''Electronically Tuned Erbium-doped Fiber Ring Lasers,'' *Int. Phot. Res. Tech Dig.*, **8**, pp. 142-143, April 1991.

Smith. P.W., ''Mode Selection in Lasers,'' *Proc. IEEE*, **60**, 4, pp. 422-440, Apr. 1972.

Tang, C.L., Statz, H. and de Mars, G., ''Spectral Output and Spiking Behaviour of Solid-State Lasers,'' *J. Appl. Phys.*, **34**, pp. 2289-2295, Aug. 1963.

Wyatt, R., ''High-power Broadly-tunable Erbium-doped Silica Fibre Laser'', *El. Lett.*, **25**, 22, pp. 1498-1499, Oct. 1989.

Zyskind, J.L., Desurvire, E., Sulhoff, J.W. and Di Giovanni, D.J., "Determination of Homogeneous Linewidth by Spectral Gain Hole-Burning in an Erbium-Doped Fiber Amplifier with GeO_2:SiO_2 Core", *IEEE Photon. Tech. Lett.*, **2**, 12, pp. 869-871, Dec. 1990.

Zyskind, J.L., Sulhoff, J.W., Stone, J., DiGiovanni, D.J., Stulz, L.W., Presbt, H.M., Piccirilli, A. and Pramayon, P.E., "Diode-Pumped, Electrically Tunable Erbium-Doped Fiber Ring Laser with Fiber Fabry-Perot Etalon", *Opt. Amplifiers and Their Applications Topical Meeting*, Colorado, July 24-26, 1991

Chapter Six

Optical Amplification of Narrow-Linewidth Signals

6.1 INTRODUCTION

To achieve high output power from a single-frequency erbium-doped fibre laser operating in the 1.5μm region, the pump power introduced to the laser resonator can be increased significantly above the lasing threshold, as is seen in a standard laser characteristic. An alternative approach to producing a high power single-longitudinal-mode fibre laser source is to optically amplify the output of a fibre laser or equivalently to distribute the gain medium partly in what is the conventional laser cavity and partly at the output port of the resonator. In this manner that part of the

gain produced at the output port is not used to overcome the cavity losses, but is used purely in converting pump light to narrow-band signal light. The amplifying medium at the output port could either be pumped with the same pump source or by a different pump source, in the latter case it could be treated as a conventional erbium-doped fibre amplifier located on the output port of the single-frequency fibre laser. This approach to high-power operation is attractive for lossy resonators.

An important consideration in using the gain medium to amplify a narrow-bandwidth signal is to ensure that the direct optical amplification of the laser signal does not significantly degrade the spectral purity of the source. This same consideration is important when using erbium-doped fibre amplifiers in coherent communication systems, which are currently the subject of much research effort and may be used in the future. Any significant broadening would have a detrimental effect on the bit-error-rate performance of the coherent communication system. For systems employing phase-sensitive detection, phase noise induced by an EDFA needs to be studied in addition to simple gain and amplitude considerations. It has been noted that using semiconductor laser amplifiers in this application may induce significant amounts of spectral broadening and it is important that if fibre amplifiers are used for this purpose they do not have similar drawbacks [Hinton].

This chapter describes the first measurements to have been performed to characterise the spectral broadening to be induced to a narrow-band signal passing through a fibre amplifier. Section 6.3 describes an experimental system developed to measure spectral broadening in an EDFA. The amount of broadening resulting will be seen to be very small, less than 0.1% of the input signal spectral width. Section 6.3.1 describes the measurement technique while Section 6.3.2 presents the results of the measurements. A statistical model is employed to model the origins of the spectral broadening and predict broadening levels. The model and its predictions for spectral broadening are discussed in Section 6.3.3. Because of the very small impact of the amplifier on the signal spectral width, direct optical amplification could be used to produce a single-longitudinal-mode high power fibre laser source in the 1.5μm region. It will be

evident from the measurements that spectral broadening is unlikely to impact on the performance of future coherent communication systems.

6.2 AMPLIFICATION OF NARROW-BAND SIGNALS

Erbium-doped fibre amplifiers (EDFAs) operating in the 1.5μm telecommunications window [Mears][Desurvire] have in recent years had a considerable impact on the thinking concerning communications systems architecture, and will play an important role in future communication systems. They will see applications in trunk and undersea networks, often eliminating the need for regenerative repeaters and improving the performance of local communication systems [Henry] [Marcuse]. Used as pre- or post-amplifiers, or as intermediate line amplifiers such devices offer high gain, low noise and high efficiency [Laming 1989], and have been characterised for amplitude and frequency modulation at frequencies up to 15GHz [Laming 1989a]. To date most experimental systems have concentrated on intensity-modulated direct-detection schemes. Advanced coherent communication systems employing optical amplifiers in combination with phase or frequency modulation will allow for greatly increased system capacity and are therefore of considerable interest for long-haul routes and for high-capacity local area networks [Okoshi]. The work presented in this chapter represents the first time the phase-noise statistics of amplified light from an erbium-doped fibre amplifier have been investigated, that is, the effect of amplified spontaneous emission (ASE) within the signal bandwidth on the signal spectrum. The statistics of the signal spectrum are important when coherent phase or frequency detection are employed. As will be seen, amplified spontaneous emission photons result in a small change in the power spectral density of the signal, which is however unlikely to have an effect on most applications. It is nevertheless a real effect which may ultimately have to be accounted for.

Recent results in which 25 amplifiers were employed, inserted every 80km in an experimental communication link [Saito] have demonstrated the possibility of concatenating many amplifiers in series to achieve coherent transmission over long distances without the use of regenerative repeaters. However, coherent systems require narrow-linewidth signals to achieve good bit-error-rate performance to take advantage of the available bandwidth [Linke]. Homodyne detection of phase shift keying (PSK) modulation can achieve a theoretical receiver sensitivity of 9 photons per bit, but requires a beat linewidth of 0.05 times the bit rate. Asynchronous heterodyne detection of narrow deviation frequency shift keying (FSK) can achieve sensitivity of 36 photons per bit, but requires a beat linewidth at the detector of 0.3 times the bit rate [Henry].

High sensitivity coherent communication systems require narrow-linewidth signals and may suffer reduced performance if significant spectral broadening to the signal were to be introduced in the optical link, in particular by phase noise in optical amplifiers or other system components. Early work on direct detection amplification for communication systems looked at semiconductor optical amplifiers [O'Mahony]. Besides being capable of less gain than EDFAs and suffering from polarisation sensitivity, it has been shown that these devices suffer from considerable phase noise, imposing limits on the number of devices which may be concatenated in a coherent optical link [Hinton]. It is of interest to determine whether similar problems will impact on the performance of the EDFA for the amplification of narrow-bandwidth signals.

Phase noise in fibre amplifiers can be caused by various effects in the active fibre, but is thought to be dominated by the addition of randomly-phased spontaneous photons to the signal field. These phase variations add to the intrinsic phase variations of the signal passing through the amplifier, thereby causing the signal linewidth to be broadened. The statistical content of the signal at the amplifier output must be altered since the randomly-phased spontaneous photons not correlated to the signal are added

within the signal bandwidth. For coherent system applications and for the amplification of narrow-band signals it is important that these phase variations must be insignificant compared to those of the signal field.

6.3 SPECTRAL BROADENING DUE TO FIBRE AMPLIFIER PHASE NOISE

In order to determine the effect of phase noise originating from the addition of amplified spontaneous emission to a amplified narrow-linewidth signal, measurements were performed to determine the amount of spectral broadening induced by an Er^{3+}-doped fibre amplifier to a narrow-linewidth signal passing through the amplifier.

6.3.1 Measurement Technique

To measure spectral broadening due to phase noise in a fibre amplifier, a measurement system was required which had sufficient resolution to a measure signal broadening component a small fraction of the signal width passing through the amplifier. A direct measurement such as a self-heterodyne measurement of the amplifier output is unlikely to provide sufficient accuracy. To realise such measurements an EDFA was incorporated in a balanced Mach-Zehnder single-mode fibre interferometer, as shown in Figure 6.1. As will be shown, if the paths of the interferometer are accurately matched the phase noise of the probe signal passing through the amplifier is cancelled at the detector and the power spectral density (PSD) of the signal at the detector is simply the spectral broadening response of the fibre amplifier.

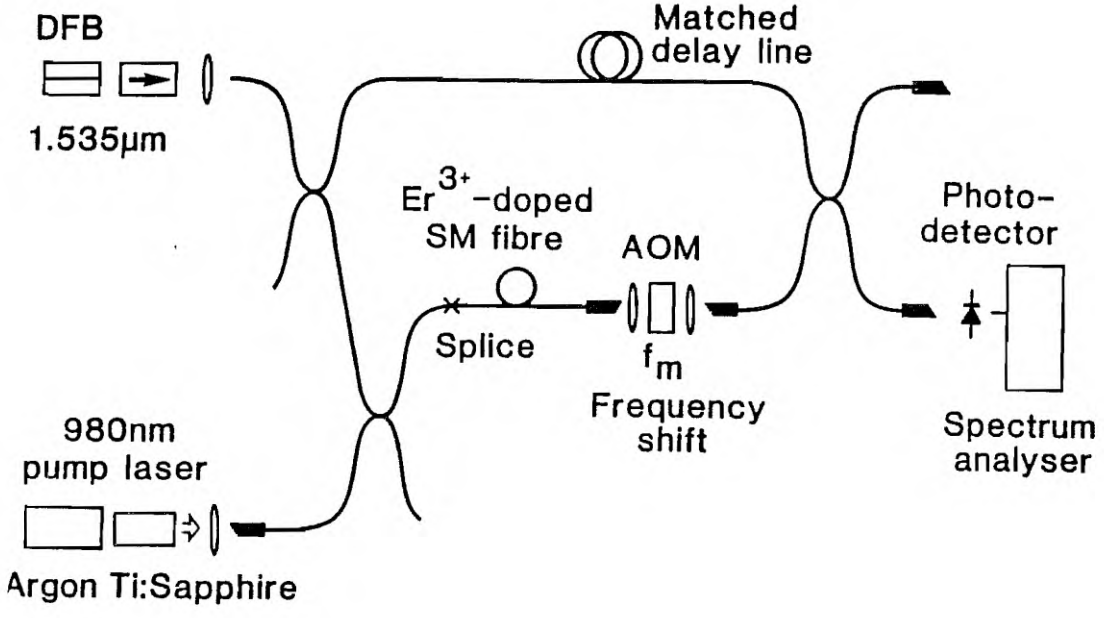

Figure 6.1 Experimental set-up for measuring spectral broadening due to EDFA phase noise. Mach-Zehnder interferometer has exactly matched paths.

The response of the measurement system and its ability to measure spectral broadening can be seen by calculating the power spectral density of the system output. The first step is to calculate the optical signals incident on the photodetector. The output from the probe CW signal laser, which was either a distributed feedback (DFB) semiconductor injection laser or a narrow-linewidth external-cavity semiconductor laser was split into two paths by the 3dB fibre coupler. One path passed through the EDFA and is up-shifted in frequency by an acousto-optic modulator

(AOM), while the other passed through a single-mode fibre delay line. The two paths were recombined in a 3dB coupler and detected.

The system response can be analysed by assuming that the time-varying field of the signal laser, E(t), is of the form:

$$E(t) = E\, e^{j(\omega t - \phi_l(t))} \tag{1}$$

where ω is the laser frequency and $\phi_l(t)$ is the time-varying phase of the laser field, while the amplitude E of the signal is assumed to be constant. It is assumed that the phase variations introduced by the amplifier from amplified spontaneous emission gives rise to an additional phase term $\phi_a(t)$ to the signal passing through the first arm including the EDFA. It is also assumed that as the signal strength is significantly stronger than the ASE strength that amplitude fluctuations can be ignored. The signals from the two paths which are combined onto the photodetector via a 3dB coupler can be written as:

$$E_1(t) = E_1\, e^{j(\omega_l t - \phi_l(t) + \omega_m t - \phi_a(t))} \tag{2}$$

$$E_2(t) = E_2\, e^{j(\omega_l(t-\tau_d) - \phi_l(t-\tau_d))} \tag{3}$$

where ω_m is the modulation frequency of the acousto-optic frequency shifter and τ_d is the propagation time difference between the light passing through the two fibre arms from the probe signal laser to the detector. The frequency shifter gives rise to a beat component in the photo-detector current, centred at frequency f_m, and of the form (when shifted to baseband):

$$i(t) \propto e^{j\phi_a(t)}\, e^{j(\phi_l(t) - \phi_l(t-\tau_d))} \tag{4}$$

The PSD of the beat component of the detector signal can be determined by taking

the autocorrelation and then Fourier Transform of the detector current in Equation 6.4. The autocorrelation R(t) can be expressed as:

$$\begin{aligned} R(t) &= \left\langle \left(e^{j\phi_a(t)}\ e^{j(\phi_l(t)-\phi_l(t-\tau_d))}\right)^* \left(e^{j\phi_a(0)}\ e^{j(\phi_l(0)-\phi_l(-\tau_d))}\right)\right\rangle \\ &= \left\langle e^{-j\phi_a(t)}\ e^{j\phi_a(0)}\ e^{j(\phi_l(0)-\phi_l(t))}\ e^{j(\phi_l(t-\tau_d)-\phi_l(-\tau_d))}\right\rangle \\ &= \left\langle e^{j(\phi_a(0)-\phi_a(t))}\ e^{j(\Delta\phi_l(t-\tau_d)-\Delta\phi_l(t))}\right\rangle \end{aligned} \tag{5}$$

where $\Delta\phi_l(t) = \phi_l(t) - \phi_l(0)$. Assuming that the phase noise of the amplifier is independent of the phase noise of the signal laser, Equation 6.5 can be written as:

$$\begin{aligned} R(t) &= \left\langle e^{j(\phi_a(0)-\phi_a(t))}\right\rangle \left\langle e^{j(\Delta\phi_l(t-\tau_d)-\Delta\phi_l(t))}\right\rangle \\ &= R_a(t)\ R_l(t) \end{aligned} \tag{6}$$

where $R_a(t) = \langle\exp(j(\phi_a(0)-\phi_a(t)))\rangle$ is the autocorrelation of the amplifier phase variations and $R_l(t) = \langle\exp(j(\Delta\phi(t-\tau_d)-\Delta\phi_l(t)))\rangle$ is related only to the laser beat signal.

To obtain the PSD the Fourier Transform (FT) is taken:

$$PSD = FT\left\{R_a(t)\right\} * FT\left\{R_l(t)\right\} \tag{7}$$

Looking at the two terms in the above equation separately, it can be shown (for example see the derivation of the self-heterodyne scheme in Appendix 1) that the second term, the Fourier Transform of the autocorrelation of the laser signal, S(f), can be expressed:

$$S(f)=\frac{\tau_c}{1+\pi^2 f^2 \tau_c^2}\left\{1-e^{-\frac{2\tau_d}{\tau_c}}\left(\cos(2\pi f\tau_d)+\frac{\sin(2\pi f\tau_d)}{\tau_c \pi f}\right)\right\}+e^{-\frac{2\tau_d}{\tau_c}}\delta(f) \tag{8}$$

where τ_c is the coherence time of the signal laser, defined by [Moslehi]:

$$\tau_c = \frac{2}{\Delta\omega_{FWHM}} \tag{9}$$

where $\Delta\omega_{FWHM}$ is the angular full width at half maximum spectral width of the laser spectrum.

Examining Equation 6.8 it can be seen that if the delay time, τ_d, between the two paths from the signal laser to the detector is much less than the coherence time of the signal laser, i.e., $\tau_d \ll \tau_c$, then the power spectral density in Equation 6.8 reduces to a delta function. In this limit the measured PSD from the experimental system reduces to:

$$PSD = FT\{R_a(t)\} = FT\left\{\left\langle e^{j(\phi_a(0)-\phi_a(t))}\right\rangle\right\} \tag{10}$$

This term represents the contribution of spectral broadening introduced by the fibre amplifier phase noise. Hence by measuring the PSD with the set-up of Figure 6.1 with the optical paths matched so that $\tau_d \ll \tau_c$, the spectral broadening due to the fibre amplifier can be determined by cancelling the phase noise of the probe signal. The actual spectrum of the signal at the output of the amplifier, $S_{out}(f)$, is given by the convolution of the spectral broadening term of Equation 6.10 with the PSD of the input signal, $S_{in}(f)$ to obtain:

$$S_{out}(f) = S_{in}(f) * FT\left\{\left\langle e^{j(\phi_a(0)-\phi_a(t))}\right\rangle\right\} \tag{11}$$

6.3.2 Spectral Broadening Measurements

Spectral broadening due to fibre amplifier phase noise was measured using the technique described in Section 6.3.1 and illustrated in Figure 6.1 with two laser sources, one with a 30MHz spectral width and one with a 50kHz spectral width. The amplifier fibre used for the series of measurements was an 11 metre length of germano-silicate composition Er^{3+}-doped single-mode optical fibre, with an Er^{3+} concentration of 250ppm, NA=0.2 and λ_c=975nm. Pump light was introduced through a dichroic or wavelength division multiplexing coupler from a CW Ti:sapphire laser operating at 980nm. The gain characteristic of the amplifier configuration for constant signal power of 61μW at 1.535μm from the DFB laser is shown in Figure 6.2. A frequency shift of either 40MHz or 100MHz was introduced by one of two acousto-optic modulators following the fibre amplifier.

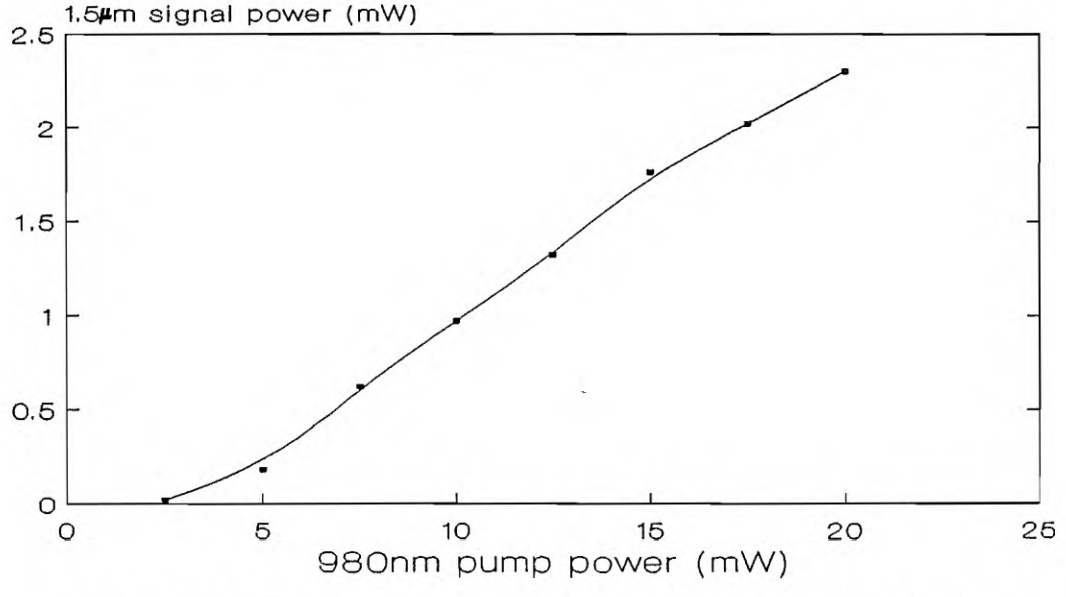

Figure 6.2 Gain characteristic of EDFA used for spectral broadening measurements. Probe signal at 1.535μm with constant power of 61μW. Amplifier pumped by Ti:sapphire laser operating at 980mn.

The first signal source employed was a DFB semiconductor laser operating at 1.535μm, with a spectral width of ~30MHz. This spectral width corresponds to a coherence length of about 6 metres in optical fibre, thus to ensure that the condition $\tau_d \ll \tau_c$ was satisfied, the two optical paths of the Mach-Zehnder were matched from one fibre coupler to the other to a path difference of within a few millimetres. In order to confirm that the two arms of the Mach-Zehnder were accurately matched the length of doped fibre was replaced by an equal length of undoped fibre. The PSD centred at the frequency shift f_m arising from the DFB signal passing through the control system was measured and is shown in Figure 6.3. As expected from Equation 6.8 the PSD is a delta function, since in this case $\phi_a=0$ with no EDFA. Expanding the scale when measuring this PSD it was possible to resolve this signal to have a width of less than 15Hz, being the limit of the detector and spectrum analyser response. This figure of 15Hz is an indication of the ultimate absolute resolving power of the Mach-Zehnder in this arrangement.

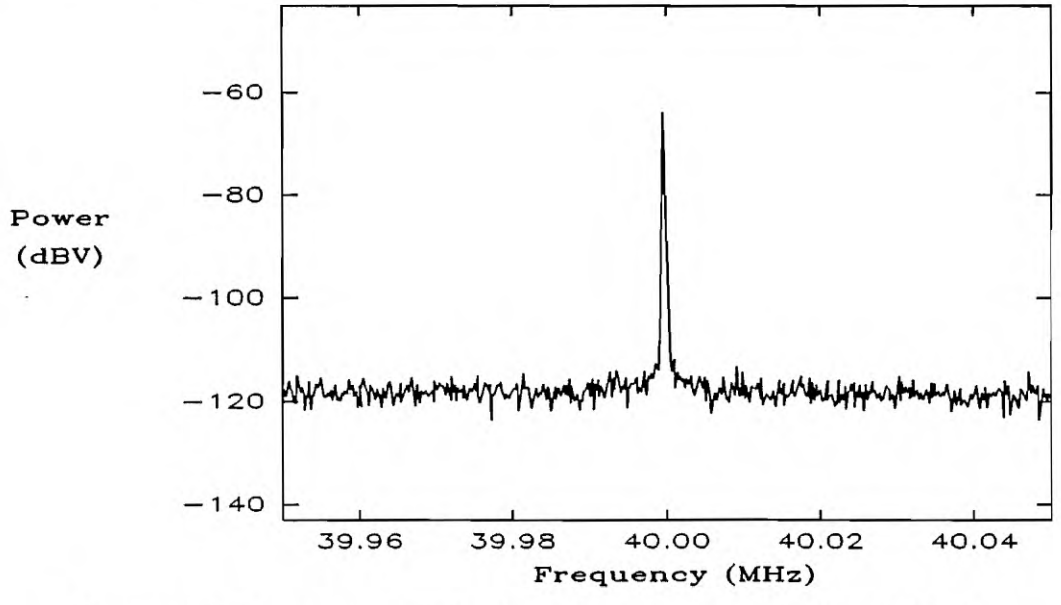

Figure 6.3 Power spectral density of output of matched-path Mach-Zehnder interferometer without amplifier. Delta function width <15Hz.

With the amplifier fibre in place the PSD of Figure 6.4 was measured, centred at the beat frequency f_m. The measurement conditions for the plotted results were a pump power of 20mW and signal power 50μW, with the amplifier providing 17dB gain. Comparison with Figure 6.3 shows that with the amplifier in place the PSD is quite different from the delta function of the control-configuration. The spectral broadening due to phase noise in the EDFA gives rise to a PSD with an approximately Lorentzian lineshape, with a half-power width of about 15kHz for these measurement conditions. The control experiment indicates that the path lengths were accurately matched when the experiment was configured and that the PSD of Figure 6.4 is due to spectral broadening arising from phase noise generated in the fibre amplifier from amplified spontaneous emission photons.

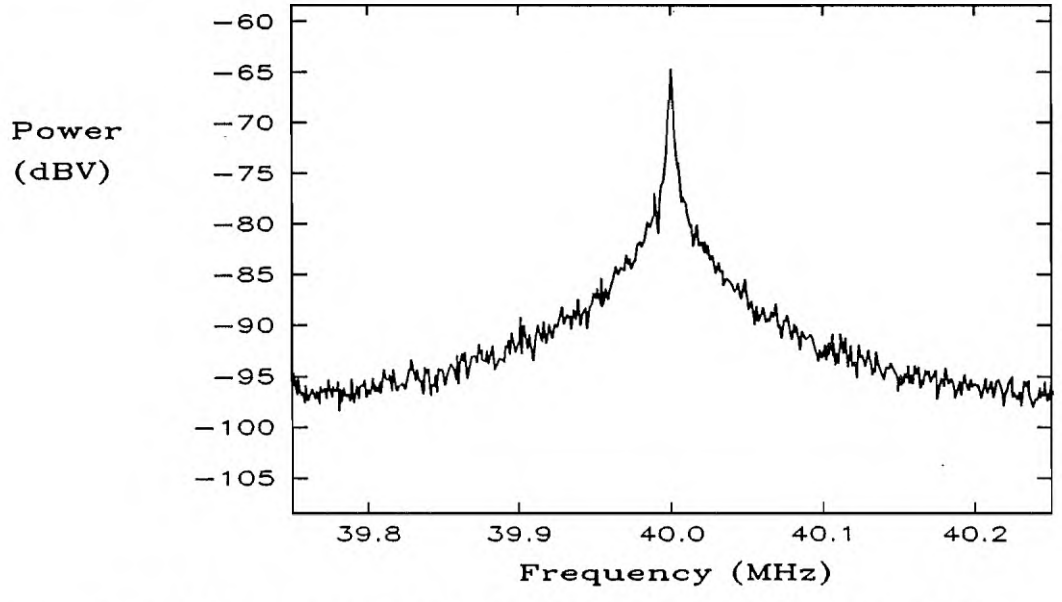

Figure 6.4 Power spectral density of spectral broadening measured by balanced Mach-Zehnder interferometer. Signal at 1.535μm with 30MHz width, amplifier providing 17dB gain. Half-power width of broadening ~ 15kHz.

The degree of spectral broadening indicated in Figure 6.4 shows a spectral width of about 15kHz, however the amount of broadening induced by the amplifier was

observed to change with input signal power with constant 980nm pump power, as shown in Figure 6.5. The signal power was varied by introducing attenuation to the laser output while keeping the DFB drive conditions constant in order to prevent linewidth changes of the signal source. It can be seen from Figure 6.5 that the degree of spectral broadening introduced by the amplifier decreases with increasing signal power. This behaviour is expected if the spectral broadening is due to spontaneous photons, since increasing the signal power brings about an increase in the ratio of signal to amplified spontaneous emission, the ASE photons within the signal bandwidth giving rise to the spectral broadening. Another contribution to the decrease in spectral broadening with increasing signal power could be that as the signal power increases for fixed pump power, the population inversion decreases, thereby reducing ASE power. When the signal power was kept constant and the pump power was varied the change in spectral broadening was not quantifiable, being very small. In this case there is very little change in the ratio of signal to ASE.

Thus the Er^{3+}-doped fibre amplifier contributes to the phase noise of a signal passing through the amplifier, resulting in a small degree of spectral broadening. The measurements above, performed with a 30MHz width signal passing through the amplifier show that the amount of spectral broadening is very small, typically less than 15kHz, or less than 0.05% of the signal width for a 30MHz probe signal width.

In order to determine whether the amount of spectral broadening was affected by the signal source spectral linewidth, additional measurements were performed, replacing the DFB laser source by an external-cavity semiconductor laser source with a spectral width of ~50kHz. A typical PSD measurement of the beat signal centred at f_m is shown in Figure 6.6, for a signal power of 100μW and a pump power of 20mW. Under these conditions no spectral broadening was measurable. A small amount of change in the PSD was detectable approaching the noise floor of the measurement, but insufficient to accurately quantify a change in the 3dB width of the PSD. Bearing in mind that the measurement scheme could resolve a delta-function width down as

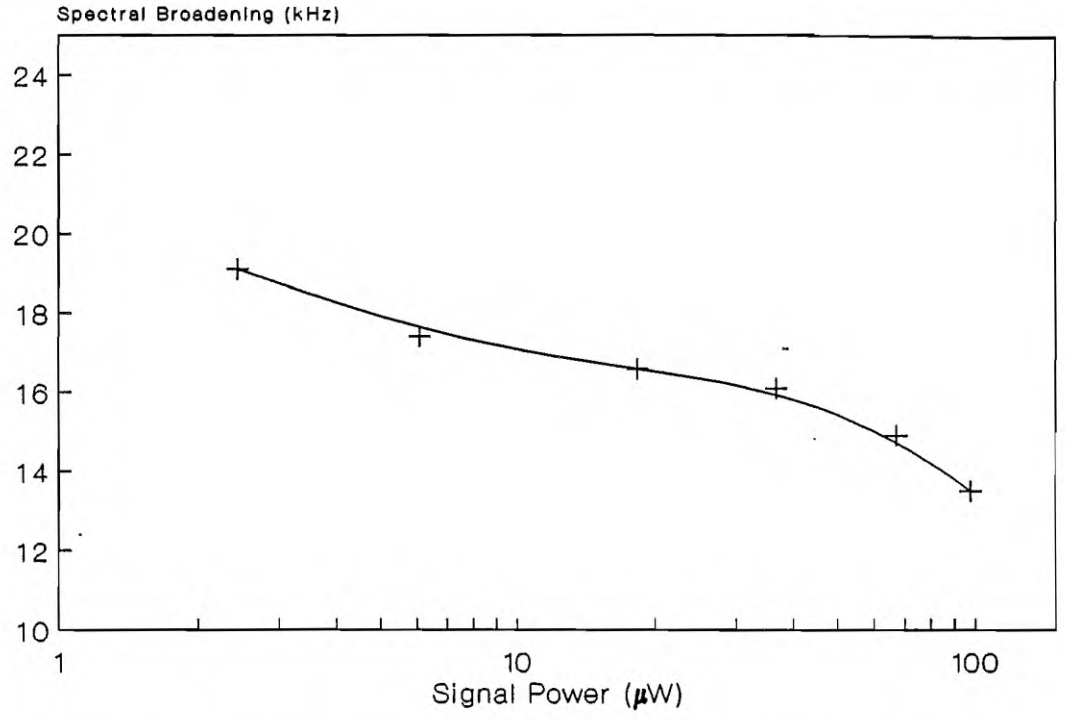

Figure 6.5 Variation of spectral broadening PSD with signal power. Signal at 1.535μm with spectral width 30MHz.

far as 15Hz, this implies that any spectral broadening is of this order of magnitude or less, this resolution corresponding to 0.03% of the signal spectral width. Although broadening could not be quantified, the absolute magnitude of the spectral broadening was determined to be dependent on the signal spectral width passing through the amplifier.

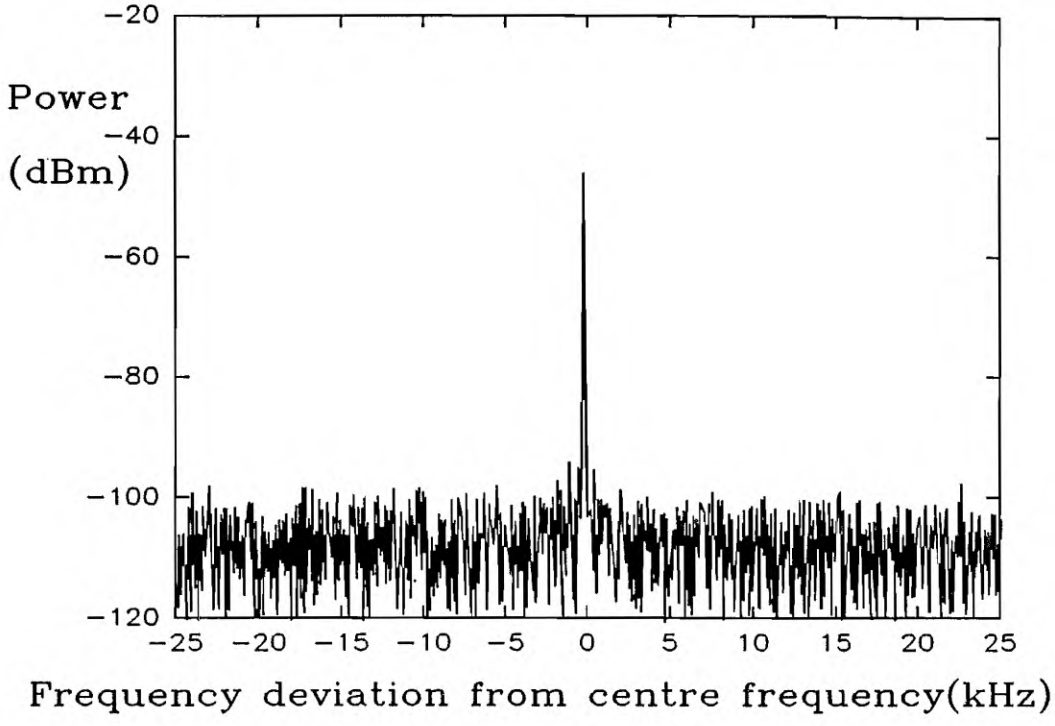

Figure 6.6 Power spectral density of spectral broadening measured with 43kHz width signal at 1.55μm. Broadening is not measurable, minimum measurable width 15Hz. Centre frequency 100MHz.

6.4 MODELLING OF FIBRE AMPLIFIER SPECTRAL BROADENING

The amount of broadening induced by the phase noise of the fibre amplifier measured in Section 6.3.2 was very small, and as such is unlikely to impact on the amplification of narrow-linewidth signals or on the performance of coherent communication systems. For coherent systems, other factors such as accumulation of ASE, power penalties due to Rayleigh backscattering, and signal broadening due to non-linear effects in the transmission fibre, will predominate in the accumulation of noise to limit system performance [Yariv 1990] [Gordon] [Staubli]. However, the spectral characteristics of a signal at the output of an amplifier will be different from those at the input of the amplifier, and hence it is useful to calculate the amount of spectral variation arising from the use of an EDFA. The spectral nature of the signal at the

amplifier output must be altered since randomly-phased spontaneous photons which are not correlated with the signal are added to the signal field.

In order to calculate the effect of the addition of ASE photons to the amplified signal field a statistical model is used in this section, as the PSD of the measured field is fundamentally a statistical phenomenon. The model assumes that the total signal at the output of the amplifier consists of a narrow-band amplified signal and broadband ASE noise, however the detection process is not able to determine the origin of individual photons and hence it is not possible to distinguish signal photons from ASE photons within the signal bandwidth. This is why spectral broadening is measured from the detector current power spectral density. It is assumed that the amplification process directly amplifies the signal photons without altering their statistics, whilst the ASE photons are assumed to be randomly phased across the signal bandwidth and are hence effectively white noise compared to the signal bandwidth.

The signal is modelled as the sum of a rotating phasor and a random phasor sum, as indicated in Figure 6.7. This type of model is commonly used when calculating laser linewidth, however in this case we work backwards from a known linewidth to the fundamental phasor components. The ASE noise is included as an additional statistically independent, random phasor sum added on top of the rotating vector of the signal field. Hence the modelling can simply be viewed as the addition of white noise due to ASE to the signal with a known spectrum, or the shifting of the power level of this known spectrum by the effect of white noise. The average rate of arrival of the ASE photons or the average number of ASE spontaneous noise vectors added in a given time determines the amount of spectral broadening, in the same way that the rate of arrival of spontaneous photons into the laser mode determines the laser linewidth. The model proceeds by calculating the arrival rate of spontaneous photons making up the input signal. This is compared with the arrival rate of amplified spontaneous emission photons to calculate the increase in spectral width of the signal at the amplifier output.

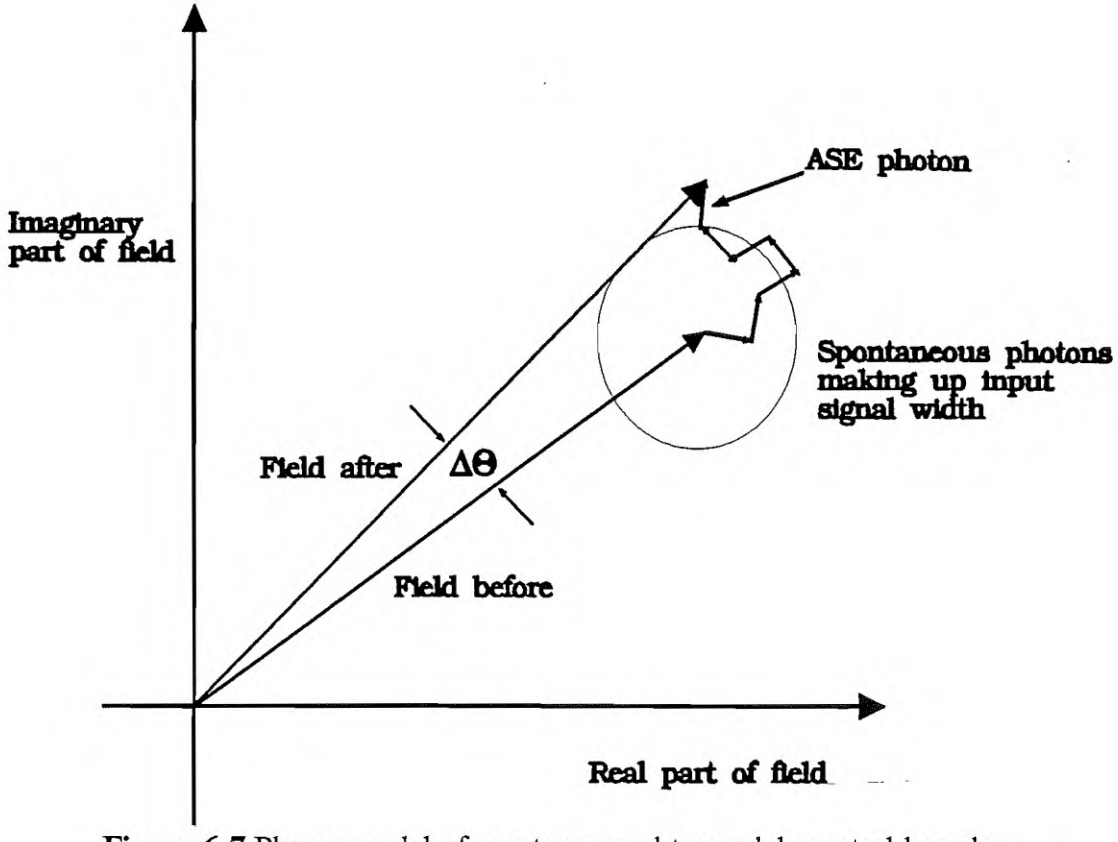

Figure 6.7 Phasor model of spectrum used to model spectral broadening. Signal is represented by a rotating vector, spontaneous emission photons add on top of the rotating vector with unit amplitude and random phase.

A Lorentzian signal is assumed for the laser signal with a linewidth $(\Delta\nu)_{laser}$, and only a CW carrier is considered. The input signal is first analysed. Using the standard phasor model of laser linewidth [Yariv] this is assumed to be modelled as a rotating phasor onto which is added a random phasor sum representing spontaneous emissions, giving rise to a finite linewidth. The laser field is represented in the form:

$$\varepsilon(t) = Re\{E(t)e^{j(\omega t+\theta(t))}\} \qquad (12)$$

where E(t) is the field amplitude, ω is the laser frequency and $\theta(t)$ is the field phase.

Without loss of generality the phasor model can be taken as the sum of a constant phasor which is entirely real and a random phasor sum made up of phasors with unit amplitude and phase uniformly distributed on $(-\pi,\pi)$. In the case under consideration, the constant phasor is also assumed to be much stronger than the random phasor sum, a valid assumption for a highly coherent light signal [Goodman].

With this assumption the angular change due to one spontaneous emission, $\Delta\theta$, is given approximately by:

$$\Delta\theta = \frac{1}{\sqrt{\bar{n}}}\cos\phi \tag{13}$$

where $\bar{n}$ is the average number of photons comprising the constant phasor signal and ϕ is the random phase of the ASE photon. ϕ is uniformly distributed on $(-\pi,\pi)$. The mean squared angular deviation after N spontaneous emissions, $\Delta\Theta(N)$, becomes:

$$\langle[\Delta\theta(N)]^2\rangle = \langle(\Delta\theta)^2\rangle\, N = \frac{1}{\bar{n}}\langle\cos^2\phi\rangle\, N \tag{14}$$

The RMS phase variation after time t can be calculated from the number of spontaneous emission photons detected in a time t in the signal bandwidth. Following the standard laser theory [Yariv] the RMS phase variation after time t can be expressed as:

$$\begin{aligned}\Delta\theta(t) &= \langle[\Delta\theta(t)]^2\rangle^{\frac{1}{2}} \\ &= \sqrt{\frac{1}{2\bar{n}}\,\frac{\mu t}{t_c}}\end{aligned} \tag{15}$$

where the variables are μ, the laser inversion factor and t_c, the photon lifetime in the resonator, which are constants characteristic of the laser source. If we calculate

directly the laser field spectrum, by taking the autocorrelation and Fourier transform of $\epsilon(t)$ from Equation 6.11, the spectral density function can be shown to be of the form:

$$S(\omega) = \frac{\langle E^2 \rangle}{4\pi} \frac{\frac{1}{4\bar{n}t_c}}{\left(\frac{\mu}{4\bar{n}t_c}\right)^2 + (\omega - \omega_0)^2} \tag{16}$$

which is a Lorentzian lineshape with FWHM linewidth given by:

$$(\Delta\omega)_{laser} = \frac{\mu}{2\bar{n}t_c} \tag{17}$$

The RMS angular deviation in the phasor description can hence be expressed in terms of the laser linewidth by:

$$\begin{aligned} \Delta\theta(t) &= \langle [\theta(t)]^2 \rangle^{\frac{1}{2}} \\ &= \sqrt{\frac{1}{2\bar{n}} \frac{\mu t}{t_c}} \\ &= \sqrt{(\Delta\omega)_{laser}\, t} \end{aligned} \tag{18}$$

To calculate the effect of the ASE noise on the phasor model and hence the measured linewidth we must add a second random phasor sum to that used in modelling the laser linewidth. Since the ASE photons are uncorrelated to the laser photons we can simply add them to the original random phasor sum, thus increasing the inter-arrival time of the noise photons, from both the signal laser and the amplifier spontaneous emissions, at the amplifier output. Using the ASE power at the amplifier output, we can calculate the average inter-arrival time of ASE photons at the amplifier output. Hence if the ASE power P_{ASE} at the amplifier output in a single polarisation is given

by:

$$P_{ASE} = \mu_a h\nu \, \Delta\nu \, (G-1) \tag{19}$$

where $h\nu$ is the photon energy, $\Delta\nu$ is the bandwidth over which the ASE power is measured, which in this case is the probe signal spectral width, as only spontaneous photons within the signal bandwidth are of interest, μ_a is the amplifier inversion factor and G is the amplifier gain, then the average time between the emission of ASE photons from the amplifier end is:

$$t_{ASE} = \frac{1}{\mu \, \Delta\nu \, (G-1)} \tag{20}$$

Thus in the average time for one ASE photon to be emitted by the amplifier the RMS angular deviation in the phase of the laser signal is:

$$\Delta\theta(t_{ASE}) = \sqrt{\frac{2\pi(\Delta\nu)_{laser}}{\mu \, \Delta\nu \, (G-1)}} \tag{21}$$

In order to modify the random phasor inter-arrival time by the addition of the amplifier ASE photons, we must know the angular deviation induced by one spontaneous emission in the laser model. Assuming the case of a large constant phasor and a random phasor sum, the angular deviation from one spontaneous emission can be approximated by:

$$\Delta\theta_1 = \frac{1}{\sqrt{n_{sig}}} \cos\phi \tag{22}$$

and hence the RMS angular change due to one spontaneous photon is:

$$\left\langle (\Delta\theta_1)^2 \right\rangle^{\frac{1}{2}} = \frac{1}{\sqrt{2n_{sig}}} \tag{23}$$

The number of signal photons in the time t_{ASE} at the amplifier output can be expressed simply as:

$$n_{sig} = \frac{P_{in} G}{h\nu} \frac{1}{\mu \Delta\nu (G-1)} \tag{24}$$

The average number of laser signal noise photons in the output signal during the average time for one ASE photon to be detected is simply the RMS angular deviation during the time t_{ASE} divided by the RMS angular deviation induced by one ASE photon:

$$n_{spont} = \frac{\Delta\theta(t_{ASE})}{\left\langle (\Delta\theta_1)^2 \right\rangle^{\frac{1}{2}}} = \sqrt{\frac{4\pi P_{in} G(\Delta\nu)_{laser}}{\mu^2 (\Delta\nu)^2 h\nu (G-1)^2}} \tag{25}$$

If we take $\Delta\nu = k(\Delta\nu)_{laser}$, then:

$$n_{spont} = \sqrt{\frac{4\pi P_{in} G}{\mu^2 h\nu k^2 (\Delta\nu)_{laser} (G-1)^2}} \tag{26}$$

The model assumes that spectral broadening occurs due to the addition of randomly-phased spontaneous photons during the time t_{ASE}. The spectral width at the amplifier output hence scales with the mean square angular deviation, which is proportional to

the number of noise photons detected. Spectral broadening is thus in the ratio:

$$\frac{n_{spont} + 1}{n_{spont}} \tag{27}$$

Hence the amount of spectral broadening measured by the detector can be approximated in proportion to the signal spectral width as:

$$\delta\nu = \frac{1}{n_{spont}} (\Delta\nu)_{laser} \tag{28}$$

To verify the validity of this model to predict spectral broadening due to randomly-phased ASE photons adding to the signal field calculations were made using constants taken to approximate the experimental conditions described in Section 6.3.2. Figure 6.8 shows the predicted spectral broadening to a 30MHz signal passing through an amplifier providing 17dB of gain. As can be seen, for input powers in the range 10μW to 100μW the predicted spectral broadening is of the order 20kHz, with slowly decreasing spectral broadening resulting as the signal power is increased. These predictions agree well with the measured results plotted in Figure 6.5, particularly for signal strengths greater than 10μW. The accuracy of the model decreases for signals less than 10μW. This is due to the assumption of the rotating vector length being much greater than a single photon becoming less valid.

The projections of the model for a 50kHz signal passing through an amplifier are plotted in Figure 6.9. As can be seen, the predicted amount of spectral broadening in this case is typically less than 2Hz. Recalling the measurements of spectral broadening for a 50kHz signal, it was not possible to resolve any spectral broadening. The model predicts broadening of $\sim$2Hz, while the resolution of the Mach-Zehnder interferometer was $\sim$15Hz, so in this case the amount of broadening in the half-power width of the PSD would not be measurable.

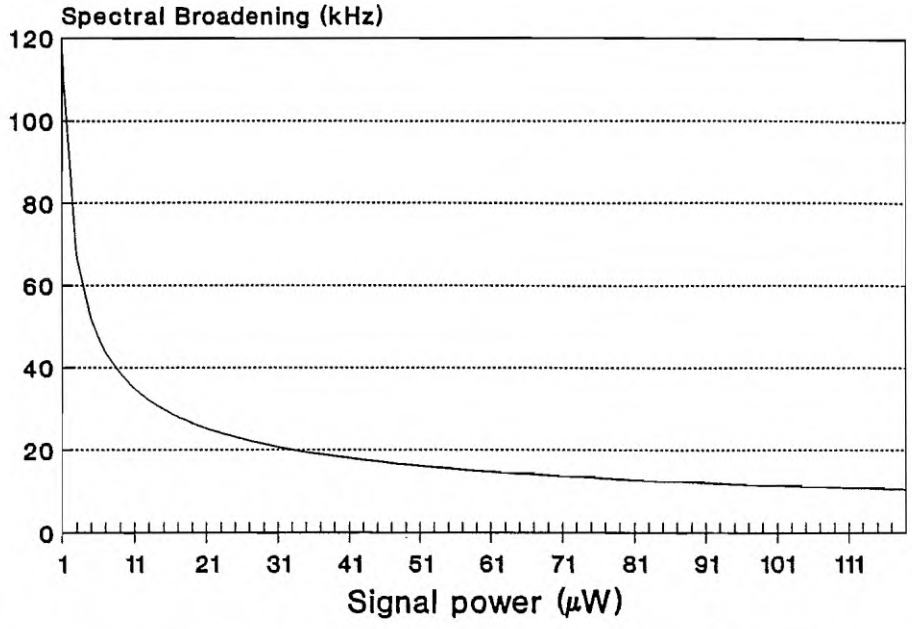

Figure 6.8 Predicted spectral broadening as a function of signal power for a signal with spectral width 30MHz.

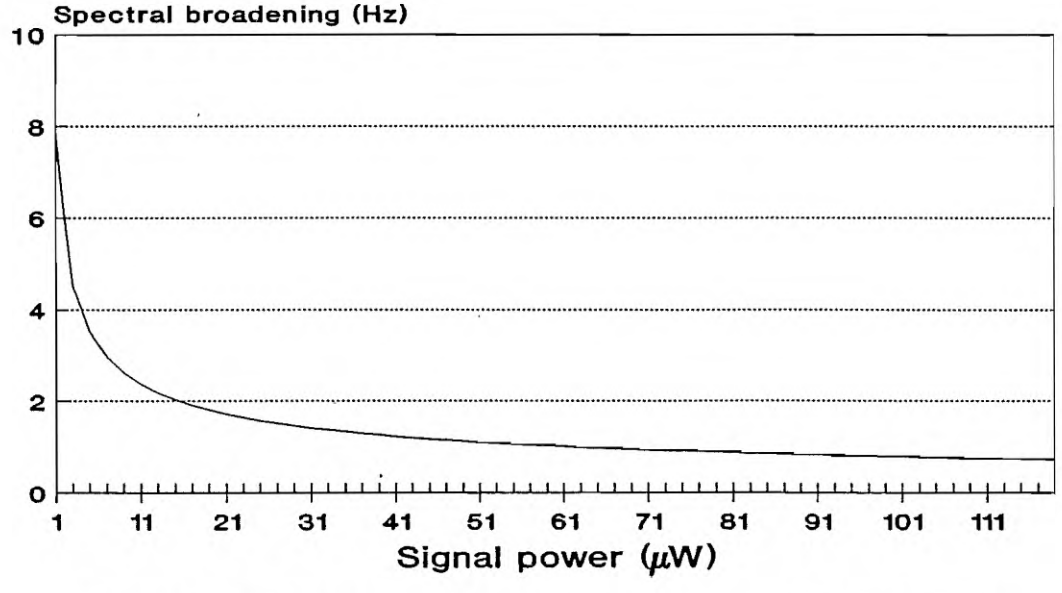

Figure 6.9 Predicted spectral broadening as a function of signal power for a signal with spectral width 50kHz.

Prompted by the publication of the measurements previously described in Section 6.3.2, Okamura and Iwatsuki attempted to measure spectral broadening from an erbium-doped fibre amplifier using a 1.4kHz linewidth input source [Okamura]. They were not able to measure any broadening, however their measurements were performed by passing the amplified signal through a self-heterodyne interferometer, not a system as developed in this work and described in Section 6.3.1. The measurement scheme of Okamura and Iwatsuki does not have the same resolving power as the measurement scheme described in Section 6.3.1, and is probably only capable of accurately measuring spectral width changes of $\sim 10\%$. Figure 6.10 shows predictions of spectral broadening for a 1kHz signal passing through an amplifier, indicating that spectral broadening in this case will be of the order of milli-Hertz, unmeasurable with the previously described matched Mach-Zehnder, and well beyond the resolution capabilities of a self-heterodyne measurement.

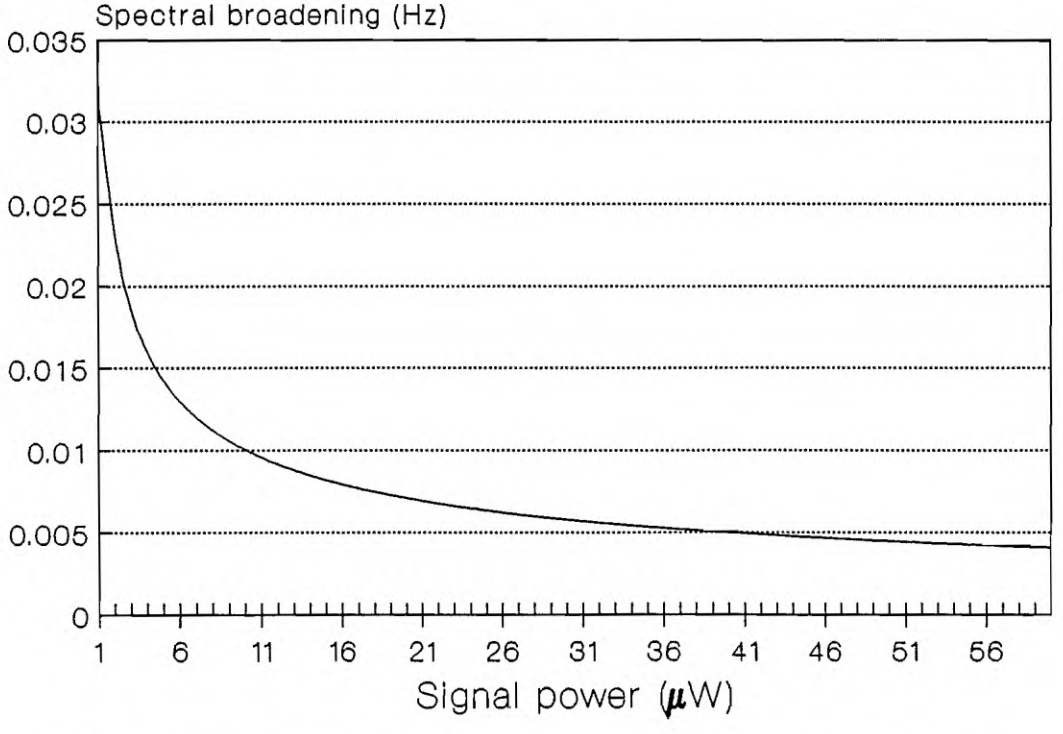

Figure 6.10 Predicted spectral broadening as a function of signal power for a signal with spectral width 1kHz.

The predicted variation of spectral broadening as a function of the spectral width of the signal is plotted in Figure 6.11 for a range of spectral widths from 100kHz to 1MHz. As can be seen the function is a monotonically increasing function with increasing slope with increasing signal width, indicating than the effect of spectral broadening becomes more dominant for larger signal spectral widths. This can be understood intuitively by seeing that the spectral width of the signal does not affect the amplification within the EDFA, while greater spectral width allows a greater number of randomly-phased spontaneous photons to fall within the signal bandwidth. Thus if two signals containing the same number of photons pass through the amplifier, both will be amplified by the same amount while the broader signal will have more ASE photons added within its signal bandwidth, causing a more significant change in the statistical nature of the field.

The other important prediction of the model, which was borne out in the experimental results, can be seen from Figure 6.8, which shows that spectral broadening becomes more pronounced as the input signal power decreases. As the ratio of signal to ASE increases the effect of the spontaneous emissions on the laser field becomes less pronounced. Only when the ASE power becomes close to the signal power will drastic spectral broadening occur. From the point of systems applications of fibre amplifiers it would thus be favourable to employ amplifiers before the signal power approaches the ASE power in the signal bandwidth. For the application of making high-power single-longitudinal-mode fibre lasers the use of an amplifier on the laser output port will have negligible impact on the laser signal spectral width.

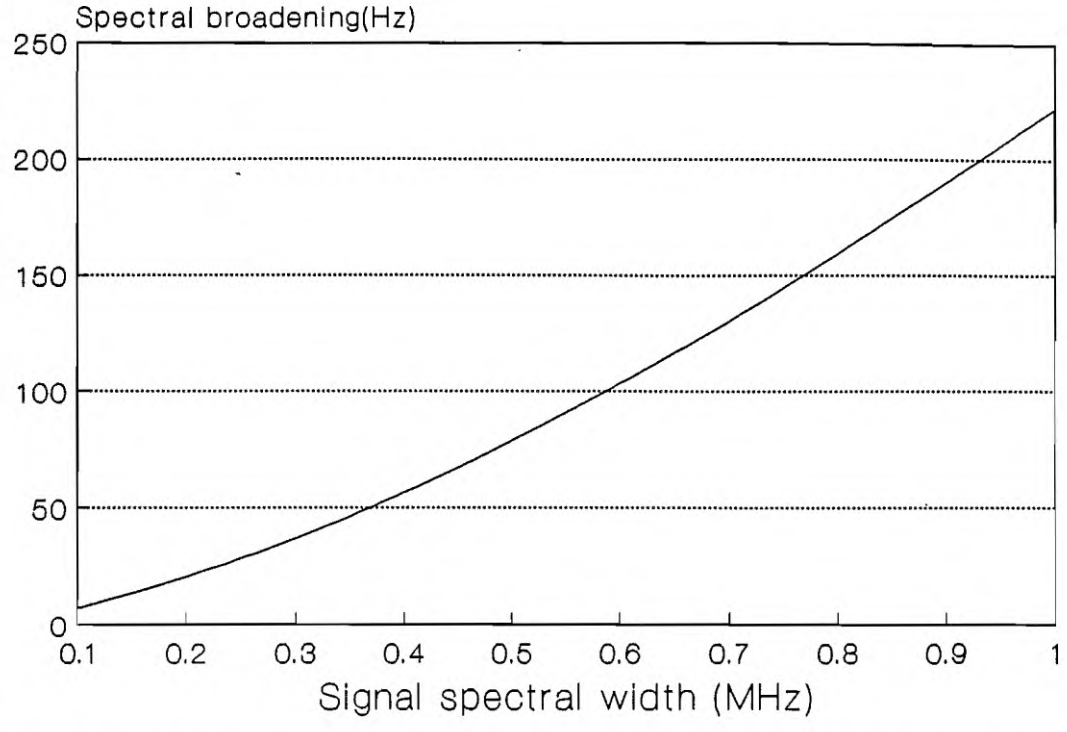

Figure 6.11 Predicted spectral broadening as a function of signal spectral width for a 10μW signal and an EDFA producing gain of 50

6.5 SUMMARY

This chapter has presented the first measurements looking at the fundamental phase properties of the spontaneous emission photons generated in an erbium-doped fibre amplifier and their effect on the statistics of a signal passing through the amplifier. Spectral broadening of a narrow-band signal passing through an EDFA has been measured with a matched-path Mach-Zehnder interferometer capable of resolving power spectral densities with 15Hz width.

Measurements with a 30MHz linewidth signal revealed spectral broadening of less than 20kHz for typical values of signal power and amplifier gain. Such levels of broadening, less than 0.1% of the signal width are unlikely to have any consequences for the bit-error-rate performance of future coherent communication systems or cause

any significant broadening when amplifying narrow-band optical signals to produce high-power single-frequency sources. Measurements with narrowband (<50kHz) signals found that the amount of broadening was too small to measure. It was determined that the amount of broadening was a function of the input signal spectral width. The amount of broadening also decreased with increasing input signal strength. A statistical model was developed to predict levels of spectral broadening, the results of the model agreeing well with the measured trends and levels of broadening.

6.6 REFERENCES

Desurvire, E., Simpson, J.R. and Becker, P.C., "High-gain Erbium-doped Travelling-wave Fiber Amplifier", *Opt. Lett.*, **12**, 11, 1987.

Goodman, J.W., *Statistical Optics*, John Wiley & Sons, New York, 1985.

Gordon, J.P. and Mollenauer, L.F., "Phase Noise in Photonic Communications Systems Using Linear Amplifiers", *Opt. Lett.*, **15**, 23, pp. 1351-1353, Dec. 1990.

Henry, P.S., "Lightwave Primer", *IEEE J. Quant. El.*, **21**, 12, pp. 1862-1879, 1985.

Hinton, K., "Analytical Model For Semiconductor Laser Amplifiers in Coherent Optical Systems", *El. Lett.*, **24**, 17, pp. 1116-1117, 1988.

Laming, R.I., Farries, M.C., Morkel, P.R., Reekie, L., Payne, D.N., Scrivener, P.L., Fontana, F. and Righetti, A., "Efficient Pump Wavelengths of Erbium-doped Fibre Optical Amplifier", *El. Lett.*, **25**, 1, 1989.

Laming, R.I. and Vodhanel, R.S., "0.1-15GHz AM and FM Response of Erbium-doped Fibre Amplifier", *El. Lett.*, **25**, 17, 1989.

Linke, R.A. and Gnauck, A.H., "High-Capacity Coherent Lightwave Systems", *J. Lightwave Tech.*, **6**, 11, 1988.

Marcuse, D., "Derivation of Analytical Expressions for the Bit-Error Probability in Lightwave Systems with Optical Amplifiers", *J. Lightwave Tech.*, **8**, 12, pp. 1816-1823, Dec. 1990.

Mears, R.J., Reekie, L., Jauncey, I,M. and Payne, D.N., "High Gain Erbium-doped Travelling-wave Fibre Amplifier Operating at 1.55μm", *Proc. OFC'87,* Reno, Nevada, 1987.

Moslehi, B., ''Analysis of Optical Phase Noise in Fiber-Optic Systems Employing a Laser Source with Arbitrary Coherence Time'', *J. Lightwave Tech.*, **LT-4**, 9, pp. 1334-1351, Sept. 1986.

Okamura, H. and Iwatsuki, K., ''Spectral Linewidth Broadening in Er-doped-fibre Amplifiers Measured With Less Than 1.4kHz Linewidth Light Source'', *El. Lett.*, **26**, 23, pp. 1965-1967, 1990.

Okoshi, T., Emura, K., Kikuchi, K. and Kersten, R. Th., ''Computation of Bit-Error Rate of Various Heterodyne and Coherent-Type Optical Communication Schemes'', *J. Opt. Comm.*, **2**, pp. 89-96, 1981.

O'Mahony, M.J., ''Semiconductor Laser Optical Amplifiers for Use in Future Fiber Systems'', *J. Lightwave Tech.*, **6**, 4, pp. 531-544, 1988.

Saito, S., Imai, T., Sugie, T., Ohkawa, N., Ichihashi, Y. and Takeshi, I., ''An Over 2,200km Coherent Transmission Experiment at 2.5Gbit/s Using Erbium-doped-fiber Amplifiers'', *Proc. OFC'90,* Paper PD2, San Francisco, California, 1990.

Staubli, R.K., Gysel, P. and Hofstetter, R.U., ''Power Penalties Due to Multiple Rayleigh Backscattering in Coherent Transmission Systems Using In-Line Optical Amplifiers'', *IEEE Phot. Tech. Lett.*, **2**, 12, pp. 872-874, Dec. 1990.

Yariv, A., *Optical Electronics*, Third Edition, Holt, Rinehart and Winston, New York, 1985.

Yariv A., ''Signal-to-noise Considerations in Fiber Links With Periodic or Distributed Optical Amplification'', *Opt. Lett.*, **15**, 19, pp. 1064-1066, Oct. 1990.

Chapter Seven

Summary and Conclusions

This thesis has been concerned with techniques for achieving single-longitudinal-mode operation in Er^{3+}-doped fibre lasers operating in the principal telecommunications window. The approach has been to experimentally develop novel fibre laser resonators for narrow-linewidth and single-longitudinal-mode operation. Several significant results have been described which contribute to the development of the technology of fibre lasers. These include the first demonstration of a travelling-wave fibre ring laser, and the operation of the travelling-wave fibre loop laser.

Resonator design for narrow-linewidth and single-frequency operation has been

investigated both for standing-wave and travelling-wave configurations. Although the standing-wave designs investigated did not reliably achieve single-frequency operation, novel resonator configurations have been fabricated and analyzed, with the modifications necessary for achieving single-frequency operation noted. An empirical observation is that to achieve single-longitudinal-mode operation the passive cavity mode spacing must be such that less than 50 passive cavity modes fall within the passive cavity bandwidth.

Very narrow-bandwidth distributed Bragg reflectors have been seen to be extremely important elements in narrow-linewidth operation of fibre lasers, and fabrication techniques under development for achieving such devices were described. The fabrication techniques improve the length and uniformity of surface-relief gratings, and initial results indicate that reflection bandwidths less than 0.2nm are achievable. These fabrication techniques will see application beyond fibre devices, to the production of narrow-band gratings on planar waveguide lasers.

A novel coupled-cavity fibre laser resonator was described, which operates by the interaction of orthogonal polarisation modes in a high birefringence resonator. The resonator took the form of a polarimetric Michelson cavity. A spectral width of less than 5GHz or 0.04nm was achieved in this configuration.

It has been demonstrated that although single-frequency operation is possible in standing-wave fibre lasers, the nature of the erbium-doped fibre gain medium and techniques for resonator construction indicate that single-frequency operation is very difficult to achieve in practice. This work has seen the pioneering of travelling-wave operation in fibre lasers to achieve single-frequency operation. Travelling-wave operation overcomes the obstacle of spatial holeburning, which limits the performance of standing-wave fibre laser resonators.

The first demonstration of travelling-wave operation in fibre lasers is described, in

the form of a uni-directional ring laser. Another novel travelling-wave fibre loop laser is also reported. Such laser resonators have been demonstrated to be capable of linewidths of less than 10kHz. It has been demonstrated by these results that all that is required to achieve single-longitudinal-mode operation in erbium-doped fibre lasers is to eliminate the effects of spatial-holeburning. By these results it has been demonstrated that although the phospho-alumino-silicate host erbium-ion fibre gain medium has mixed homogeneous and inhomogeneous broadening components it acts as a homogeneous medium. This demonstration of single-frequency operation by the elimination of spatial holeburning operates in a gain medium in which the homogeneous and inhomogeneous broadening have similar widths, so although substantial inhomogeneous broadening exists the gain medium acts as if homogeneously broadened. The measured linewidth of these lasers appears at this stage to be limited by thermal and mechanical design limitations.

This thesis has also considered the amplification of narrow-linewidth signal in the 1.55μm region by erbium-doped fibre amplifiers. It has been identified and measured for the first time that the use of fibre amplifiers results in spectral broadening to a signal passing through the amplifier. Although this phenomenon exists, the magnitude of the broadening has been identified to be very small. This noise source is unlikely to impact on the performance of coherent communication systems or cause significant broadening when amplifying narrow-bandwidth signals to produce high-power single-longitudinal-mode sources. A novel measurement scheme was described which was capable of measuring the small changes in spectral width of a signal passing through a fibre amplifier, and a model proposed to predict the effects of spectral broadening.